

# Flow and Heat Transport of Maxwell Fluid Induced by Stretching and Rotating Surfaces



By  
*Awais Ahmed*

**Department of Mathematics  
Quaid-i-Azam University  
Islamabad, Pakistan  
2021**

# Flow and Heat Transport of Maxwell Fluid Induced by Stretching and Rotating Surfaces



By  
*Awais Ahmed*

Supervised By  
*Prof. Dr. Masood Khan*

Department of Mathematics  
Quaid-i-Azam University  
Islamabad, Pakistan  
2021

# Flow and Heat Transport of Maxwell Fluid Induced by Stretching and Rotating Surfaces



By

*Awais Ahmed*

A DISSERTATION SUBMITTED IN THE PARTIAL FULFILLMENT OF THE  
REQUIREMENT FOR THE DEGREE OF

DOCTOR OF PHILOSOPHY

IN

**MATHEMATICS**

*Supervised By*

*Prof. Dr. Masood Khan*

**Department of Mathematics**

**Quaid-i-Azam University**

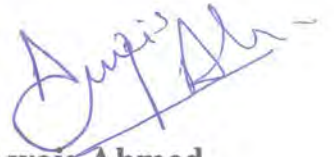
**Islamabad, Pakistan**

**2021**

## Author's Declaration

I, Awais Ahmed hereby state that my PhD thesis titled “Flow and Heat Transport of Maxwell Fluid Induced by Stretching and Rotating Surfaces” is my own work and has not been submitted previously by me for taking any degree from the Quaid-i-Azam University Islamabad, Pakistan or anywhere else in the country/world.

At any time if my statement is found to be incorrect even after my graduate the university has the right to withdraw my PhD degree.



Name of Student: Awais Ahmed

Date: 23-08-2021

## Plagiarism Undertaking

I solemnly declare that research work presented in the thesis titled "Flow and Heat Transport of Maxwell Fluid Induced by Stretching and Rotating Surfaces" is solely my research work with no significant contribution from any other person. Small contribution/help wherever taken has been duly acknowledged and that complete thesis has been written by me.

I understand the zero tolerance policy of the HEC and Quaid-i-Azam University, Islamabad towards plagiarism. Therefore, I as an Author of the above titled thesis declare that no portion of my thesis has been plagiarized and any material used as reference is properly referred/cited.

I undertake that if I am found guilty of any formal plagiarism in the above titled thesis even afterward of PhD degree, the University reserves the rights to withdraw/revoke my PhD degree and that HEC and the University has the right to publish my name on the HEC/University Website on which names of students are placed who submitted plagiarized thesis.

Student/Author Signature: \_\_\_\_\_



Name: Awais Ahmed

*CERTIFICATE*

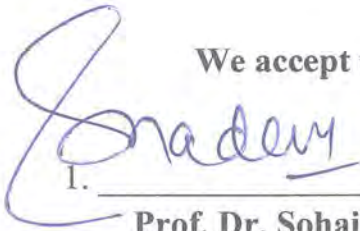
**Flow and Heat Transport of Maxwell Fluid  
Induced by Stretching and Rotating Surfaces**

By

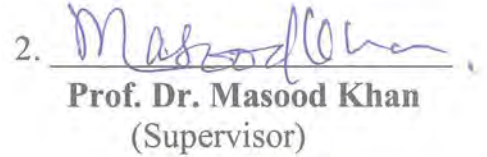
***Awais Ahmed***

A THESIS SUBMITTED IN THE PARTIAL FULFILLMENT OF THE  
REQUIREMENTS FOR THE DEGREE OF THE  
***DOCTOR OF PHILOSOPHY IN MATHEMATICS***

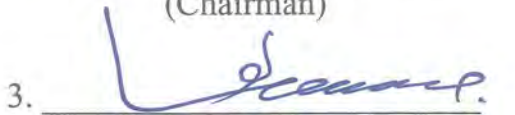
We accept this thesis as conforming to the required standard

1. 

**Prof. Dr. Sohail Nadeem**  
(Chairman)

2. 

**Prof. Dr. Masood Khan**  
(Supervisor)

3. 

**Assoc. Prof. Abdullah Shah**  
(External Examiner)

4. 

**Prof. Dr. Nasir Ali**  
(External Examiner)

Department of Mathematics  
COMSATS University Islamabad,  
Park Road Chak Shahzad, Islamabad

Department of Mathematics & Statistics  
International Islamic University  
H-10 Sector, Islamabad

**Department of Mathematics  
Quaid-i-Azam University  
Islamabad, Pakistan  
2021**



## Certificate of Approval

This is to certify that the research work presented in this thesis entitled **Flow and Heat Transport of Maxwell Fluid Induced by Stretching and Rotating Surfaces** was conducted by Mr. **Awais Ahmed** under the kind supervision of **Prof. Dr. Masood Khan**. No part of this thesis has been submitted anywhere else for any other degree. This thesis is submitted to the Department of Mathematics, Quaid-i-Azam University, Islamabad in partial fulfillment of the requirements for the degree of Doctor of Philosophy in field of Mathematics from Department of Mathematics, Quaid-i-Azam University Islamabad, Pakistan.

Student Name: **Awais Ahmed**

Signature: \_\_\_\_\_

External committee:

a) **External Examiner 1:**

Name: **Dr. Abdullah Shah**

Designation: Associate Professor

Office Address: Department of Mathematics, COMSATS University  
Islamabads, Park Road Chak Shahzad, Islamabad.

Signature: \_\_\_\_\_

b) **External Examiner 2:**

Name: **Prof. Dr. Nasir Ali**

Designation: Professor

Office Address: Department of Mathematics & Statistics, Faculty of Basic  
& Applied Sciences, International Islamic University, Islamabad.

Signature: \_\_\_\_\_

c) **Internal Examiner**

Name: **Prof. Dr. Masood Khan**

Designation: Professor

Office Address: Department of Mathematics, QAU Islamabad.

Signature: \_\_\_\_\_

**Supervisor Name:**

**Prof. Dr. Masood Khan**

Signature: \_\_\_\_\_

**Name of Dean/ HOD**

**Prof. Dr. Sohail Nadeem**

Signature: \_\_\_\_\_

**Dedicated to**

**My beloved parents**



# Acknowledgement

In the name of **ALLAH**, the Most Glorious and the Most Merciful Lord, the creator and all praises to **ALLAH** who guide me in darkness, helps me in troubles and empowers me to view tentative blocks as stepping stones to the stars to reach the eventual stage with courage. I am nothing without my **ALLAH** but I can achieve everything with assistance. All of my reverence and commitment goes to our **Prophet Hazrat Muhammad SAWW** the source of humanity, kindness and guidance for the whole creatures and who advised the mankind to pursue knowledge from cradle to grave.

First and foremost I would like to express my special appreciation and thanks to my PhD advisor Prof. Dr. Masood Khan, you have been a tremendous mentor for me. I would like to thank you for encouraging my research and for allowing me to grow as a research scientist. Your advice on both research as well as on my career have been invaluable. In short, your tireless work, unique way of research and devotion to your profession cannot be expressed in words.

I would like to thank my mother and father, whose love, prayers and guidance are with me to follow my dreams. I am very thankful to my loving parents for their guidance, support and encouragement. I owe my heartiest gratitude for their assistance and never ending prayers for success. I highly commend the cooperative behavior of my brothers who endeavored for my edification and betterment.

I gratefully acknowledge the Department of Mathematics, Quaid-i-Azam university Islamabad for this wonderful facilitation sources that made my PhD work possible. My sincere thanks also goes to chairman Department of Mathematics Prof. Dr. Sohail Nadeem, who provide me the opportunity for this milestone achievement.

I thank my fellow labmates in for the stimulating discussions, for the sleepless nights we were working together, and for all the fun we have had in the last four years. A very special thank you to Dr. Jawad Ahmed for his invaluable advice and feedback on my research and for always being so supportive of my work. My time at Quaid-i-Azam University was also enriched by the graduates and fellows Abdul Hafeez, Zahoor Iqbal, Mahnoor Sarfraz, Muhammad Yasir, Dr. Muhammad Irfan, Dr. Aamir Hamid.

In the end I would like to thank to all my research fellows and to those people who directly and indirectly helped me during my research work.

**Best Regards**

**Awais Ahmed**

## **Abstract**

The viscoelasticity of rate type non-Newtonian fluids exhibits two major phenomena, due to viscous and elastic components, which are termed as creep and relaxation phenomena. The researchers have developed the Kelvin-Voigt and Maxwell empirical models for the viscoelastic fluids. These two models successfully predict the creep and relaxation phenomena. Most of fluids in nature are viscoelastic types e.g., polymers, paints, and some biological fluids. The flow of viscoelastic non-linear fluids with heat and mass transport is of great important in many areas of engineering applications such as plastic coating and polymer sheet production etc. The heat transfer rate greatly affects the quality of these products. Thus, the study of rheological features of viscoelastic fluids with thermal and solutal energy transport mechanisms is a foremost interest of the current era of research.

Several studies have been devoted in analyzing the flow and energy transport phenomena of Maxwell fluid engender by stretching and rotating surfaces. The present thesis is structured from this point of view. Both flow and energy transport phenomena over various stretching and rotating surfaces, which include stretching and rotating sheet, disk as well as cylinder are modeled in the form of highly non-linear partial differential equations (PDEs). The diverse physical effects which can considerably affect the flow and heat transport mechanisms are contemplated. Convective transport of thermal and solutal energy is studied in both modes, forced and free convective. Analytical and numerical computations are carried out to similar equations for the flow and heat transfer. The well-known homotopy analysis method (HAM) and `bvp4c` built-in MATLAB function are utilized for construction of solutions. The outcomes for the flow and energy transport controlling parameters are explored through the tabular and graphical abstracts. It is interesting to observed that an increment in the stress relaxation phenomenon of viscoelastic Maxwell fluid

declines the flow velocity however enhances significantly both the thermal and solutal energy transport from surface to free stream. The thermal and mass relaxation times in higher trend, which are the features of Cattaneo-Christov theory, decrease the energy transport in fluid flow over both stretching and rotating geometries. The rate of thermal energy transport in Maxwell fluid boosts up in case of constant wall temperature as compared to prescribed surface temperature. On the other hand, in swirling flow induced by rotating cylinder the higher value of Reynolds number declines the velocity field and fluid motion confined to the surface of cylinder together with temperature and concentration distributions are also reduced. The present results are also verified by making comparison with the results available in the literature.

# Contents

<b>1</b>	<b>Introduction</b>	<b>4</b>
1.1	Background and Literature Review . . . . .	4
1.2	Motivation and Research Objectives . . . . .	12
1.3	Fundamental and Constitutive Relations (Laws) of Continuum Mechanics . . . . .	14
1.3.1	Fundamental Relations . . . . .	14
1.3.2	Constitutive Relations . . . . .	16
1.4	Methods of Computation . . . . .	17
1.4.1	Homotopy Analysis Method (HAM) . . . . .	18
1.4.2	Bvp4c (Numerical Method) . . . . .	19
1.5	Thesis Structure . . . . .	20
<b>2</b>	<b>Mixed Convective Flow of Maxwell Nanofluid over a Stretching Sheet</b>	<b>24</b>
2.1	Problem Formulation . . . . .	25
2.1.1	Similarity Transformation . . . . .	28
2.2	Homotopic Solution . . . . .	29
2.3	Results and Discussion . . . . .	30

2.3.1	Results Authentication . . . . .	32
<b>3</b>	<b>Unsteady Stagnation Point Flow of Maxwell Nanofluid due to Stretchable Disk</b>	<b>39</b>
3.1	Mathematical Formulation . . . . .	40
3.2	Solution Procedure . . . . .	43
3.3	Discussion of Results . . . . .	44
3.4	Surface Thermal Gradient and Analysis Authentication . . . . .	47
<b>4</b>	<b>Analysis of Cattaneo-Christov Model for Unsteady Flow of Maxwell Fluid due to Stretchable Cylinder</b>	<b>57</b>
4.1	Mathematical Formulation . . . . .	58
4.2	Computational Procedure . . . . .	62
4.3	Analysis of Results . . . . .	63
4.4	Outcomes Validation and Surface Thermal and Soutal Grandients . . . . .	65
<b>5</b>	<b>Buoyancy Driven Unsteady Stagnation Point Flow of Maxwell Fluid over a Stretchable Cylinder</b>	<b>72</b>
5.1	Mathematical Formulation . . . . .	73
5.2	Numerical Methodology . . . . .	76
5.3	Physical Interpretation of Outcomes . . . . .	78
5.4	Validation of Present Outcomes . . . . .	85
<b>6</b>	<b>Boundary Layer Flow of Maxwell Fluid Due to Stretchable Rotating Cylinder</b>	<b>87</b>

6.1	Mathematical Modelling . . . . .	88
6.1.1	Analysis for Large Re . . . . .	92
6.2	Quantities of Interest . . . . .	93
6.3	Numerical Solution . . . . .	94
6.4	Presentation of Results . . . . .	96
<b>7</b>	<b>Thermal Analysis in Swirl Motion of Maxwell Nanofluid over a Rotating Cylinder</b>	<b>105</b>
7.1	Problem Development . . . . .	106
7.2	Physical Quantities . . . . .	111
7.3	Numerical Solution . . . . .	111
7.4	Discussion of Results . . . . .	113
<b>8</b>	<b>Von Kármán Flow of Maxwell Nanofluid Featuring the Cattaneo-Christov Theory with Buongiorno Model</b>	<b>121</b>
8.1	Mathematical Formulation . . . . .	122
8.2	Solution Procedure . . . . .	126
8.3	Convergence of Solution . . . . .	127
8.4	Discussion of Results . . . . .	128
<b>9</b>	<b>Thesis Summary and Future Recomendations</b>	<b>139</b>
9.1	Conclusions . . . . .	139
9.2	Future Recomendations . . . . .	141



# Chapter 1

## Introduction

A comprehensive literature survey with motivation and objectives of the present theoretical study is provided in this chapter. Some material and fundamental mathematical relations are given which are helpful in this study. Moreover, solution schemes for the governing equations are also explained here.

### 1.1 Background and Literature Review

In current era of fast-growing technology, the study of non-Newtonian fluid flow has fascinated the scientists due to its numerous applications in the fields of engineering, such as the glass blowing, processing of adhesive tapes, and coating applications often required the flow of non-Newtonian fluids over the rigid surface. Many engineering equipments used the non-Newtonian fluids e.g. for the reduction of friction in oil-pipeline, soldiers suits fill with some non-linear fluids that turn into solid when built hit them, use as a surfactant in large-scale heating and cooling systems, use in the manufacturing of lubricants for vehicles. Despite the Newtonian

fluids whose flow mechanism is described by the simple linear relationship of shear rate and shear stress, the non-Newtonian fluids have complex rheological properties depending on their viscosity behavior as a function of deformation history, shear rate, stress and time, etc. Each non-Newtonian fluid has its own characteristics and thus there is no single mathematical relation that can explain the flow behavior of all non-linear fluids. Therefore, scientists classified the non-Newtonian fluids into three main types: (i) differential type, (ii) integral type and (iii) rate type by defining the mathematical model for each specified non-Newtonian fluid. For the study of non-Newtonian fluids, the term "rheology" is also important which is defined as deformation and flow of matter. The flow of non-Newtonian fluids in various geometries with the various physical assumptions were reported in the studies (see *Refs.* [1 – 4]). The Phan-Thien–Tanner model was employed by Dhinakaran *et al.* [5] to investigate the steady flow of viscoelastic fluid between parallel plates under the influence of electro-osmotic forces. Prasad *et al.* [6] studied the MHD flow of viscoelastic fluid with variable viscosity and heat transport over the stretching sheet. Their analysis revealed that a higher magnitude of Lorentz force decreases the surface temperature gradient and skin friction. Malaspinas *et al.* [7] utilized the Lattice Boltzmann method to simulate linear and non-linear viscoelastic fluids. Siddiqa *et al.* [8] numerically examined the free convection flow of non-Newtonian fluid over a vertical surface. In the recent studies of non-Newtonian fluid, the non-axisymmetric Homann flow problem for the viscoelastic fluid over a fixed plate was investigated numerically by Mahapatra *et al.* [9]. Dimensionless velocities and displacement thickness were analyzed for different values of the viscoelastic parameter in their study.

In non-linear fluids, the viscoelastic fluids are those which exhibit both the elastic and viscous effects and in addition these fluids the stress-strain relationship depends on time. Two

major phenomena are observed in the viscoelastic fluids, one of which is stress relaxation and the other is a creep. Thus, researchers have proposed the two mathematical models for this type of fluids which are the Maxwell model and the kelvin Voigt model. The Maxwell fluid model is the simplest model for linear viscoelastic type material which describes the phenomenon of stress relaxation. On the other hand, the Kelvin Voigt model predicts the creep phenomenon, but this model is poor for stress relaxation. Most of the materials found in industries are encountered with the flow viscoelastic fluids under stress relaxation behavior, such as the process of manufacturing plastic, paints, polymers, and rubber sheets. On the other hand, there are some limitations of the present Maxwell fluid model. This model only predicts the stress relaxation phenomenon in the viscoelastic fluid and the model is poor for the prediction of creep phenomenon. Moreover, the shear thinning and shear thickening features can not be described by this model. Attention has been paid by researchers to study the rheology of Maxwell fluid flow subject to various physical effects. Wenchang *et al.* [10] reported the investigation on an unsteady flow of Maxwell fluid between parallel plates. The Laplace and Fourier transforms were used for solution of the problem. Nadeem *et al.* [11] numerically studied the flow of Maxwell fluid induced by stretchable sheet in the presence of the magnetic field. They revealed that the higher values of the relaxation time parameter decline the flow velocity and enhance the temperature distribution. Falkner–Skan flow of MHD Maxwell fluid was studied by Abbasbandy *et al.* [12]. In this study, both the analytical and numerical solutions were presented. In a recent investigation, Ahmed *et al.* [13] studied the swirling flow of Maxwell between two coaxially rotating disks. Their results explored that for higher Reynolds number, the pressure field drop near the surface of the lower disk. Rauf *et al.* [14] examined the multi-layer flows of immiscible fractional Maxwell fluids. They obtained the analytical solution of the problem with the help of

Laplace transform coupled with the Hankel and Weber transforms of order zero. It was shown that due to increment in the fractional parameter the flow velocity decreases.

In the subject of fluid dynamics, the flow induced by stretching and rotating surfaces attract the researchers to investigate its characteristics due to its diverse applications in engineering mechanism such as wire drawing, glass fiber, hot rolling, paper production, etc. In a wide range of applications, from shafts and axles to spinning projectiles, flow over rotating cylinders is also critically important. Crane [15] was the first who inspected the flow induced by a stretching cylinder. In 1984, Wang [16] performed the analysis of 3D flow of viscous fluid caused by a stretching sheet. In this investigation, he introduced the flow ansatz for the conversion of governing PDEs into similar ODEs. Moreover, an asymptotic analysis for small values of stretching strength parameter was also done. Afterward, many researchers investigated the flow phenomenon over stretching surfaces (*see Refs.*[17 – 19]). Fang and Yao [20] studied the flow of a Newtonian fluid due to stretchable rotating cylinder with the assumption of axisymmetry. They considered the rotation of cylinder to be constant because a constant rotation of the cylinder does not induce secondary axial flow. Sprague and Weidman [21] investigated the flow of Newtonian fluid caused by a purely rotating solid cylinder. Subhashini *et al.* [22] found dual solutions for the flow over a stretching sheet with thermal diffusivity. Numerical investigation of MHD boundary layer flow of viscous fluid over an exponentially stretchable sheet was explored by Mukhopadhyay [23]. An analytical study performed by Dandapat *et al.* [24] on the unsteady thin film flow of bi-viscosity fluid over a stretching sheet. Their solution revealed that in comparison of Newtonian and the thin film is faster for bi-viscosity. Ahmed *et al.* [25] carried out the numerical investigation on the thin film flow of Maxwell nanofluid over a rotating disk in an unsteady state. The outcomes of this study show that for higher values of magnetic

parameter the film thickness reduces. In recent studies, the flow of Casson fluid over a swirling cylinder in axisymmetry and energy transport was analyzed by Javed *et al.* [26]. The viscous fluid impinging radially on the swirling cylinder was examined by Weidman [27].

Now a days, researchers paid too much attention to the analysis of heat and mass transfer due to their plenteous applications in the field of engineering and industrial appliances such as cooling process in nuclear reactor, heat exchanger, manufacturing of plastic and polymer. Moreover, understanding the mechanism of heat and solutal energy transport in the flow of fluid over a stretched surface is also decisive because the quality of the product in the extrusion process mainly depends on it. Thus, the scientists explore new ideas for the investigation of these phenomena and discussed them deeply. Fourier's and Fick's laws are the basic fundamental mathematical relations that are used to describe the mechanism of the transport of heat and mass in a given medium due to temperature and concentration difference, respectively. Fourier's law leads to the equation of parabolic type for the temperature distribution which means heat transport has infinite speed and propagate throughout the medium with initial disturbance. To resolve this heat transport paradox the Fourier's law needs some modifications. Many attempts have taken to clear up this paradox but not at all have been successful. Cattaneo [28] modified Fourier's approach by introducing a relaxation time parameter multiply with the time derivative of heat flux which yields to the hyperbolic type equation for heat transport phenomenon and as result, transport of heat has finite speed in the entire medium. This new model is termed as Maxwell-Cattaneo (MC) model. Due to the frame invariance property Christov [29] amend the MC model by replacing the time derivative to upper-convective time derivative which includes the higher spatial gradients. Yousif *et al.* [30] numerically studied the momentum and heat transport by using Fourier's law in the flow of Carreau nanofluid under the impact of magnetic

field and internal sink/source. Sarafraz *et al.* [31] examined the characteristics of heat transport by employing Fourier's approach of heat conduction in the process of pool boiling in the presence of the constant magnetic field.

Recently, scientists explored the heat and mass transport phenomena by using the Cattaneo-Christov double diffusion theory for the flow of both Newtonian and non-Newtonian fluids in different geometries. Han *et al.* [32] studied the flow of viscoelastic fluid with thermal energy transport in view of non-Fourier's approach. They presented the graphical outcomes for thermal and concentration fields. Energy transport in MHD flow of viscous fluid flow with Cattaneo-Christov model over the stretching sheet was explored by Upadhya *et al.* [33]. Cattaneo-Christov double diffusion theory was employed for thermal analysis in the rotating flow of Oldroyd-B fluid over the stretching sheet with variable thermal conductivity by Khan *et al.* [34]. The numerical investigation was performed by Ibrahim [35] on the 3D rotating flow of Powell-Eyring fluid and heat transfer with the help of non-Fourier's law. Farooq *et al.* [36] analyzed the Cattaneo-Christov model for the thermal energy transport in the flow of viscous fluid with temperature-dependent thermal conductivity and mass diffusivity. Their results revealed that both thermal and concentration distributions decline due to large thermal and mass relaxation time parameters, respectively. Alamri *et al.* [37] investigated the flow of second-grade fluid with heat transport over a stretching cylinder with the perspective of Cattaneo-Christov heat flux model. Furthermore, numerous investigations have been performed for the analysis of Fourier's and Cattaneo-Christov approaches for the heat and solutal energy transport in the flow of various types of fluids (*see Refs.*[38 – 47]).

Heat transfer enhancement is a crucial task for scientists in both conduction and convection modes of heat transport. The old technique which was used to remove the heat from the high



flux area was the fins. For example, removing heat from the high heat flux area around the chips becomes an important factor in the design of a reliable computer system. The higher transport of heat in the plastic extrusion process also makes the quality of the product better. Recently, nanofluid is a remarkable approach in the subject of fluid dynamics for the enhancement of convective transport of thermal energy in fluid flow. There are many applications for nanofluids such as the use of nanofluids in a heat exchanger for energy saving, solar collector, etc. Numerous studies on thermophysical properties as well as the heat and fluid flow characteristics of nanofluids have been carried out in different systems to discover their advantages over typical working fluids. Huminic *et al.* [48] provided a review on applications of nanofluids in various types of heat exchangers such as plate heat exchangers, shell and tube heat exchangers, compact heat exchangers. This study focused on the analysis of published results of theoretical and experimental investigation.

Nanofluids, as a new type of liquid/solid suspension, could not only greatly improve the solutal and thermal conductivity of bulk liquids, but also improve the stability and flexibility of the suspension compared to conventional liquid/solid compounds. While in the exploration of advanced cooling technology in 1995, Choi [49] first introduced the concept of nanofluids. The Buongiorno model [50] for nanofluids measures the distribution of nanoparticles through the fluid flow more realistically by defining the Brownian diffusion and thermophoresis slip mechanisms. This model has been extensively used by researchers to study the thermal conduction enhancement of conventional fluids. Nanofluid research has been significantly increased worldwide in the development of highly efficient cooling devices and enhanced heat transfer technology, especially in the past two decades. Sulochan *et al.* [51] reported the numerical study of MHD boundary layer flow of nanofluids with the impact of Joule heating and radiative

source over moving needle. Turkyilmazoglu [52] applied the Buongiorno model to investigate the laminar fully developed flow of nanofluid within the asymmetric channel with the impact of zero net particle flux at the walls. Rostami *et al.* [53] presented the multiple solutions of mixed convection stagnation point flow of hybrid nanofluid, in assisting and opposing mode, over a vertical sheet. In this study, the heat transfer rate of nanofluids and hybrid nanofluids with different values of the volume fraction of nanoparticles was compared and it was noted that HNF3 ( $\phi_{SiO_2} = \phi_{Al_2O_3} = 0.1$ ) having the highest heat transfer rate in all cases. Ahmadi *et al.* [54] conducted theoretical and experimental studies on the thermal conduction of the nanofluids and investigated results reveal that an increase in thermal and concentration conduction of nanoparticles boost up the conductivity of nanofluids. Recently, Yang *et al.* [55] investigated the combined heat and solutal energy transport application of nanofluids as well as fields of photocatalysis and sterilization in air purification. The different forced convection mechanisms for the flow of nanofluid, hybrid nanofluid and their uses in the field of engineering for the heat transfer enhancement can be found in the following studies (see *Refs.* [56 – 60]). The haphazard motion and thermo-migration of nanoparticles in the flow of nanofluids is also critically important. The large and small value of thermophoretic and Brownian forces significantly affected the temperature and concentration distribution in the flow. Much theoretical analysis is reported to the thermophoresis and Brownian motion of nanoparticles. Wakif *et al.* [61] and Animasaun *et al.* [62] presented a detailed analysis on the thermo-migration and haphazard motion of nanoparticles in different fluid models, respectively. The outcomes of the whole analysis indicated that the large values of Brownian motion and thermophoretic force enhance the thermo-migration and haphazard motion of nanoparticles, respectively. Thus, as a result, the temperature distribution increased in fluid flow. Moreover, a higher rate of heat

transport can be obtained due to Brownian motion in the presence of thermal radiation and convective heat and mass transfer in the wall 3D flow.

Mixed convective flow, in both classes of fluids (Newtonian and non-Newtonian fluids), is an important topic for researchers and scientists currently for the enhancement of thermal energy transport rate. Both external and internal flow systems in many engineering processes deal with the MHD mixed convection flow e.g., cooling of nuclear reactors, cooling of electronic equipment and energy conversion in nuclear reactors. Moreover, the working of the DCLL (Dual-Coolant Lead-Lithium) blanket uses the concept of mixed convection. The well-known Boussinesq approximation is used to investigate the effect of buoyancy force on heat transport in mixed convection, which is in either an aiding or an opposing mode in the direction of forced convection, regardless of whether the fluid flow is laminar or turbulent. Buoyancy-driven flow over a vertical sheet in opposing/aiding modes was reported by Cheng *et al.* [63]. Correlation for the mixed convective flow of a nanofluid in the horizontal pipe for a very large Prandtl number was found by Li *et al.* [64] in an experimental study. Hayat *et al.* [65] performed an analytical computation to study the mixed convective flow of Sisko nanofluid. Their findings revealed that large values of the buoyancy parameter reduce the temperature distribution, while the solutal field showed the opposite trend.

## 1.2 Motivation and Research Objectives

An extensive literature survey for non-Newtonian viscoelastic fluids flow with energy transport phenomenon in the previous section proved that the flow analysis of various non-Newtonian fluids with heat and mass transport by considering different physical aspects shows an increasing

interest of researchers up till now. Most of the investigations have been devoted to exploring this area of research. Based on works that were so far reported in the literature, some gaps have been identified in the study of the flow field of non-Newtonian viscoelastic Maxwell fluid with energy transport induced by stretching and rotating surfaces geometry. Furthermore, this area of research is perhaps not focused extensively and properly. Thus, there is huge space to explore the rheological properties of Maxwell fluid flow induced by stretching and rotating surfaces. Therefore, the primary objective of this thesis is to find the analytical and numerical solutions of these highly non-linear phenomena such that we can deeply predict the rheological characteristics of viscoelastic Maxwell fluid and transportation of thermal energy. The physical considerations in this study are relevant to a number of applications that involve polymers, plastic extrusion, rotating machinery, gas turbine rotors, centrifugal pumps, the cooling system in electronic devices, and many more. Accordingly, in this study, we emphasize these matters and try to fill up the gaps in this field. Thus, the key objectives of the present theoretical investigation are the following:

- Flow phenomenon of Maxwell nanofluid over stretching and rotating surfaces is modeled in form of governing partial differential equations and these equations are then transformed into similar ordinary differential equations with the help of suitable flow ansatz.
- Transport mechanisms of heat and solutal energy in flow are examined with various physical effects such as thermal radiation, Joule heating, chemical reaction and heat source in the system.
- Flow structure of viscoelastic Maxwell fluid with energy transport is assessed with the help of analytical and numerical solutions of the governing equations and results are presented

graphically. A comprehensive physical justification of each outcome is provided. Besides, results validation in good agreement with published literature is shown.

## 1.3 Fundamental and Constitutive Relations (Laws) of Continuum Mechanics

### 1.3.1 Fundamental Relations

There are some fundamental laws in the continuum mechanics which are always true. These include the law of conservation of mass, momentum and energy. For laminar and incompressible fluid flow the mathematical expressions are:

*Mass balance:*

$$\frac{\partial \rho}{\partial t} + \nabla \cdot (\rho \mathbf{V}) = 0, \quad (1.1)$$

*Momentum balance:*

$$\rho \frac{d\mathbf{V}}{dt} = \nabla \cdot \hat{\boldsymbol{\sigma}} + \rho \hat{\mathbf{b}}, \quad (1.2)$$

*Energy balances:*

$$\rho c_p \frac{dT}{dt} = -\nabla \cdot \hat{\mathbf{q}}, \quad (1.3)$$

$$\frac{dC}{dt} = -\nabla \cdot \hat{\mathbf{J}}. \quad (1.4)$$

In the above relations,  $\rho$  is the fluid density,  $\mathbf{V}$  the velocity field vector,  $\nabla$  the vector differential operator,  $\frac{d}{dt}$  the material derivative,  $\hat{\boldsymbol{\sigma}}$  the Cauchy stress tensor,  $\hat{\mathbf{b}}$  the body force,  $c_p$  heat capacity of fluid at constant pressure,  $(\hat{\mathbf{q}}, \hat{\mathbf{J}})$  heat and solutal fluxes, respectively,  $(T, C)$  denote temperature and concentration, respectively,  $\hat{\boldsymbol{\sigma}}$  can be break down as  $\hat{\boldsymbol{\sigma}} = -p\mathbf{I} + \mathbf{S}$  with  $p$  as

the fluid pressure,  $\mathbf{I}$  the identity tensor and  $\mathbf{S}$  the extra stress tensor. Moreover, the deformation of non-Newtonian fluid is related to  $\mathbf{S}$  and this is defined by the specific mathematical relation for a particular non-Newtonian fluid model.

In case of magnetohydrodynamic (MHD) and buoyancy driven flow Eq. (1.2) is modified as

$$\rho \frac{d\mathbf{V}}{dt} = -\nabla p + \nabla \cdot \mathbf{S} + \mathbf{J}_1 \times \mathbf{B} + \rho g [B_T(T - T_\infty) + B_C(C - C_\infty)]. \quad (1.5)$$

Here  $\mathbf{J}_1 = \sigma(\mathbf{V} \times \mathbf{B})$  the current density,  $\sigma$  the electric conductivity of fluid,  $\mathbf{B}$  applied magnetic field and  $(T_\infty, C_\infty)$  temperature and concentration of quiescent fluid at infinity, respectively and the last term in above equation is the result from Boussinesq approximation for buoyancy force in the system where  $(B_T, B_C)$  are the thermal and solutal volumetric expansion coefficients.

### Modification of Energy Equations for Nanofluids

According to Buongiorno [50], the contribution of thermophoresis and Brownian diffusion slips phenomena enhance the convective energy transportation in nanofluids. Therefore, the energy Eqs. (1.3) and (1.4) are transformed by adding these two forces as:

$$\frac{dT}{dt} + \frac{1}{\rho c_p} \nabla \cdot \hat{\mathbf{q}} = \tau \left[ D_B \nabla C \cdot \nabla T + \frac{D_T}{T_\infty} (\nabla T \cdot \nabla T) \right], \quad (1.6)$$

$$\frac{dC}{dt} + \nabla \cdot \hat{\mathbf{J}} = \frac{D_T}{T_\infty} (\nabla \cdot \nabla T). \quad (1.7)$$

In the above equations,  $D_B$  is the coefficient of Brownian diffusion,  $D_T$  the coefficient of thermophoresis and  $\tau$  the heat capacity ratio of nanoparticles to the base fluid.



### 1.3.2 Constitutive Relations

There are also some other mathematical relations that are true considerably and proposed empirically from the properties of matter. Such relations are called constitutive laws. Also, these laws are completely based on observations. Some of the relevant laws to the present study are described below:

#### Fourier's and Fick's Laws

The thermal and solutal energy conduction in the fluid is done by the following mathematical expressions:

$$\hat{\mathbf{q}} = -k\nabla T, \quad (1.8)$$

$$\hat{\mathbf{J}} = -D_B\nabla C, \quad (1.9)$$

where  $k$  denotes the thermal conductivity of fluid.

#### Cattaneo-Christove Theory

As mentioned before the Fourier's approach for heat conduction is not realistic and violates the principle of causality. Therefore, Cattaneo-Christove [28, 29] modified the mathematical relations of Fourier's and Fick's for heat and mass fluxes, respectively, by introducing the relaxation time with upper convective derivative as:

$$\hat{\mathbf{q}} + \lambda_t \frac{D\hat{\mathbf{q}}}{Dt} = -k\nabla T, \quad (1.10)$$

$$\hat{\mathbf{J}} + \lambda_c \frac{D\hat{\mathbf{J}}}{Dt} = -D_B\nabla C, \quad (1.11)$$

where  $(\lambda_t, \lambda_c)$  are the thermal and solutal relaxation times, respectively.

### Maxwell Fluid Model

The phenomena of stress relaxation and creep are observed in the viscoelastic materials, thus, in such materials the Maxwell fluid model, which is key part of this study, is good to predict stress relaxation phenomenon. This model is also empirical and observational based. The constitutive relation for this model is defined as:

$$\left(1 + \lambda_1 \frac{D}{Dt}\right) \mathbf{S} = \mu \mathbf{A}_1, \quad (1.12)$$

where  $\lambda_1$  is the relaxation time,  $\mu$  the dynamic viscosity,  $\frac{D}{Dt}$  the upper convective time derivative and  $\mathbf{A}_1 = \nabla \mathbf{V} + \nabla \mathbf{V}^T$  the first Rivlin–Ericksen tensor.

## 1.4 Methods of Computation

In order to compute the solutions of highly non-linear similar ordinary differential equations which arised in the present theoretical analysis of Maxwell nanofluid flow with energy transport phenomenon, under the influence of different physical factors such as magnetic field, a force of buoyancy and Joule heating, produced by stretching and rotating surfaces both semi-analytical and numerical techniques are employed. These methods include the homotopy analysis method and bvp4c approach. A brief introduction to the working of these methods is presented in this section.

### 1.4.1 Homotopy Analysis Method (HAM)

In 1992 Liao [66] proposed the semi-analytical technique to obtain the series solution of the highly non-linear differential equations which is called the homotopy analysis method (HAM). The concept of homotopy is purely topological on which this method is based. It provides the continuous deformation of the initial approximation to the desired solution of the given problem. The homotopy function is defined as  $\tilde{H} : \hat{\mathbf{X}} \times [0,1] \longrightarrow \hat{\mathbf{Y}}$  such that  $\tilde{H}(\hat{\mathbf{x}},0) = \psi_{\circ}(\hat{\mathbf{x}})$  and  $\tilde{H}(\hat{\mathbf{x}},1) = \psi(\hat{\mathbf{x}})$  with  $\hat{\mathbf{x}} \in \hat{\mathbf{X}}$  where  $\psi_{\circ}(\hat{\mathbf{x}})$  and  $\psi(\hat{\mathbf{x}})$  two continuous deformable functions defined on topological space  $\hat{\mathbf{X}}$  and  $\hat{\mathbf{Y}}$ . The method is preferable over the other conventional analytical methods such as the perturbation technique because it is independent of the small/large parameters. Moreover, it provides the assurance of convergence for highly non-linear problems.

Consider the non-linear differential equation

$$\hat{A}[s(\xi)] = 0, \quad (1.13)$$

where  $\hat{A}$  is the non-linear operator and  $s$  the unknown function. Suppose  $s_{\circ}(\xi)$  is the initial approximation of  $s(\xi)$  and  $\hat{L}$  the auxiliary linear operator.

By introducing the non-zero auxiliary linear parameter  $\hbar$  the homotopy is constructed as the zeroth order deformation equation

$$(1 - \kappa)\hat{L}[\hat{s}(\xi, \kappa) - s_{\circ}(\xi)] = \kappa\hbar\hat{A}[s(\xi)], \quad (1.14)$$

where  $\kappa \in [0, 1]$  is the embedding parameter, when  $\kappa = 0$  and  $\kappa = 1$  we get

$$\hat{s}(\xi, 0) = s_{\circ}(\xi) \text{ and } \hat{s}(\xi, 1) = s(\xi), \quad (1.15)$$

The variation of  $\hat{s}(\xi, \kappa)$  from  $s_o(\xi)$  to  $s(\xi)$  as  $\kappa$  varies from 0 to 1 is called continuous deformation.

This is the basic concept of HAM and  $\hat{s}(\xi, \kappa)$  can be represented as Taylor series expansion

$$\hat{s}(\xi, \kappa) = s_o(\xi) + \sum_{m=1}^{\infty} s_m(\xi) \kappa^m, \quad s_m = \frac{1}{m!} \frac{\partial^m \hat{s}(\xi, \kappa)}{\partial \kappa^m}. \quad (1.16)$$

The above series is convergent at  $\kappa = 1$ . The  $m$ th order deformation equation is defined as:

$$\hat{L}[s_m(\xi) - \varkappa_m s_{m-1}(\xi)] = \hbar \check{R}_m(s_{m-1}), \quad (1.17)$$

with

$$\check{R}_m(s_{m-1}) = \frac{1}{(m-1)!} \left. \frac{\partial^{m-1} \hat{s}(\xi, \kappa)}{\partial \kappa^{m-1}} \right|_{\kappa=0}, \quad \varkappa_m = 0, \quad m \leq 1 \text{ and } \varkappa_m = 0, \quad m > 1. \quad (1.18)$$

The above whole computation is performed with the help of Mathematica software.

### 1.4.2 Bvp4c (Numerical Method)

The bvp4c is a Runge-Kutta method that employs the Lobatto IIIa formula in three phases.

The Simpson's quadrature rule is used in well-known Lobatto methods. On the given interval,

this is a collocation method, and the collocation polynomial provides a C1-continuous solution

with fourth order accuracy. The mesh and error control are highly dependent on the solution's

residual in this method. To utilize the bvp4c for the solution of given non-linear boundary

value problem the first step is to reduce the higher order differential equation into the system

of first order equations.

## 1.5 Thesis Structure

The presented work is an outcome of the numerical and analytical study in which we have analyzed the various aspects of incompressible viscoelastic Maxwell fluid flow generated due to different stretching and rotating geometries, namely the rheology of Maxwell fluid flow, buoyant fluid motion and impact of magnetic field. Moreover, the convective transportation of thermal energy, role of Brownian motion and thermophoresis slip mechanism of nanofluids in heat transport with a number of physical effects are also studied. All the published material produced in this thesis is specified clearly in this section with a brief description of each chapter as follows:

**Chapter 1:** In this chapter, a relevant literature survey to present work with motivation is presented. The objectives of the thesis are also mentioned here. The conservation laws and some particular material relations of continuum mechanics for current study are given. In addition, solution methodologies used in the mathematical analysis are discussed concisely.

**Chapter 2:** This chapter presents the thermal and solutal energy transport analysis via Cattaneo-Christov theory in the flow of Maxwell nanoliquid. The flow is a 3D, laminar, steady and incompressible and generated by a vertical bilateral stretching sheet. The transport mechanism of energy is considered as both forced and free convective. The semi-analytical technique namely the homotopy analysis method is used to acquire the solutions of similar ordinary differential equations of the considered physical problem. The outcomes of this chapter are published in "**Proceedings of the Institution of Mechanical Engineers, Part C: Journal of Mechanical Engineering Science, (2020) DOI: 10.1177/0954406220973242**".

**Chapter 3:** The unsteady stagnation point flow of a Maxwell nanofluid due to radially stretchable disk is scrutinized in this chapter. The heat and mass transfer analysis is performed

under the impact of Joule heating, heat source, magnetic field and chemical reaction. The Brownian motion and thermophoresis phenomena of nanofluid are investigated with help of the Buongiorno model. The surface temperature of the disk is taken as constant and radially varying. The outcomes of the problem are computed numerically and discussed briefly with appropriate physical justification for each pertinent parameter. The results of this chapter are published in "**Arabian Journal for Science and Engineering, 45 (2020) 5529–5540**".

**Chapter 4:** In this chapter, an analysis of Cattaneo-Christov double diffusion theory for thermal and solutal energy transfer in unsteady, axisymmetric and laminar flow of Maxwell fluid induced by stretching cylinder is carried out. The thermal conductivity of Maxwell fluid is assumed as temperature-dependent. A system of non-linear ordinary differential equations is found by using the suitable group of flow similarities into the partial differential equations which governs the physical problem. The results for flow mechanism, thermal and solutal distributions are acquired numerically. Moreover, a graphical illustration of outcomes with physical reasoning is provided via each pertinent parameter. The work furnished in this chapter is published in "**Journal of Thermal Analysis and Calorimetry, (2020) DOI: 10.1007/s10973-020-09343-1**".

**Chapter 5:** This chapter explores the thermal characteristics of buoyancy-driven unsteady stagnation flow of viscoelastic Maxwell liquid over a vertical cylinder executing stretching under the impact of a magnetic field which is applied normally to the flow field. The non-Fourier's approach is utilized to study the thermal energy transport mechanism rather than classical Fourier's law. Numerical scheme `bvp4c` is applied to find the solution of governing equations for this problem. The impact of velocity ratio parameter, thermal and solutal relaxation phenomena, unsteadiness parameter and magnetic field on temperature distribution is reported



in the graphical abstract. Furthermore, the variation in heat transport rate subject to constant and axially varying surface temperature of cylinder is also provided through graphs. This chapter is an extension of chapter 4. The findings of this chapter are published in "**Arabian Journal for Science and Engineering, 45 (2020) 9439–9447**".

**Chapter 6:** The theoretical analysis in this chapter is made to determine the rheology of Maxwell fluid over a stretchable rotating cylinder in the presence of magnetic field. The rotation of the cylinder is taken as constant. Additionally, the transport mechanism of thermal and solutal energy also part of this study. The problem is modeled in form of PDEs with the assumptions of steady, laminar and axisymmetric and the flow field of Maxwell fluid with energy distribution is found as numerical solutions of similar ODEs. The problem is governed by various physical parameters such as Reynolds number, magnetic parameter, relaxation time parameter etc. This study is the new contribution in the literature of rheology of non-Newtonian fluids. The outcomes of this chapter have been published in "**Applied Mathematics and Mechanics, 41 (2020) 667–680**".

**Chapter 7:** This chapter is proposed as an extension of chapter 6 for the thermal analysis in a broad context. The heat and mass transportation are investigated in the swirling flow of Maxwell nanofluid with the addition of different heat transport enhancement physical factors such as Joule heating, thermal radiation, heat constraint and thermophoresis. Moreover, the heat transport from the surface to fluid is assumed as convective. The impact of all these factors is examined through numerical outcomes of governing equations in graphical presentation. The work furnished in this chapter is published in "**Applied Mathematics and Mechanics, 41 (2020) 1417–1430**".

**Chapter 8:** In this chapter, an investigation of the heat transport mechanism in the well-

known Von Kármán flow of Maxwell nanofluid is performed. Here the Cattaneo-Christov theory and Buongiorno model for nanofluid are jointly applied for thermal analysis in flow phenomenon. The impact of the magnetic field, heat source and chemical reaction on thermal and solutal energy transport are also studied. Von Kármán flow ansatz are employed to transform the governing PDEs into non-linear ODEs. Series solutions of governing equations are developed as function of physical parameters with help of the homotopy analysis method (HAM) and presented graphically. The findings of this chapter are published in "**Applied Mathematics and Mechanics, 41 (2020) 1195–1208**".

**Chapter 9:** Finally, the work of thesis is accomplished in chapter-9 with the summary of the study, conclusions and some recommendations for future work.

## Chapter 2

# Mixed Convective Flow of Maxwell Nanofluid over a Stretching Sheet

This chapter invokes the thermal and solutal analysis in the buoyancy driven three dimensional flow of Maxwell nanofluid subject to Cattaneo-Christov theory. The flow of non-Newtonian fluid is induced above the vertical bi-directional stretching sheet. The slip mechanisms of Brownian diffusion and thermophoresis of nanoparticles in the flow of Maxwell liquid are analyzed with the help of the Buongiorno model for nanofluid. The suitable ansatz for flow phenomenon is employed to reduce the governing boundary layer partial differential equations (PDEs) into the non-linear ordinary differential equations (ODEs). Moreover, the homotopic approach is utilized for the solution of the governing ODEs to investigate the flow of Maxwell fluid along with energy transport mechanism. The outcomes are presented graphically and discussed the physical reasoning behind them. The analysis revealed that both buoyancy and mixed convection parameters enhanced  $x$ -component of the velocity field but declined  $y$ -component. Additionally, these two parameters are also increased the thermal and solutal energy

transport in nanofluid for assisting buoyant motion. It is observed that the thermophoretic force boosts up the thermal energy transportation in the flow in the presence of the thermal relaxation phenomenon.

The present results are confirmed through tabular data with some previous studies.

## 2.1 Problem Formulation

Consider an incompressible, laminar flow of viscoelastic Maxwell nanofluid generated by vertical elastic bi-directional stretching sheet as shown in **Fig. 2.1**. The velocity field of the problem is assumed as  $\mathbf{V} = [u, v, w]$  and Cartesian coordinates  $(x, y, z)$  are taken in such way that the velocities of the fluid particles on the surface of sheet are  $u = ax$ ,  $v = by$  and  $w = 0$ , respectively, where  $a$  and  $b$  are positive constants. As sheet is vertical hence the force of gravity  $\mathbf{g} = [g, 0, 0]$  is taken along  $x$  - axis. Thus, the dynamics of the Maxwell nanofluid flow with the help of basic laws of conservation given in Eqs. (1.1) and (1.5) (cf. Chapter 1) with mathematical relation for Maxwell model (see Eq. (1.12)) is expressed in the form of following boundary layer

partial differential equations (PDEs)

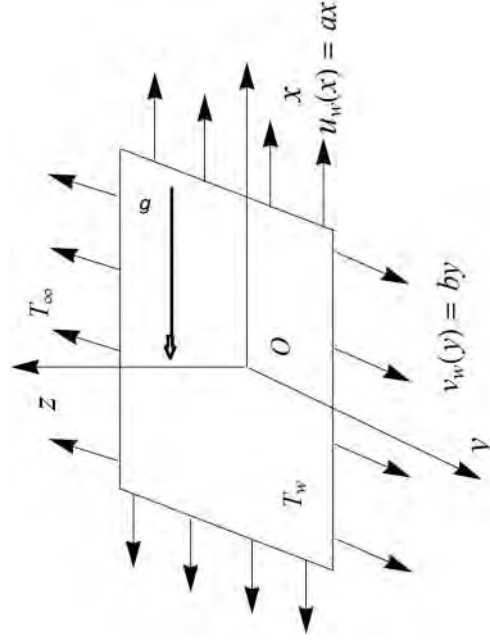


**Figure 2.1:** Flow configuration.

$$\frac{\partial u}{\partial x} + \frac{\partial v}{\partial y} + \frac{\partial w}{\partial z} = 0, \quad (2.1)$$

$$\begin{aligned} & u \frac{\partial u}{\partial x} + v \frac{\partial u}{\partial y} + w \frac{\partial u}{\partial z} = \nu \left[ \frac{\partial^2 u}{\partial z^2} \right] \\ & -\lambda_1 \left[ u^2 \frac{\partial^2 u}{\partial x^2} + v^2 \frac{\partial^2 u}{\partial y^2} + w^2 \frac{\partial^2 u}{\partial z^2} + 2uv \frac{\partial^2 u}{\partial x \partial y} + 2vw \frac{\partial^2 u}{\partial y \partial z} + 2uw \frac{\partial^2 u}{\partial x \partial z} \right] \\ & + g[B_T(T - T_\infty) + B_C(C - C_\infty)] + \lambda_1 g B_T \left( u \frac{\partial T}{\partial x} + v \frac{\partial T}{\partial y} + w \frac{\partial T}{\partial z} - (T - T_\infty) \frac{\partial u}{\partial x} \right) \\ & + \lambda_1 g B_C \left( u \frac{\partial C}{\partial x} + v \frac{\partial C}{\partial y} + w \frac{\partial C}{\partial z} - (C - C_\infty) \frac{\partial u}{\partial x} \right), \end{aligned} \quad (2.2)$$

$$\begin{aligned}
& u \frac{\partial v}{\partial x} + v \frac{\partial v}{\partial y} + w \frac{\partial v}{\partial z} = \nu \left[ \frac{\partial^2 v}{\partial z^2} \right] \\
& -\lambda_1 \left[ u^2 \frac{\partial^2 v}{\partial x^2} + v^2 \frac{\partial^2 v}{\partial y^2} + w^2 \frac{\partial^2 v}{\partial z^2} + 2uv \frac{\partial^2 v}{\partial x \partial y} + 2vw \frac{\partial^2 v}{\partial y \partial z} + 2uw \frac{\partial^2 v}{\partial x \partial z} \right]. \quad (2.3)
\end{aligned}$$

Moreover, for the phenomena of thermal and soluatl energy transport in viscoelastic Maxwell nanofluid the following PDEs are obtained by using Eqs. (1.6, 1.7) and Eqs. (1.10, 1.11) (cf. Chapter 1)

$$\begin{aligned}
& u \frac{\partial T}{\partial x} + v \frac{\partial T}{\partial y} + w \frac{\partial T}{\partial z} - \tau \left[ D_B \left( \frac{\partial C}{\partial z} \frac{\partial T}{\partial z} \right) + \frac{D_T}{T_\infty} \left( \frac{\partial T}{\partial z} \right)^2 \right] \\
& + \lambda_t \left[ u^2 \frac{\partial^2 T}{\partial x^2} + v^2 \frac{\partial^2 T}{\partial y^2} + w^2 \frac{\partial^2 T}{\partial z^2} + 2uv \frac{\partial^2 T}{\partial x \partial y} + 2vw \frac{\partial^2 T}{\partial y \partial z} + 2uw \frac{\partial^2 T}{\partial x \partial z} + u \frac{\partial u}{\partial x} \frac{\partial T}{\partial x} + u \frac{\partial v}{\partial x} \frac{\partial T}{\partial y} \right. \\
& \quad \left. + u \frac{\partial w}{\partial x} \frac{\partial T}{\partial z} + v \frac{\partial u}{\partial y} \frac{\partial T}{\partial x} + v \frac{\partial v}{\partial y} \frac{\partial T}{\partial y} + v \frac{\partial w}{\partial y} \frac{\partial T}{\partial z} + w \frac{\partial u}{\partial z} \frac{\partial T}{\partial x} + w \frac{\partial v}{\partial z} \frac{\partial T}{\partial y} + w \frac{\partial w}{\partial z} \frac{\partial T}{\partial z} \right] \\
& - \lambda_t \tau D_B \left[ u \frac{\partial^2 C}{\partial x \partial z} \frac{\partial T}{\partial z} + u \frac{\partial C}{\partial z} \frac{\partial^2 T}{\partial x \partial z} + v \frac{\partial^2 C}{\partial y \partial z} \frac{\partial T}{\partial z} + v \frac{\partial C}{\partial z} \frac{\partial^2 T}{\partial y \partial z} + w \frac{\partial^2 C}{\partial z^2} \frac{\partial T}{\partial z} + w \frac{\partial C}{\partial z} \frac{\partial^2 T}{\partial z^2} \right] \\
& - 2\lambda_t \tau \frac{D_T}{T_\infty} \left[ u \frac{\partial T}{\partial z} \frac{\partial^2 T}{\partial x \partial z} + v \frac{\partial T}{\partial z} \frac{\partial^2 T}{\partial y \partial z} + w \frac{\partial T}{\partial z} \frac{\partial^2 T}{\partial z^2} \right] = \alpha_1 \left[ \frac{\partial^2 T}{\partial z^2} \right], \quad (2.4)
\end{aligned}$$

$$\begin{aligned}
& u \frac{\partial C}{\partial x} + v \frac{\partial C}{\partial y} + w \frac{\partial C}{\partial z} + \lambda_c \left[ u^2 \frac{\partial^2 C}{\partial x^2} + v^2 \frac{\partial^2 C}{\partial y^2} + w^2 \frac{\partial^2 C}{\partial z^2} + 2uv \frac{\partial^2 C}{\partial x \partial y} + 2vw \frac{\partial^2 C}{\partial y \partial z} + 2uw \frac{\partial^2 C}{\partial x \partial z} \right. \\
& \quad \left. + u \frac{\partial u}{\partial x} \frac{\partial C}{\partial x} + u \frac{\partial v}{\partial x} \frac{\partial C}{\partial y} + u \frac{\partial w}{\partial x} \frac{\partial C}{\partial z} + v \frac{\partial u}{\partial y} \frac{\partial C}{\partial x} + v \frac{\partial v}{\partial y} \frac{\partial C}{\partial y} \right. \\
& \quad \left. + v \frac{\partial w}{\partial y} \frac{\partial C}{\partial z} + w \frac{\partial u}{\partial z} \frac{\partial C}{\partial x} + w \frac{\partial v}{\partial z} \frac{\partial C}{\partial y} + w \frac{\partial w}{\partial z} \frac{\partial C}{\partial z} \right] \\
& - \lambda_c \frac{D_T}{T_\infty} \left[ u \frac{\partial^3 T}{\partial x \partial z^2} + v \frac{\partial^3 T}{\partial y \partial z^2} + w \frac{\partial^3 T}{\partial z^3} \right] = D_B \left[ \frac{\partial^2 C}{\partial z^2} \right] + \frac{D_T}{T_\infty} \left( \frac{\partial^2 T}{\partial z^2} \right). \quad (2.5)
\end{aligned}$$

The appropriate boundary conditions for the flow and energy transport equations are

$$u = u_w = ax, \quad v = v_w = by, \quad w = 0, \quad T = T_w, \quad C = C_w \quad \text{at} \quad z = 0, \quad (2.6)$$

$$u \rightarrow 0, \quad v \rightarrow 0, \quad T \rightarrow T_\infty, \quad C \rightarrow C_\infty \quad \text{as} \quad z \rightarrow \infty. \quad (2.7)$$

In the above equations,  $\nu$  is the kinematic viscosity,  $(T_w, C_w)$  are the surface temperature and concentration and  $(T_\infty, C_\infty)$  the free stream temperature and concentration,  $\alpha_1 = \frac{k}{\rho c_p}$  the thermal diffusivity of fluid.

### 2.1.1 Similarity Transformation

In the view of flow ansatz used by Wang [16], letting

$$\begin{aligned} u &= axf'(\eta), \quad v = ayg'(\eta), \quad w = -\sqrt{av}(f + g), \quad \eta = z\sqrt{\frac{a}{\nu}} \\ \phi(\eta) &= \frac{C - C_\infty}{C_w - C_\infty}, \quad \theta(\eta) = \frac{T - T_\infty}{T_w - T_\infty}, \end{aligned} \quad (2.8)$$

Eq. (2.1) is satisfied automatically and Eqs. (2.2 – 2.7) yield

$$\begin{aligned} f''' + (f + g)f'' - f'^2 + \beta_1(2(f + g)f'f'' - (f + g)^2f''') + \lambda(\theta + N_1\phi) \\ - \lambda\beta_1((f + g)\theta' - f'\theta) - \lambda\beta_1N_1((f + g)\phi' - f'\phi) = 0, \end{aligned} \quad (2.9)$$

$$g''' + (f + g)g'' - g'^2 + \beta_1(2(f + g)g'g'' - (f + g)^2g''') = 0, \quad (2.10)$$

$$\begin{aligned} \theta'' + \text{Pr}(f + g)\theta' + \text{Pr}(N_b\theta'\phi' + N_t\theta'^2) - \text{Pr}\beta_t((f + g)(f' + g')\theta' + (f + g)^2\theta'') \\ - \text{Pr}\beta_tN_b((f + g)\theta''\phi' + (f + g)\theta'\phi'') - 2\text{Pr}\beta_tN_t(f + g)\theta'\theta'' = 0, \end{aligned} \quad (2.11)$$

$$\begin{aligned} \phi'' + \text{LePr}(f + g)\phi' + \frac{N_t}{N_b}\text{LePr}\theta'' - \text{LePr}\beta_c((f + g)(f' + g')\phi' + (f + g)^2\phi'') \\ - \text{LePr}\frac{N_t}{N_b}(f + g)\theta''' = 0, \end{aligned} \quad (2.12)$$

with boundary conditions

$$f(0) = 0, \quad g(0) = 0, \quad f'(0) = 1, \quad g'(0) = R, \quad \theta(0) = 1, \quad \phi(0) = 1, \quad (2.13)$$

$$f'(\infty) = 0, \quad g'(\infty) = 0, \quad \theta(\infty) = 0, \quad \phi(\infty) = 0. \quad (2.14)$$

Here  $R (= \frac{b}{a})$  denotes the stretching parameter,  $\beta_1 (= \lambda_1 a)$  the fluid relaxation time parameter,  $\beta_t (= \lambda_t a)$  the thermal relaxation time parameter,  $\beta_c (= \lambda_c a)$  the solutal relaxation time parameter,  $\lambda (= \frac{Gr}{Re_x^2})$  the buoyancy ratio parameter,  $N_1 (= \frac{Gr}{Gr^*})$  the mixed convection parameter,  $Gr (= \frac{gB_T(T_w - T_\infty)x^3}{\nu^2})$  and  $Gr^* (= \frac{gB_C(C_w - C_\infty)x^3}{\nu^2})$  are Grashof numbers for temperature and concentration, respectively,  $Re_x (= \frac{u_w x}{\nu})$  the local Reynolds number,  $N_b (= \frac{\tau D_B(C_w - C_\infty)}{\nu})$  the Brownian diffusion coefficient,  $N_t (= \frac{\tau D_T(T_w - T_\infty)}{\nu T_\infty})$  the thermophoresis parameter,  $Pr (= \frac{\nu}{\alpha_1})$  the Prandtl number and  $Le (= \frac{\alpha_1}{D_B})$  the Lewis number.

## 2.2 Homotopic Solution

In this section the series solutions of governing similar equations for flow and energy transport, given in (2.9 – 2.12) subject to the boundary conditions (2.13) and (2.14), are constructed by means of a well-known technique namely the homotopy analysis method (HAM). In order to construct the homotopic series solution with the help of homotopy approach we choose the following initial guesses  $(f_0, g_0, \theta_0, \phi_0)$  and the auxiliary linear operators  $(\mathcal{L}_f, \mathcal{L}_g, \mathcal{L}_\theta, \mathcal{L}_\phi)$  as

$$f_0(\eta) = 1 - e^{-\eta}, \quad g_0(\eta) = R(1 - e^{-\eta}), \quad \theta_0(\eta) = e^{-\eta}, \quad \phi_0(\eta) = e^{-\eta}, \quad (2.15)$$



$$\begin{aligned}
\mathcal{L}_f[f(\eta)] &= f''' - f', \quad \mathcal{L}_g[g(\eta)] = g''' - g', \\
\mathcal{L}_\theta[\theta(\eta)] &= \theta'' - \theta, \quad \mathcal{L}_\phi[\phi(\eta)] = \phi'' - \phi.
\end{aligned}
\tag{2.16}$$

## 2.3 Results and Discussion

Here in this part of the chapter the outcomes of Maxwell nanofluid flow and energy transport with the effect of embedded physical parameters are explained with physical justification. The main results of the present study are the behavior of the flow field of Maxwell fluid and thermal energy transport with the impact of buoyancy and mixed convection parameters. Moreover, the impact of thermophoresis and Brownian motion parameters on temperature and concentration profile in view of thermal and solutal relaxation phenomena are the novel findings of the present research. In computation process of the results the values of pertinent parameters are fixed as  $R = \lambda = N_1 = \beta_1 = 0.5$ ,  $N_t = N_b = \beta_t = \beta_c = 0.4$  and  $Pr = Le = 6.5$ .

**Figs. 2.2(a, b)** explore that the higher values of stretching strength parameter  $R$  decrease  $f'(\eta)$  and increase  $g'(\eta)$  components of the velocity field. Physically,  $R$  is the ratio of stretching rates in the  $y$ -direction to  $x$ -direction thus, an increase in  $R$ , the  $x$ -component of velocity field declines and  $y$ -component increases. The impact of mixed convection parameter  $N_1$  and buoyancy parameter  $\lambda > 0$  (assisting mode) on the flow field is depicted through **Figs. 2.3(a, b)** and **Figs. 2.4(a, b)**, respectively. It is noted that both parameters enhance the  $x$ -component of the velocity field but decline the  $y$ -component. These results are expected because the buoyancy force due to the thermal gradient in the fluid acts along the  $x$ -axis and normal to the  $y$ -axis. Therefore, this force act as an external driving agent for the fluid motion in  $x$ -direction which means buoyant fluid motion is same as the direction of forced convective motion of the fluid.

However, this is an opposing agent for the  $y$ -component of the velocity field. Moreover, the impact of these two parameters on the thermal and solutal energy transfer is shown in **Figs. 2.5(a, b)** and **Figs. 2.6(a, b)**. These results explored that both temperature and concentration profiles are decreasing due to increasing trends in  $\lambda$  and  $N_1$ . Physically, the buoyancy in the fluid is due to the density gradient which created by thermal gradient and body force, thus, the fixed thermal gradient in the Maxwell nanofluid is used for the buoyant motion of the fluid and as a result, the flow field increases and energy transport decreases.

The phenomenon of stress relaxation in viscoelastic Maxwell nanofluid is described by the dimensionless relaxation time parameter  $\beta_1$ . **Figs. 2.7(a, b)** reveal that the augmentation in  $\beta_1$  significantly enhances both thermal and solutal energy transport in the fluid flow because for the higher trend in  $\beta_1$  the fluid becomes more solid like due to the large magnitude of stress relaxation and conduction of energy increases between fluid particles. The plots in **Figs. 2.8(a, b)** illustrate the behavior of thermal and solutal energy transport in nanofluid flow via thermal relaxation time parameter  $\beta_t$  and solutal relaxation time parameter  $\beta_c$ , respectively. It is observed that in case of higher relaxation time parameters both heat and mass transport decrease. These parameters are the results from the Cattaneo-Christov theory, physically the higher values of  $\beta_t$  and  $\beta_c$  slow down the thermal and solutal energy waves motion in fluid flow. As a result, the transport of heat and mass declines. The haphazard motion and thermomigration of nanoparticles in Maxwell liquid produce the thermophoretic and Brownian forces according to the Buongiorno model. **Figs. 2.9(a, b)** show that the increase in  $N_t$  boosts up the temperature distribution. Physically, thermophoretic force in the nanoliquid increases for higher values of  $N_t$ , consequently, the transfer of heat energy in the flow enhances. The impact of Brownian motion parameter  $N_b$  to the temperature and concentration field is envisioned in

**Figs. 2.10(a, b).** It is found that the temperature field boots up for higher values of  $N_b$  but a converse trend is noted in the case of concentration field. Physically, when  $N_b$  is increased the Brownian force enhances and creates the resistance for the transportation of solutal energy and in result concentration profile declines. In the case of heat transport  $N_b$  enhances the effective heat capacity of the fluid and kinetic energy of fluid particles transformed into thermal energy and therefore, the thermal field in flow increases.

### **2.3.1 Results Authentication**

The outcomes of the present investigation are validated with the help of comparison tables. **Tables 2.1, 2.2** are comparison of initial and final values of similarity function for different  $R$  and **Table 2.3** is the comparison of thermal gradient for various  $R$ .

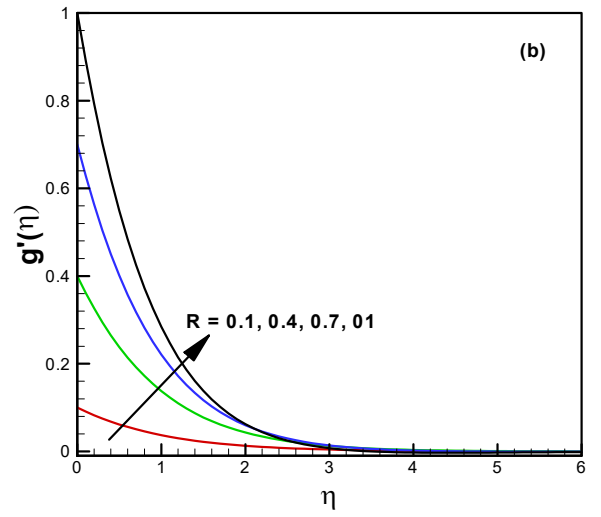
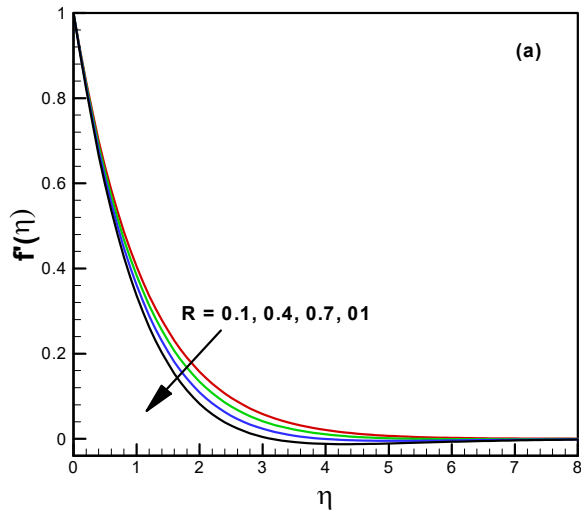


**Figure 2.2:** Impact of  $R$  on  $f'(\eta)$  and  $g'(\eta)$ .

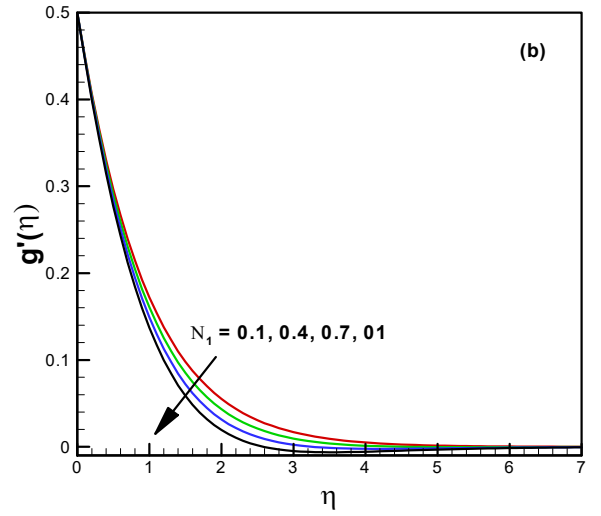
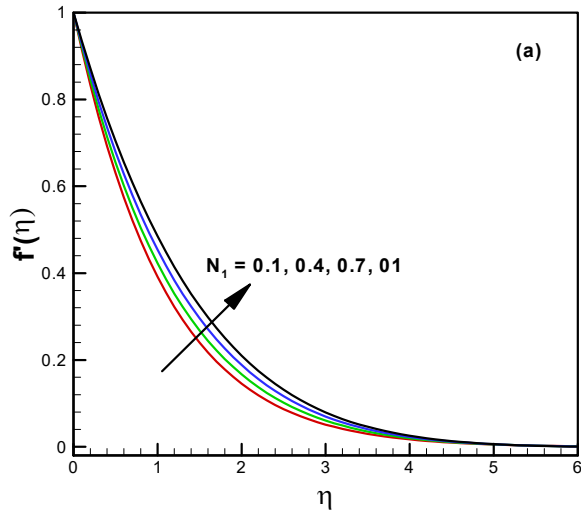


**Figure 2.3:** Impact of  $N_1$  on  $f'(\eta)$  and  $g'(\eta)$ .

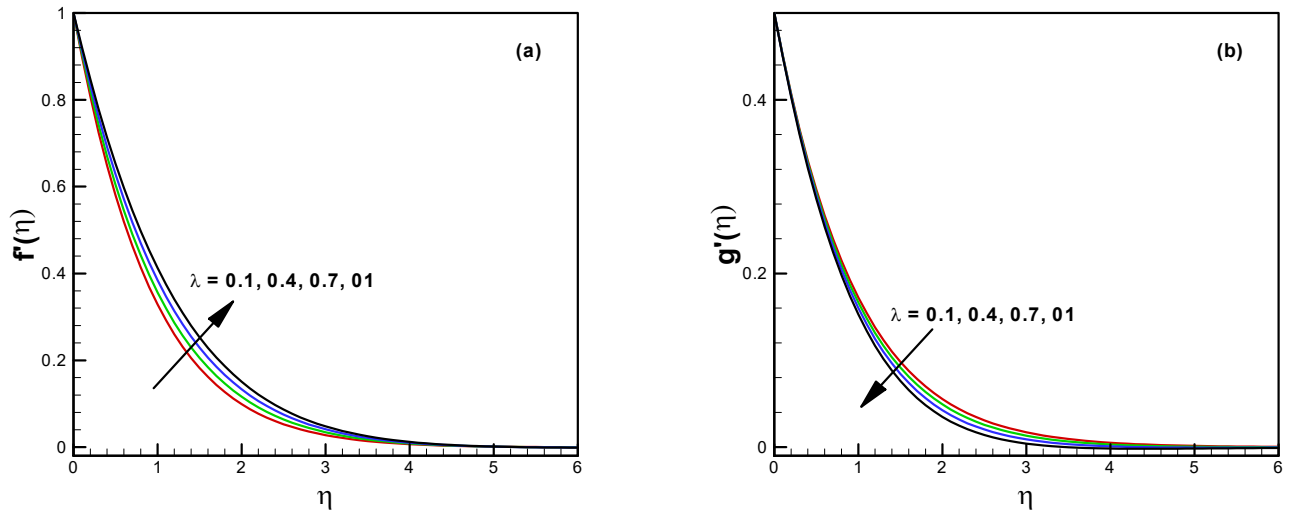


**Figure 2.4:** Impact of  $\lambda$  on  $f'(\eta)$  and  $g'(\eta)$ .

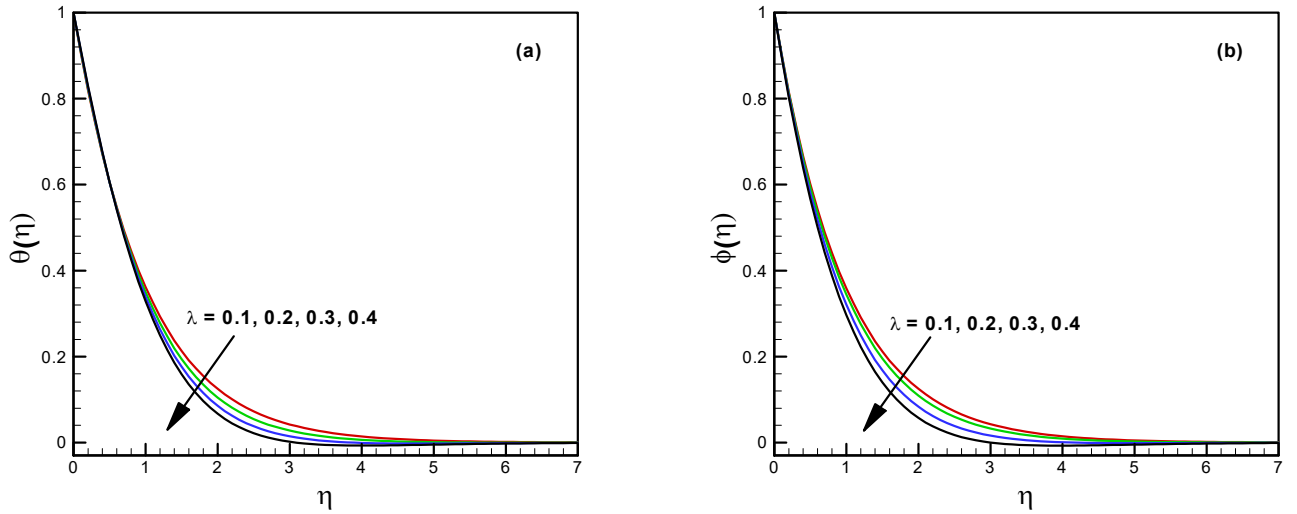


**Figure 2.5:** Impact of  $\lambda$  on  $\theta(\eta)$  and  $\phi(\eta)$ .

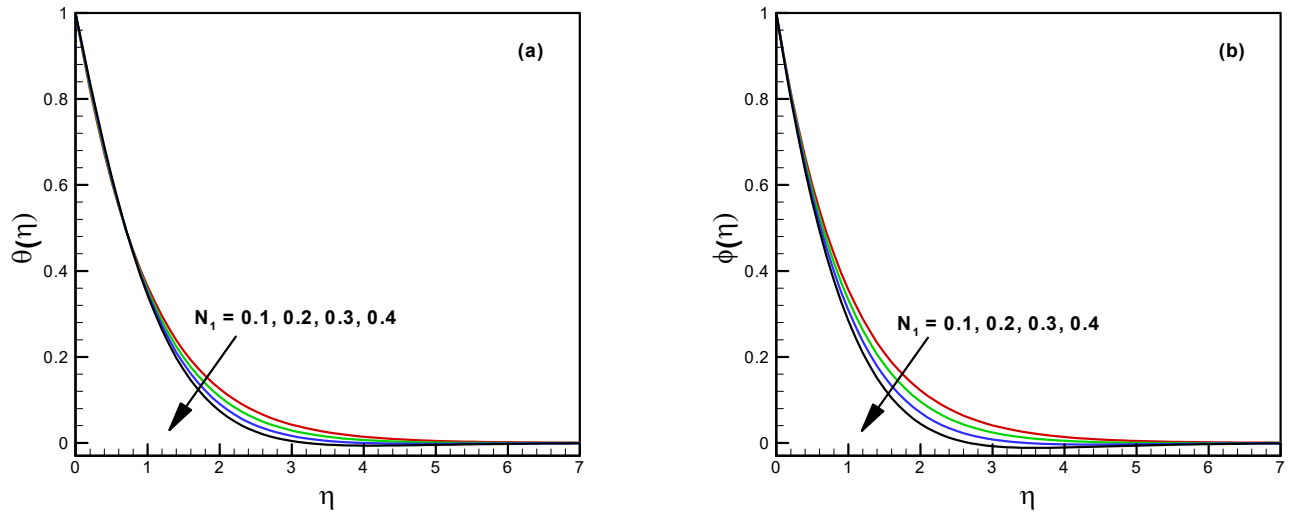


**Figure 2.6:** Impact of  $N_1$  on  $\theta(\eta)$  and  $\phi(\eta)$ .

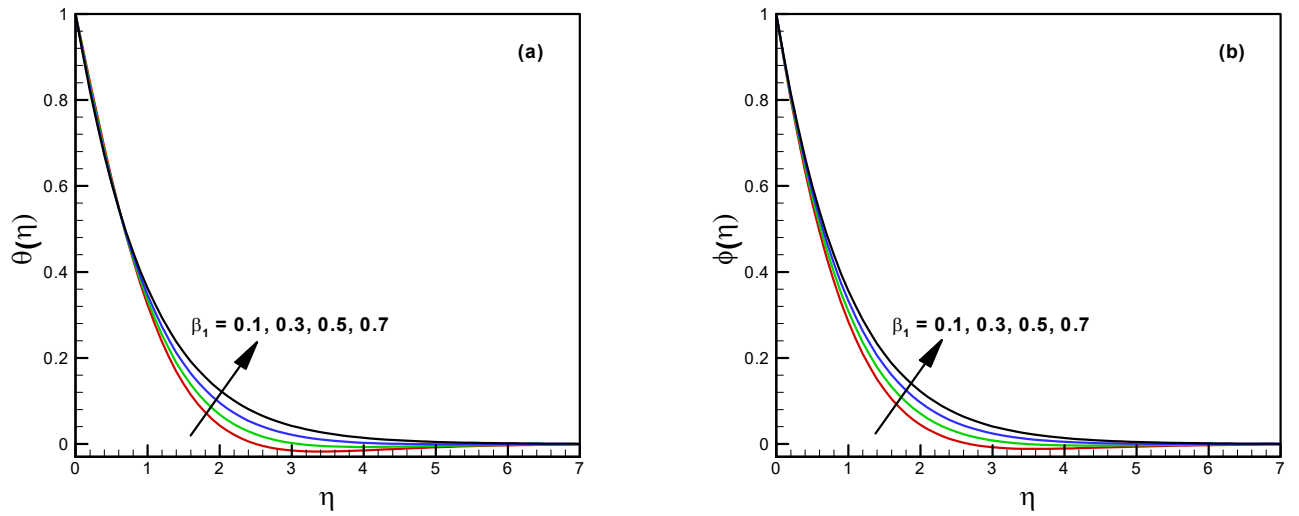


**Figure 2.7:** Impact of  $\beta_1$  on  $\theta(\eta)$  and  $\phi(\eta)$ .

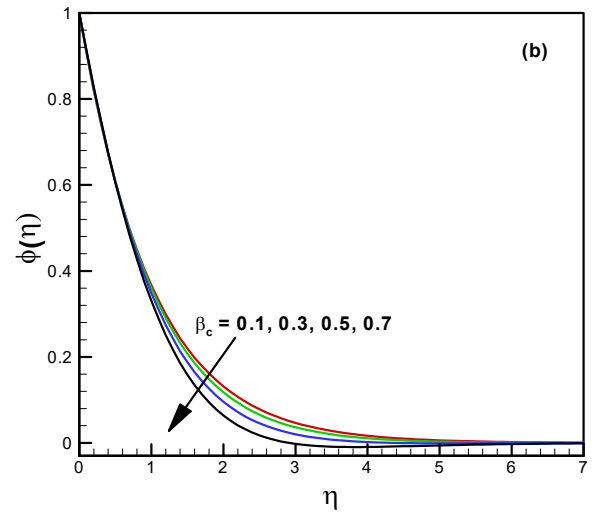
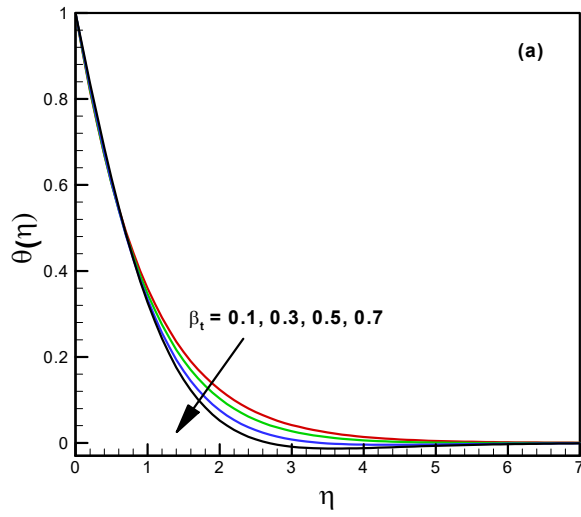


**Figure 2.8:** Impact of  $\beta_t$  on  $\theta(\eta)$  and  $\beta_c$  on  $\phi(\eta)$ .

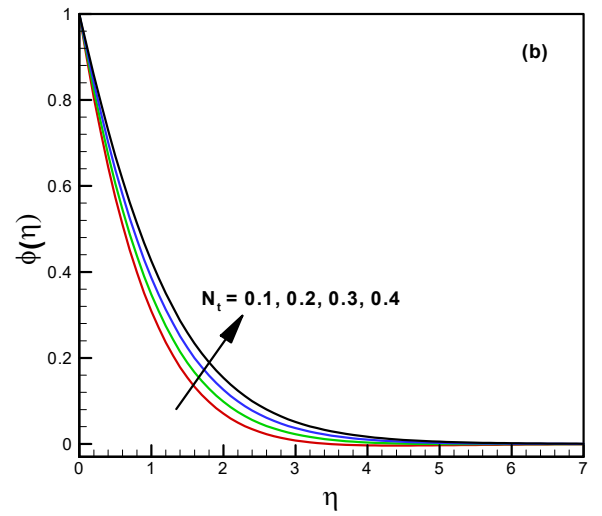
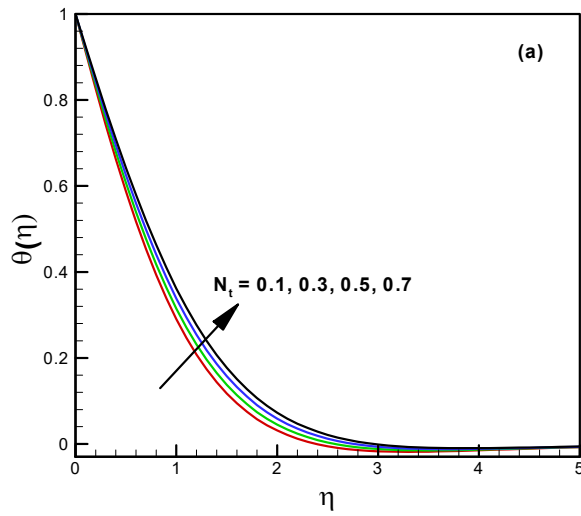


**Figure 2.9:** Impact of  $N_t$  on  $\theta(\eta)$  and  $\phi(\eta)$ .

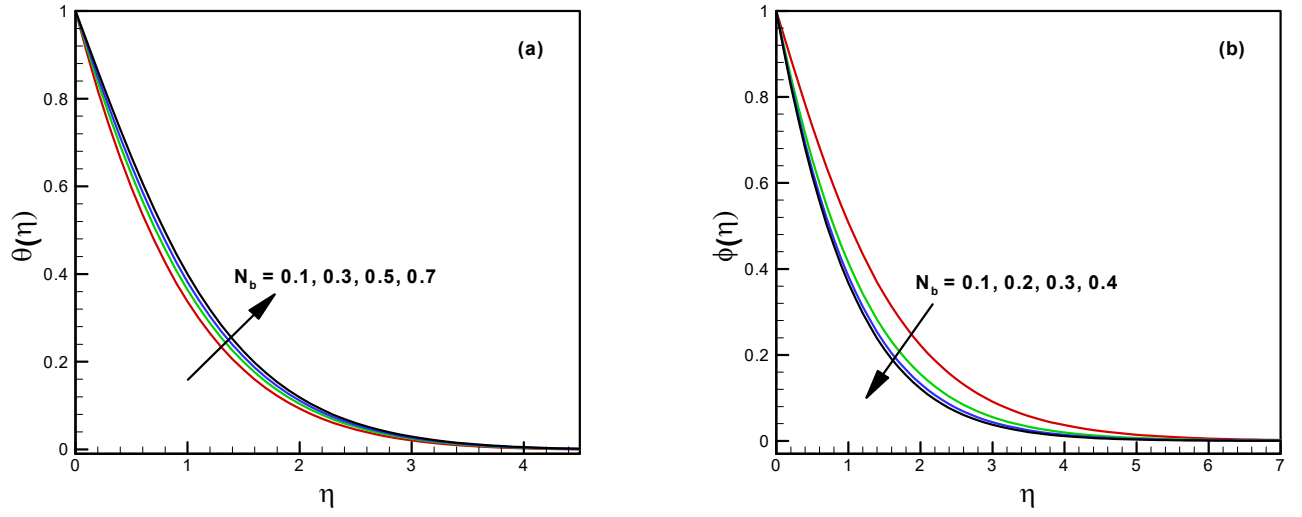


**Figure 2.10:** Impact of  $N_b$  on  $\theta(\eta)$  and  $\phi(\eta)$ .

**Table 2.1:** Numerical values of  $-f''(0)$  and  $-g''(0)$  for various  $R$  when  $\beta_1 = \lambda = N_1 = 0$ .

$R$	$-f''(0)$	$-g''(0)$	$-f''(0)$	$-g''(0)$
	Ref.[16]	Ref.[16]	Present results	Present results
0.0	1.000000	1.000000	1.000000	1.000000
0.25			1.026183	1.026190
0.50	1.051948	1.051889	1.051889	1.051892
0.75			1.077125	1.077127
1.0	1.101850	1.101903	1.101903	1.101903



**Table 2.2:** Numerical values of  $f(\infty)$  and  $g(\infty)$  for various  $R$  when  $\beta_1 = \lambda = N_1 = 0$ .

$R$	$f(\infty)$	$g(\infty)$	$f(\infty)$	$g(\infty)$
	Ref.[16]	Ref.[16]	Present results	Present results
0.0	1	0	1	0
0.25	0.907075	0.257986	0.907070	0.257985
0.50	0.842360	0.451671	0.842362	0.451668
0.75	0.792308	0.612049	0.792311	0.612050
1.0	0.751527	0.751527	0.751525	0.751525

**Table 2.3:** Numerical values of  $-\theta(0)$  for various  $R$  when  $\beta_1 = \lambda = N_1 = \beta_t = \beta_c = N_t = N_b = Le = 0$  and  $Pr = 1$ .

$R$	$-\theta(0)$		
	Ref.[67]	Ref.[68]	Present results
0.25	0.665932	0.665933	0.665930
0.50	0.735334	0.735334	0.735334
0.75	0.796472	0.796472	0.796473

## Chapter 3

# Unsteady Stagnation Point Flow of Maxwell Nanofluid due to Stretchable Disk

The main objective of this chapter is to study the thermal and solutal aspects of the magnetohydrodynamic (MHD) unsteady flow of Maxwell nanofluid under the consideration of stagnation point over a radially stretching disk. The impact of resistive heating and heat generation on the transportation of thermal energy in fluid is analyzed. Moreover, the prescribed surface temperature (PST) and constant wall temperature (CWT) are considered here. Additionally, the convective energy transport at the surface of the disk is assumed. The similar equations which govern the flow, heat and mass transport phenomena are solved numerically via `bvp4c` scheme. Also, the results for flow field and energy transport are presented graphically with comprehensive discussion. As a key outcomes, it is noted that the higher values of the unsteadiness parameter enhance the temperature field in case of CWT but decline in case

of PST. The Eckert number boosts up the temperature distribution in the Maxwell fluid significantly.

### 3.1 Mathematical Formulation

Consider the unsteady laminar boundary layer flow of Maxwell nanofluid over radially stretching disk of radius  $R_1$  with the consideration of stagnation point. Suppose that  $u$  and  $w$  are velocity components along  $r - axis$  and  $z - axis$ , respectively. The stretching velocity of the disk and free stream velocity are assumed as  $u_w(t, r) = \frac{ar}{1-\gamma t}$  and  $u_e(z) = \frac{cz}{1-\gamma t}$ , respectively, where  $a$ ,  $c$  and  $\gamma$  are positive constants. Moreover, a transverse magnetic field  $\mathbf{B} = (0, 0, B_0)$  is applied to flow of nanofluid (see **Fig. 3.1**). The influence of Joule heating, heat generation /absorption and chemical reaction to the transportation of heat and solutal energy in the nanofluid is also considered here.

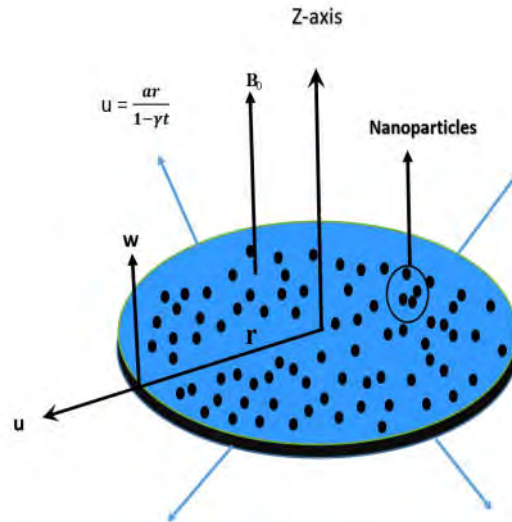


**Figure 3.1:** Flow mechanism.

The above assumptions with conservation laws (cf. Chapter 1) and Maxwell fluid model

(cf. Chapter 1) lead to the boundary layer governing PDEs as:

$$\frac{\partial(ru)}{\partial r} + \frac{\partial(rw)}{\partial z} = 0, \quad (3.1)$$

$$\begin{aligned} \frac{\partial u}{\partial t} + u \frac{\partial u}{\partial r} + w \frac{\partial u}{\partial z} + \lambda_1 \left[ \frac{\partial^2 u}{\partial t^2} + 2u \frac{\partial^2 u}{\partial t \partial r} + 2w \frac{\partial^2 u}{\partial z \partial t} + 2uw \frac{\partial^2 u}{\partial r \partial z} + w^2 \frac{\partial^2 u}{\partial z^2} + u^2 \frac{\partial^2 u}{\partial r^2} \right] \\ = -\frac{1}{\rho} \frac{\partial p}{\partial r} + \nu \left[ \frac{\partial^2 u}{\partial z^2} \right] - \frac{\sigma B_0^2}{\rho} \left[ u + \lambda_1 \left\{ \frac{\partial u}{\partial t} + w \frac{\partial u}{\partial z} \right\} \right], \end{aligned} \quad (3.2)$$

$$\begin{aligned} \frac{\partial T}{\partial t} + u \frac{\partial T}{\partial r} + w \frac{\partial T}{\partial z} = \alpha_1 \left[ \frac{\partial^2 T}{\partial z^2} \right] + \tau \left[ D_B \frac{\partial T}{\partial z} \frac{\partial C}{\partial z} + \frac{D_T}{T_\infty} \left( \frac{\partial T}{\partial z} \right)^2 \right] \\ + Q_\circ \left( \frac{T - T_\infty}{(\rho c_p)_f} \right) + \frac{\sigma B_0^2 u^2}{(\rho c_p)_f}, \end{aligned} \quad (3.3)$$

$$\frac{\partial C}{\partial t} + u \frac{\partial C}{\partial r} + w \frac{\partial C}{\partial z} = D_B \left[ \frac{\partial^2 C}{\partial z^2} \right] + \frac{D_T}{T_\infty} \left[ \frac{\partial^2 T}{\partial z^2} \right] - k_1(C - C_\infty), \quad (3.4)$$

with corresponding boundary conditions

$$u(t, r, z) = u_w(t, r) = \frac{ar}{1-\gamma t}, \quad w(t, r, z) = 0,$$

$$-k \frac{\partial T}{\partial z} = h_T (T_w - T), \quad \text{where } T_w = \text{constant (CWT) and } T_w - T_\infty = \frac{br}{1-\gamma t} \quad (\text{PST})$$

$$-D_B \frac{\partial C}{\partial z} = h_C (C_w - C) \quad \text{at } z = 0, \quad (3.5)$$

$$u = u_e = \frac{cr}{1-\gamma t}, \quad T \rightarrow T_\infty, \quad C \rightarrow C_\infty \quad \text{as } z \rightarrow \infty. \quad (3.6)$$

Here  $p$  is the fluid pressure,  $B_0$  the magnetic field strength,  $Q_\circ$  the heat source,  $k_1$  the chemical reaction constant and  $(h_T, h_C)$  are heat and mass transfer coefficients, respectively.

By invoking the following the similarity

$$\begin{aligned}
u &= \frac{ar}{1-\gamma t} f'(\eta), \quad w = -2\sqrt{\frac{a\nu}{1-\gamma t}} f(\eta), \quad T = T_\infty + (T_w - T_\infty) \theta(\eta) \quad (\text{CWT}), \\
T &= T_\infty + \frac{br}{1-\gamma t} \theta(\eta) \quad (\text{PST}), \quad \phi(\eta) = \frac{C-C_\infty}{C_w-C_\infty}, \quad \eta = \sqrt{\frac{a}{\nu(1-\gamma t)}} z.
\end{aligned} \tag{3.7}$$

After substituting the above conversions Eq. (3.1) is satisfied automatically and Eqs. (3.2) – (3.7) yield

$$\begin{aligned}
&f''' - \frac{S}{2}\eta f'' - S f' - f'^2 + 2f f'' - \frac{7}{4}\beta_1 S^2 \eta f'' - \frac{\beta_1}{4}\eta^2 S^2 f''' - 2\beta_1 S^2 f' \\
&- 2S\beta_1 f'^2 - \beta_1 \eta S f' f'' + 2S\beta_1 \eta f f''' + 6S\beta_1 f f'' + 4\beta_1 f f' f'' - 4\beta_1 f^2 f''' \\
&- M(f' + \beta_1 \frac{S}{2}\eta f'' + \beta_1 S f' - 2\beta_1 f f'' - A - \beta_1 AS) \\
&+ AS + A^2 + \beta_1(2AS^2 + 2A^2S) = 0,
\end{aligned} \tag{3.8}$$

$$\begin{aligned}
&\theta'' + \text{Pr}(2f\theta' - \frac{S}{2}\eta\theta') + \text{Pr} N_b \theta' \phi' + \text{Pr} N_t \theta'^2 \\
&+ \text{Pr} ME_{c_r} f'^2 + \text{Pr} \delta\theta = 0, \quad (\text{CWT})
\end{aligned} \tag{3.9}$$

$$\begin{aligned}
&\theta'' + \text{Pr}(2f\theta' - S\theta - \theta f' - \frac{S}{2}\eta\theta') + \text{Pr} N_b \theta' \phi' + \text{Pr} N_t \theta'^2 \\
&+ \text{Pr} ME_{c_r} f'^2 + \text{Pr} \delta\theta = 0, \quad (\text{PST})
\end{aligned} \tag{3.10}$$

$$\phi'' + Le \text{Pr}(2f\phi' - \frac{S}{2}\eta\phi') + Le \text{Pr} \frac{N_t}{N_b} \theta'' - Le \text{Pr} K_1 \theta = 0, \tag{3.11}$$

$$f(0) = 0, \quad f'(0) = 1, \quad \theta'(0) = -\gamma_1(1 - \theta(0)), \quad \phi'(0) = -\gamma_2(1 - \phi(0)), \quad (3.12)$$

$$f'(\infty) = A, \quad \theta(\infty) = 0, \quad \phi(\infty) = 0. \quad (3.13)$$

In the overhead equations,  $S$  ( $= \frac{\gamma}{a}$ ) is the unsteadiness parameter,  $\beta_1$  ( $= \frac{\lambda_1 a}{1 - \gamma t}$ ) the Deborah number,  $A$  ( $= \frac{c}{a}$ ) the velocity ratio parameter,  $M$  ( $= \frac{\sigma B_0^2 (1 - \gamma t)}{(\rho_f) a}$ ) the magnetic parameter,  $N_b$  ( $= \frac{\tau D_B (\Delta C)}{\nu}$ ) the Brownian motion parameter,  $N_t$  ( $= \frac{\tau D_T \Delta T}{\nu T_\infty}$ ) the thermophoresis parameter,  $Ec$  ( $= \frac{u_w^2}{c_p \Delta T (1 - \gamma t)}$ ) the Eckert number,  $Pr$  ( $= \frac{\nu}{\alpha_1}$ ) the Prandtl number,  $\delta$  ( $= \frac{Q_0 (1 - \gamma t)}{a (\rho c_p)}$ ) the heat source/sink parameter,  $K_1$  ( $= \frac{k_1 (1 - \gamma t)}{a}$ ) the chemical reaction parameter,  $Le$  ( $= \frac{\alpha_1}{D_B}$ ) the Lewis number and  $\gamma_1$  ( $= \frac{h_T}{k} \sqrt{\frac{\nu (1 - \gamma t)}{a}}$ ),  $\gamma_2$  ( $= \frac{h_C}{D_B} \sqrt{\frac{\nu (1 - \gamma t)}{a}}$ ) the Biot numbers for temperature and concentration, respectively.

## 3.2 Solution Procedure

The numerical method `bvp4c` (MATLAB built-in function) is adopted to acquired the results for flow field, temperature and concentration distribution in the flow. For this we transformed the governing ODEs given in Eqs. (3.8), (3.9), (3.10) and (3.11) along with corresponding boundary conditions Eqs. (3.12) and (3.13) to the system of first order ordinary differential equations.

The transformed variables are supposed as

$$f = y_1, \quad f' = y_2, \quad f'' = y_3, \quad f''' = y y_1, \quad (3.14)$$

$$\theta = y_4, \quad \theta' = y_5, \quad \theta'' = y y_2, \quad (3.15)$$

$$\phi = y_6, \quad \phi' = y_7, \quad \phi'' = y y_3. \quad (3.16)$$

The resulting first order ODEs are as follows

$$yy_1 = \frac{\begin{bmatrix} y_2^2 - 2y_1y_3 + Sy_2 + \frac{S}{2}\eta y_3 + \frac{7}{4}S^2\beta_1\eta y_3 + 2S^2\beta_1y_2 \\ -4\beta_1y_1y_2y_3 + 2S\beta_1y_2^2 + S\beta_1\eta y_2y_3 - 6S\beta_1y_2y_3 \\ +M(y_2 + \frac{S}{2}\beta_1\eta y_3 + S\beta_1y_2 - 2\beta_1y_1y_3 - A - S\beta_1A) \\ -AS - A^2 - \beta_1(2AS^2 + 2A^2S) \end{bmatrix}}{a_1}, \quad (3.17)$$

$$yy_2 = \text{Pr} \left( \frac{S}{2}\eta y_5 - 2y_1y_5 - N_b y_5 y_7 - N_t y_5^2 - MEc_r y_2^2 - \delta y_4 \right), \quad (\mathbf{CWT}) \quad (3.18)$$

$$yy_2 = \text{Pr} \left( Sy_4 + \frac{S}{2}\eta y_5 + y_2y_4 - 2y_1y_5 - N_b y_5 y_7 - N_t y_5^2 - MEc_r y_2^2 - \delta y_4 \right), \quad (\mathbf{PST}) \quad (3.19)$$

$$yy_3 = Le \text{Pr} \left( \frac{S}{2}\eta y_5 - 2y_1y_7 - \frac{N_t}{N_b} yy_2 + K_1 y_6 \right),$$

where

$$a_1 = 1 + 2S\beta_1\eta y_1 - \beta_1 \frac{S^2}{4}\eta^2 - 4\beta_1 y_1^2,$$

and boundary conditions for the above non-linear first order differential system are

$$\begin{aligned} y_1(0) = 0, \quad y_2(0) = 1, \quad y_5(0) = -\gamma_1(1 - y_4(0)), \quad y_7(0) = -\gamma_2(1 - y_6(0)), \\ y_2(\infty) = A, \quad y_4(\infty) = 0, \quad y_4(\infty) = 0. \end{aligned} \quad (3.20)$$

### 3.3 Discussion of Results

This section is composed for the physical analysis of graphical outcomes of governing flow and energy transport phenomena of Maxwell nanofluid over a stretching disk in the presence of

the magnetic field. The thermal energy transport is deliberated with constant surface temperature(CWT) and perscribed surface temperature (PST). A higher rate of thermal energy transport is observed for CWT as compared to PST. Physically, in the case of PST, the surface temperature varies with the spatial variable, so the average heat energy transport for PST is lower than CWT due to the variation in temperature at the surface. In order to obtain the physically acceptable outcomes, the values of controlling physical parameters are taken fixed as  $\beta_1 = A = S = \gamma_1 = \gamma_2 = Ec = K_1 = \delta = N_t = 0.1$ ,  $N_b = 0.4$ ,  $M = Le = 1$ ,  $Pr = 2$ . **Figs. 3.2(a – c)** describe the impact of magnetic parameter  $M$  on velocity, temperature and concentration fields, respectively. It is noted that for higher values of magnetic parameter  $M$  the fluid velocity decreases but the energy transport increases in the fluid flow. Physically, the more value of  $M$  enhances the corresponding Lorentz force due to the magnetic field. This force produces the resistance to the fluid flow thus, the velocity of fluid declines. On the other hand, conduction of energy among the fluid particles boosts up due to higher Lorentz force. One thing should be noted here that for appropriate results  $M < 1$  in the case of concentration field but for the velocity and temperature fields  $M > 1$  is acceptable. Plots in **Figs. 3.3(a – c)** are present to explore the effects of Maxwell parameter  $\beta_1$  on velocity field, thermal and solutal profiles. It is evident that for higher values of  $\beta_1$  the stress relaxation phenomenon increases in the viscoelastic fluid thus, the fluid shows a more solid-like response than liquid. Due to this solid-like behavior of fluid the flow velocity at any point decreases but temperature and concentration increase.

**Figs. 3.4(a – c)** correspondingly show the flow field, thermal and concentration fields for various values of velocity ratio parameter  $A$ . As for  $A < 1$  the stretching velocity of the disk is greater than free stream velocity thus, the increasing trend in  $A < 1$  enhances the fluid flow



velocity but it declines the temperature and concentration fields due decrease in the forced convection mechanism. The plots in **Figs. 3.5(a – c)** and **Figs. 3.6(a – c)** depict the impact of unsteadiness parameter  $S$  on thermal and solutal fields with the comparison of small and large thermophoretic and Brownian forces. It shows that the increasing values of  $S$  enhance and reduces the temperature profile in the case of CWT and PST, respectively, because for PST the dimensionless temperature  $\theta$  has the inverse relation to the unsteady surface temperature variation thus, in result the temperature field decline. Moreover, the concentration field is increasing function for higher values of  $S$ . The influence of nanoparticle in Maxwell fluid to the heat and mass transportation is described by the thermophoretic and Brownian motion parameter  $N_t$  and  $N_b$ , respectively. **Figs. 3.5(a – c)** and **Figs. 3.6(a – c)** also illustrate the variation in temperature and concentration fields for small and large values of  $N_t$  and  $N_b$ , respectively. It is concluded that heat transport increases for higher values of  $N_t$  and  $N_b$  in both cases CWT and PST. But the mass transport enhances for higher values of  $N_t$  and opposite behavior is found for  $N_b$ . Moreover, it is noted that the range of thermophoretic parameter  $N_t$  is found as  $[0.1, 3]$  and  $[0.01, 0.1]$  for the solution of temperature and concentration distributions in the flow of Maxwell nanoliquid, respectively. Physically, an increase in  $N_t$  rises the thermophoretic force which enhances the convective transport of thermal energy in nanoliquid. Furthermore, the higher value of  $N_b$  increases the Brownian force which acts as the opposing and aiding agent for mass and heat transport in the fluid, respectively. Thus, in result the concentration field declines and temperature field enlarge.

To picture the impact of heat source/sink on temperature field **Figs. 3.7(a, b)** are enlisted. It is clear that the thermal energy source in the system enhances the heat transfer rate in the fluid and the converse is true for the sink. The influence of chemical reaction to the mass

transport describes by the reaction parameter  $K_1$ . **Figs. 3.8(a, b)** show that the mass transport decreases in the constructive mode of chemical reaction  $K_1 > 0$  and increases in destructive mode  $K_1 < 0$ . The graphs in **Figs. 3.9(a, b)** elucidate the variation in temperature and concentration field versus Prandtl number  $Pr$  and Lewis number  $Le$ , respectively. It is observed that the transportation of thermal and solutal energy in nanoliquid reduces with increasing values of  $Pr$  and  $Le$ , respectively. Physically, the increasing trend of these parameters reduce the thermal and mass diffusivity of nano liquid, respectively. Thus, in consequence, both thermal and solutal fields reduce. The strength of convective energy transport for thermal and solutal phenomena are expressed by Biots number  $\gamma_1$  and  $\gamma_2$ , respectively. It reveals by the **Figs. 3.10(a, b)** that the higher thermal and solutal Biot numbers  $\gamma_1$  and  $\gamma_2$  upgrade temperature and concentration fields, respectively. Physically, higher estimation in the Biot number decreases the resistance for energy transport at the surface in consequence the higher surface temperature and concentration gradients achieved. **Fig. 3.11** envisions the increasing variation in temperature field versus Eckert number  $Ec$ . Physically,  $Ec$  corresponds to the strength of resistive heating thus, more values of  $Ec$  produce the extra heat in the fluid which enhances the temperature field and the results are in accordance with the study [69].

### 3.4 Surface Thermal Gradient and Analysis Authentication

The validation of current numerical scheme is proved with help of comparison **Table 3.1** for various values of  $M$  in good agreement. The numerical values of surface thermal gradient and solutal gradient for different  $N_t$ ,  $N_b$ ,  $Pr$  and  $Le$  are presented in **Table 3.2**. It is observed that there is higher values of thermal gradient in case of PST as compare to CWT.

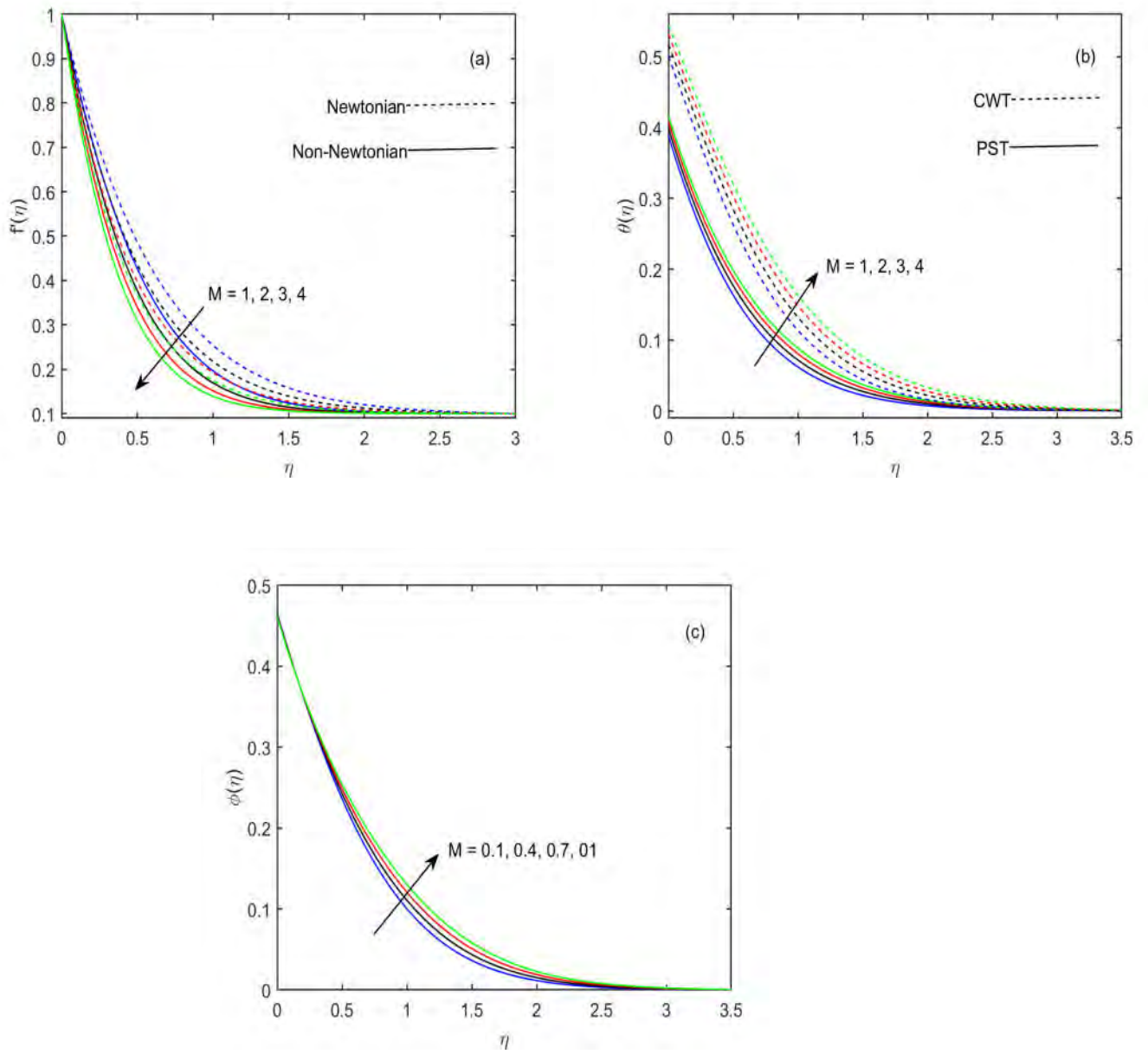


**Figure 3.2:** The velocity, temperature and concentration profiles via  $M$ .

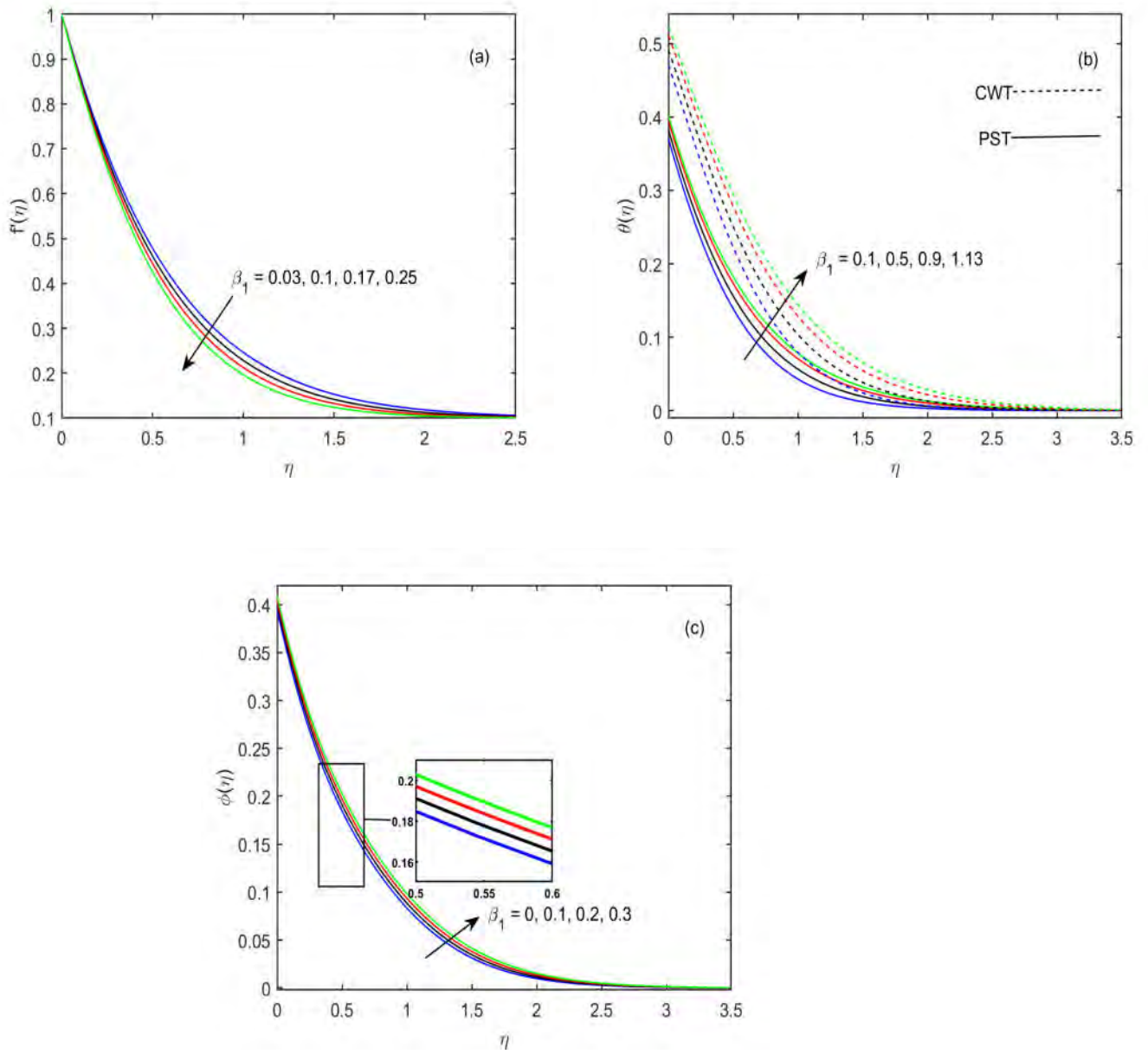


**Figure 3.3:** The velocity, temperature and concentration profiles via  $\beta_1$ .

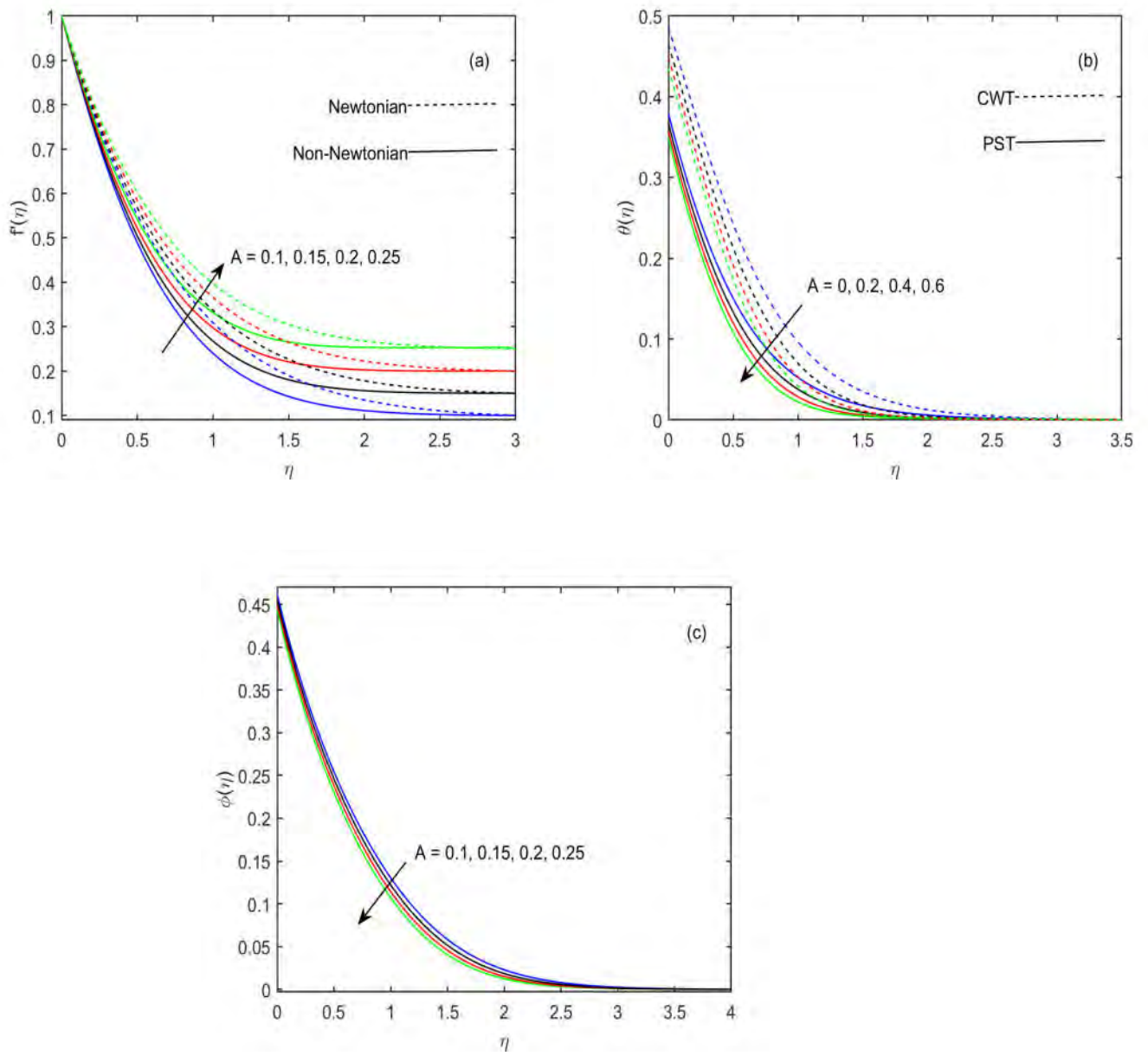


**Figure 3.4:** The temperature and concentration profiles via  $A$ .

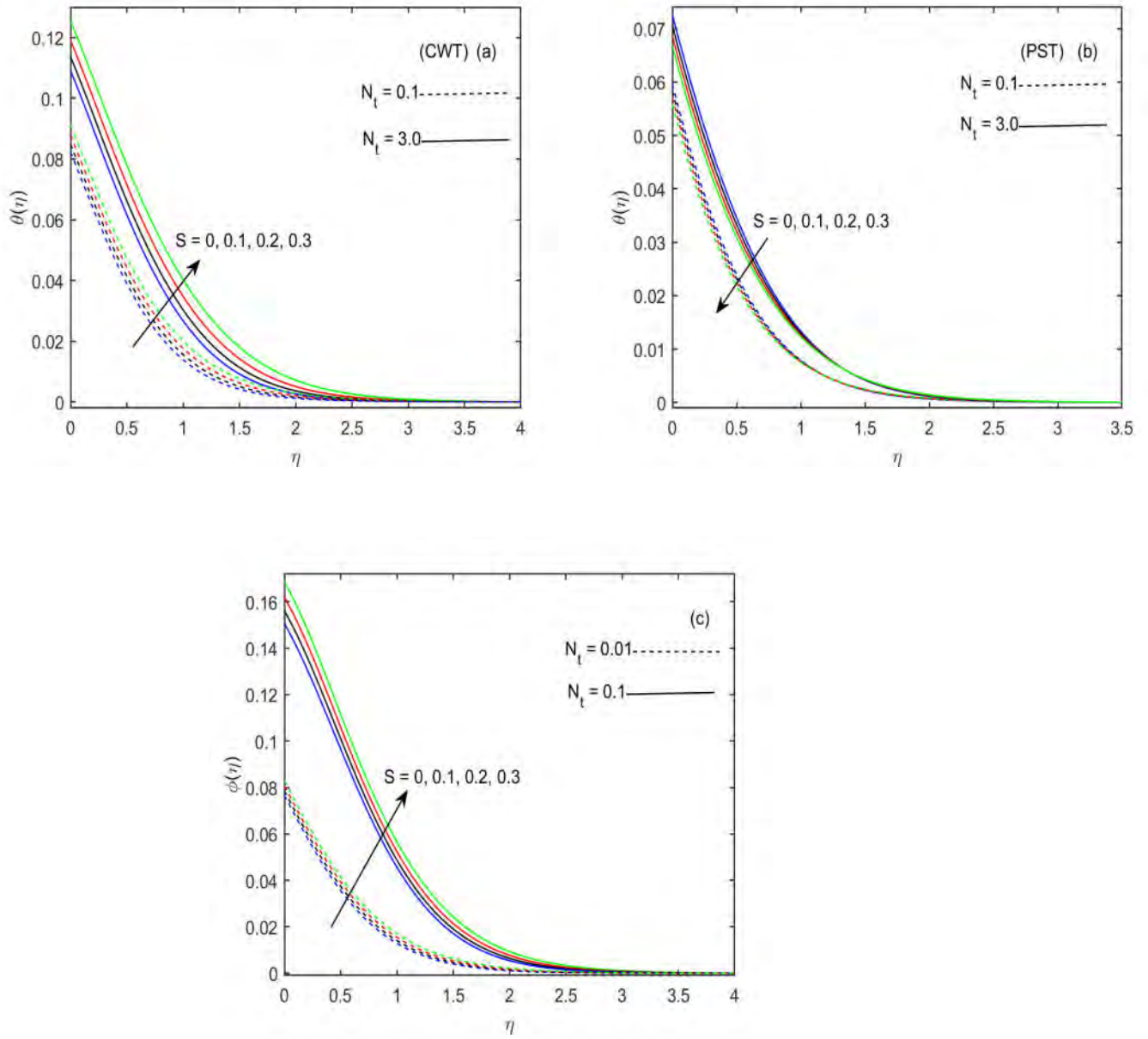


**Figure 3.5:** The temperature and concentration profiles via  $S$  with comparison of  $N_t$ .

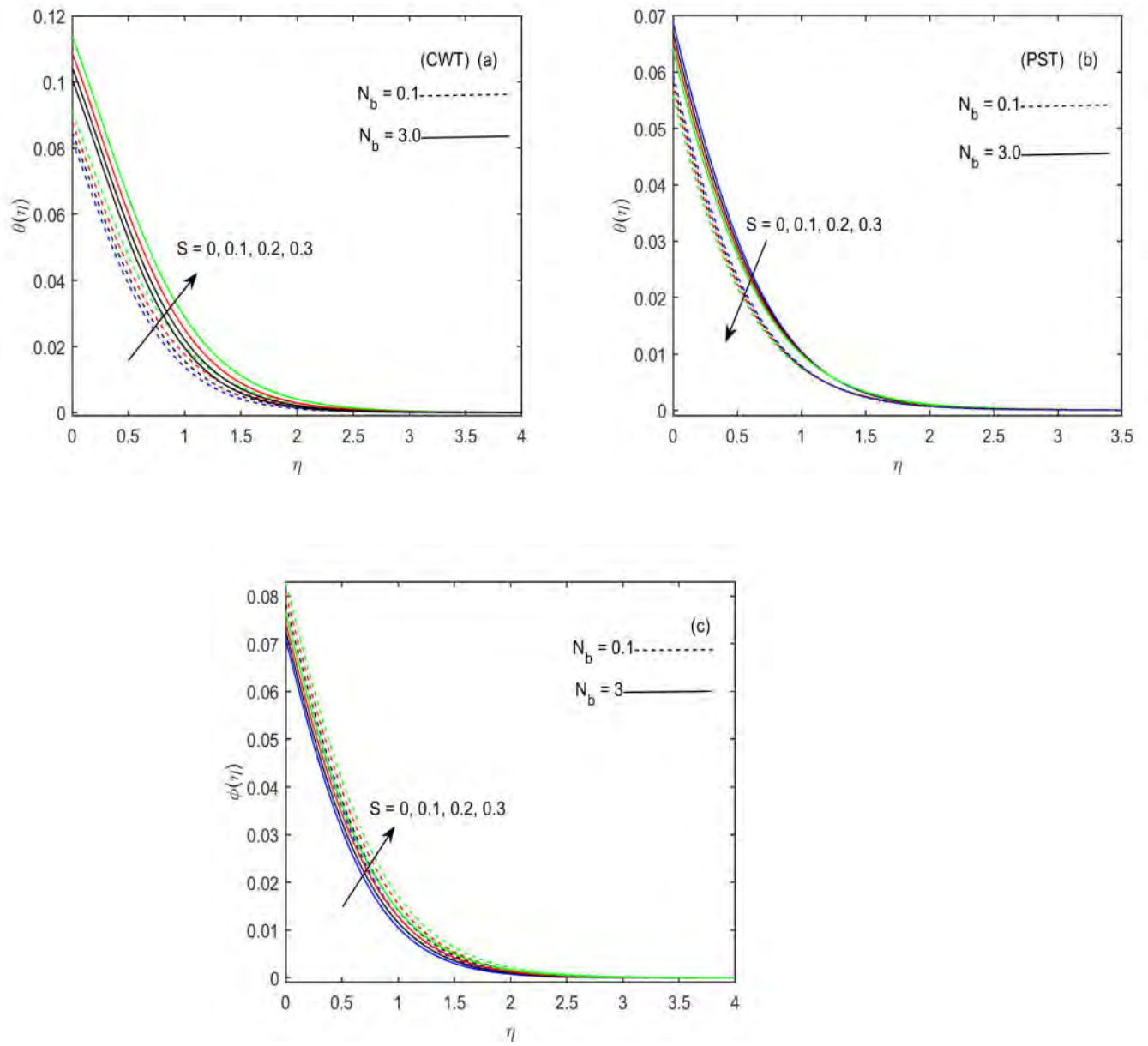


**Figure 3.6:** The temperature and concentration profiles via  $S$  with comparison of  $N_b$ .



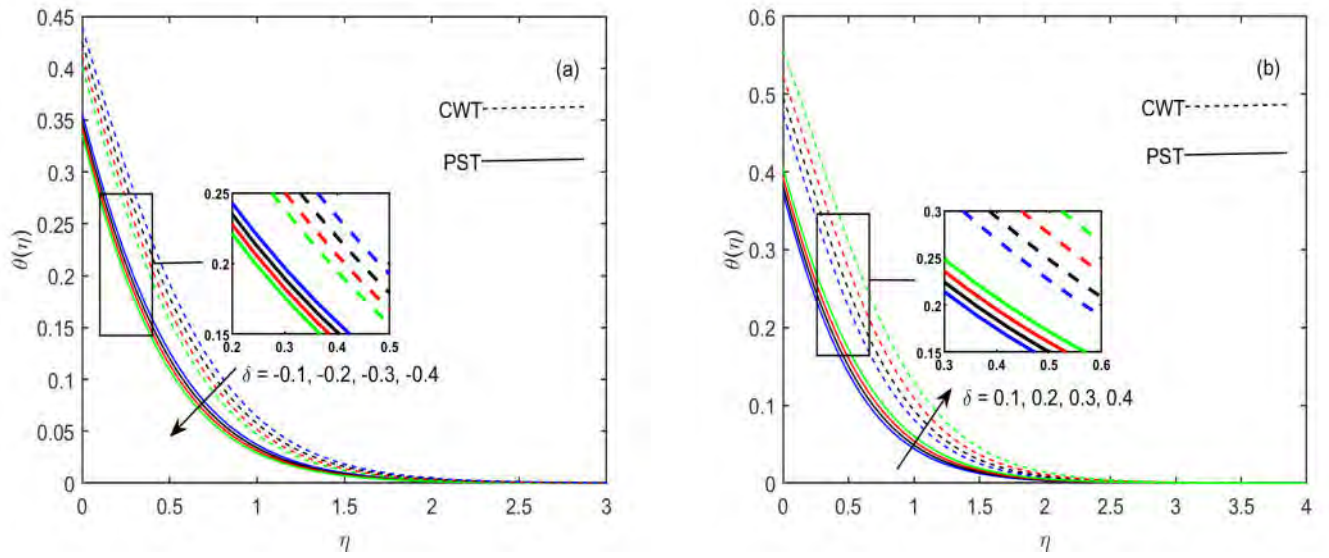


**Figure 3.7:** The temperature profile via heat source/sink parameter  $\delta$ .

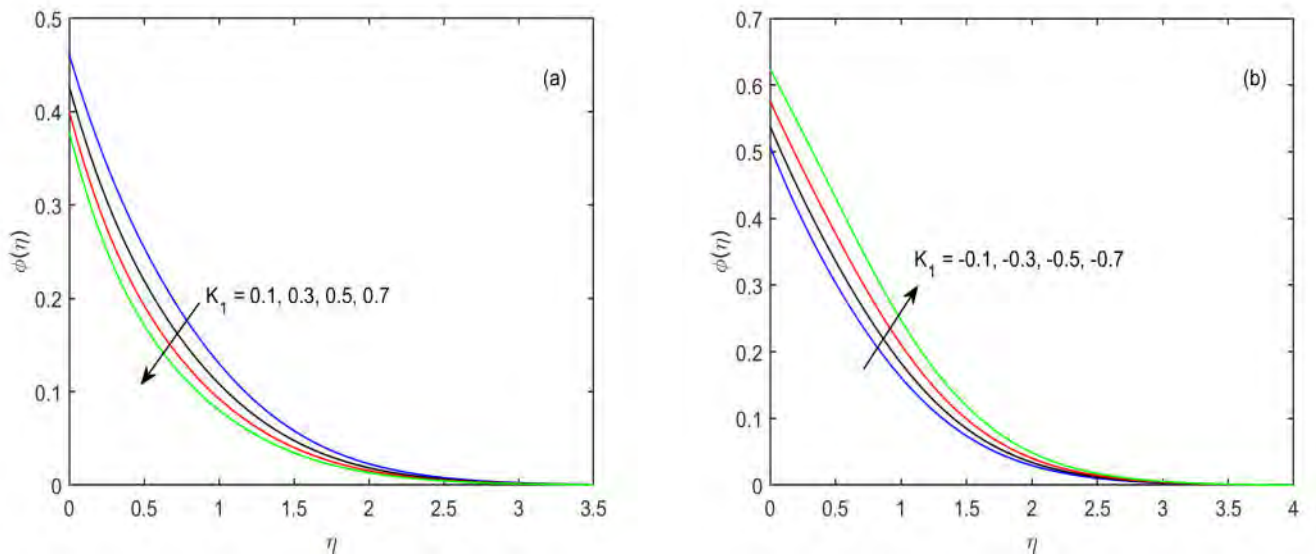


**Figure 3.8:** The concentration profile via  $K_1$ .



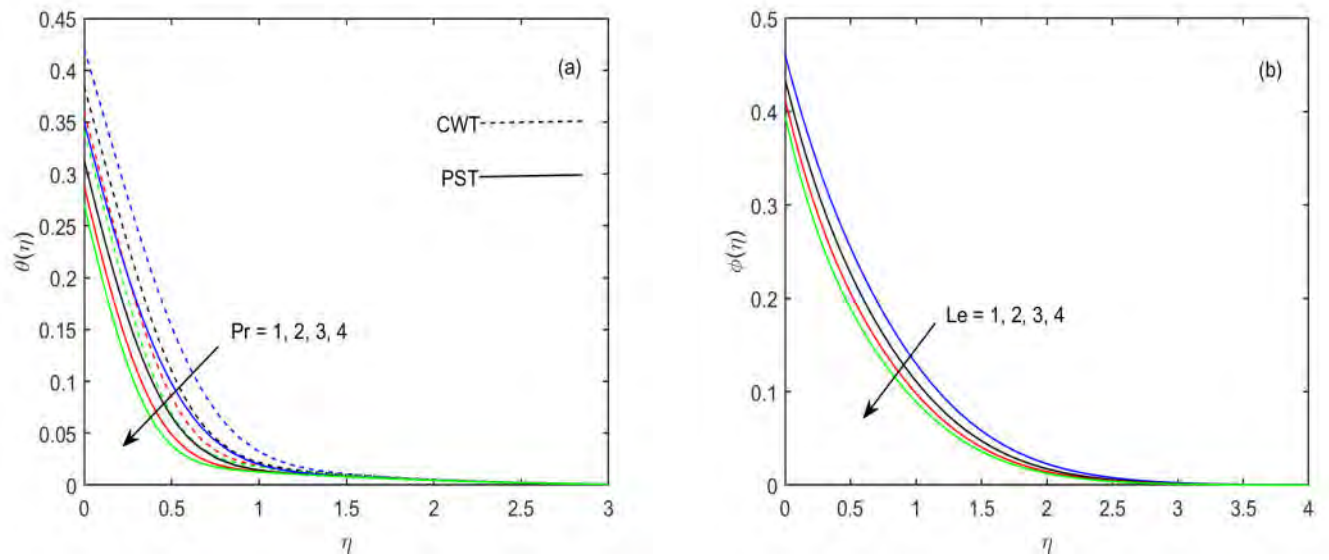


**Figure 3.9:** The temperature and concentration profiles via  $Pr$  and  $Le$ .

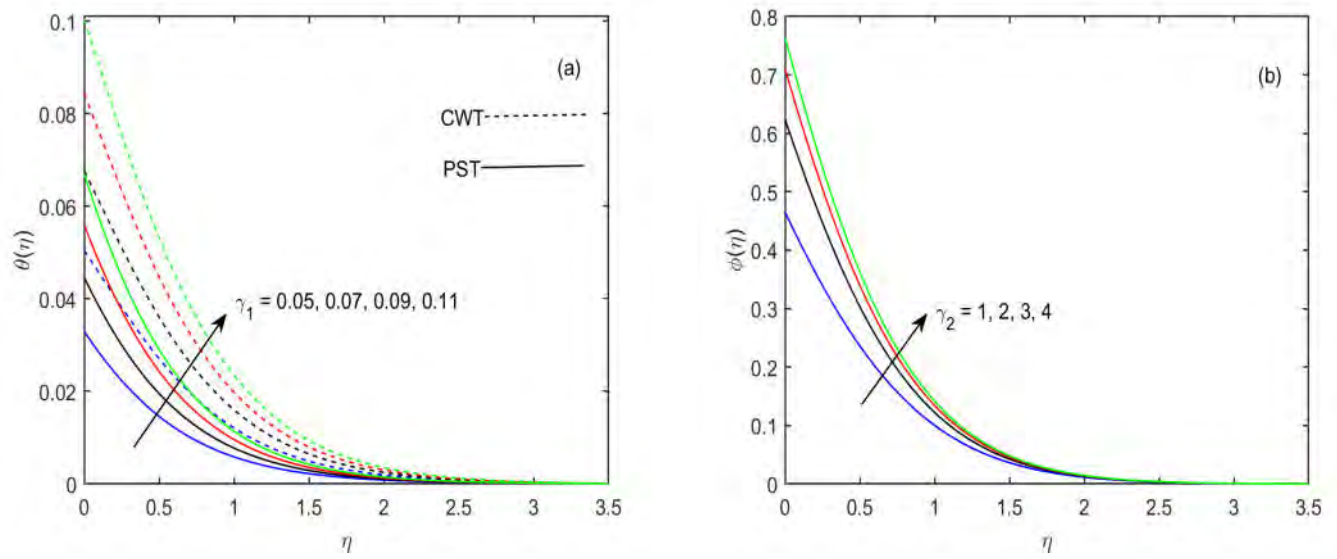


**Figure 3.10:** The temperature and concentration profiles via  $\gamma_1$  and  $\gamma_2$ , respectively.

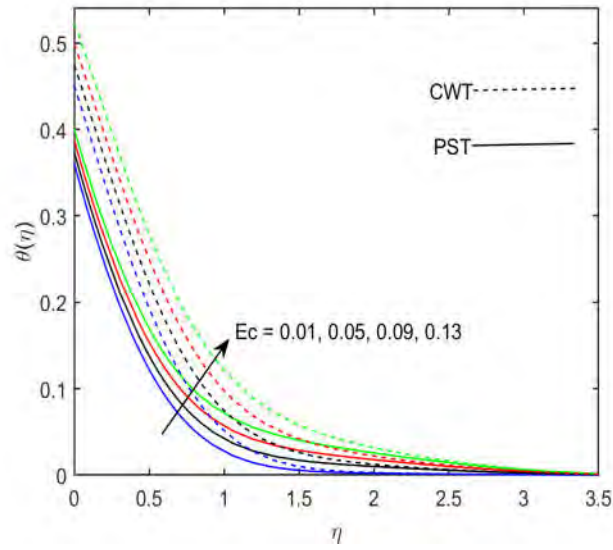


**Figure 3.11:** The temperature profile via  $Ec$ .

**Table 3.1:** The comparison of  $-f''(0)$  for various values of  $M$  in limiting case when  $S = A = \beta_1 = 0$ .

$-f''(0)$			
$M$	Ref. [70]	Ref. [71]	Present results
0.0	1.17372	1.17372088	1.1749647
0.5	1.36581	1.36581449	1.3661531
1.0	1.53571	1.53571052	1.5358086
2.0	1.83049	1.83048967	1.8307000
3.0	2.08484	2.08484656	2.0848967

**Table 3.2:** Numerical values of Nusselt and Sherwood numbers for different values  $N_t$ ,  $N_b$ , Pr and  $Le$  when  $S = A = \gamma_1 = \gamma_2 = K_1 = \delta = 0.1$ ,  $M = 1$  and  $\beta_1 = 0.01$ .

$N_t$	$N_b$	Pr	$Ec$	$Le$	$-\theta'(0)$ (CWT)	$-\theta(0)$ (PST)	$-\phi(0)$
0.1	0.1	2.0	0.5	1.0	0.091225	0.094037	0.528710
					0.091162	0.094012	0.486878
					0.091099	0.093986	0.445440
0.1	0.1	2.0	0.5	1.0	0.091225	0.094037	0.528710
					0.090836	0.093856	0.550459
					0.090425	0.093669	0.557728
0.1	0.1	0.5	0.5	1.0	0.082085	0.087591	
					0.087257	0.091413	
					0.089782	0.093084	
0.1	0.1	2.0	0.1	1.0	0.0921436	0.0944904	
					0.0889005	0.0927621	
					0.0856576	0.0910338	
0.1	0.1	2.0	0.1	0.5			0.457417
							0.561378
							0.618065

## Chapter 4

# Analysis of Cattaneo-Christov

# Model for Unsteady Flow of

# Maxwell Fluid due to Stretchable

# Cylinder

In this chapter, an analysis of thermal and solutal energy transport phenomena in Maxwell fluid flow with the help of Cattaneo-Christov double diffusion theory is performed. The unsteady 2D flow of Maxwell fluid with variable thermal conductivity over the stretching cylinder is considered here. We formulate the partial differential equations (PDEs) under given assumptions for the governing physical problem of heat and mass transport in Maxwell fluid by using double diffusion of Cattaneo-Christov model rather than classical Fourier's and Fick's laws. Numerical technique `bvp4c` is employed for the solution of ordinary differential equations (ODEs) which are obtained from governing PDEs under the appropriate similarity

transformations. In view of the acquired results, it is observed that for convenient results the values of the unsteadiness parameter should be less than one. The higher values of the Maxwell parameter decline the flow field but increase the energy transport in the fluid flow. Both thermal and concentration energy distributions in Maxwell liquid flow decline for higher values of thermal and concentration relaxation times parameters. Moreover, a small thermal conductivity parameter also enhances the temperature field. The validation of results proved with the help of comparison Table 4.1 with previous articles.

## 4.1 Mathematical Formulation

Consider the unsteady laminar 2D flow of an incompressible Maxwell fluid with variable thermal conductivity influenced by stretching cylinder of radius  $R_1$ . Suppose that  $u$  and  $w$  are velocity components along  $z - axis$  (axis of cylinder) and  $r - axis$  (normal to  $z$ -axis), respectively, as presented in **Fig. 4.1**. The time dependent cylinder stretching velocity is assumed to be  $u_w(t, z) = \frac{az}{1-\gamma t}$  where  $a, \gamma > 0$ . Transport of solutal and thermal energy in the flow is conducted by using Cattaneo-Christov double diffusion theory. By keep in the mind the above assumptions for given flow and energy transport problem and eliminating  $\mathbf{S}$  in Eqs. (1.2) and (1.12),  $\hat{\mathbf{q}}$  in Eqs. (1.3) and (1.10) and  $\hat{\mathbf{J}}$  in Eqs. (1.4) and (1.11) (cf. Chapter 1), respectively, we arrived

at following set of governing partial differential equations:

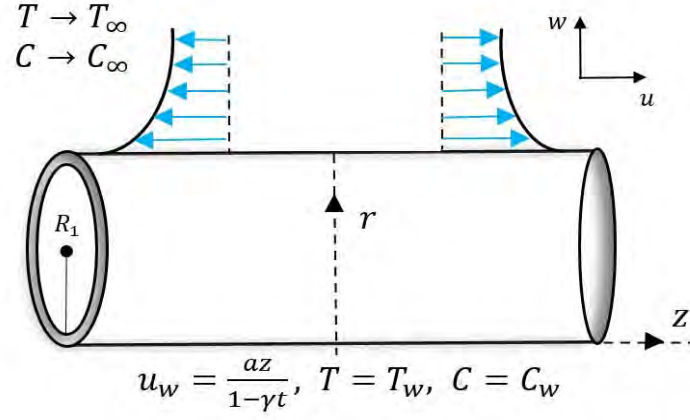


**Figure 4.1:** Graphical representation of phenomena.

$$\frac{\partial(ru)}{\partial z} + \frac{\partial(rw)}{\partial r} = 0, \quad (4.1)$$

$$\begin{aligned} \frac{\partial u}{\partial t} + u \frac{\partial u}{\partial z} + w \frac{\partial u}{\partial r} &= \nu \left[ \frac{\partial^2 u}{\partial r^2} + \frac{1}{r} \frac{\partial u}{\partial r} \right] \\ -\lambda_1 \left[ \frac{\partial^2 u}{\partial t^2} + 2u \frac{\partial^2 u}{\partial t \partial z} + 2w \frac{\partial^2 u}{\partial r \partial t} + 2uw \frac{\partial^2 u}{\partial r \partial z} + w^2 \frac{\partial^2 u}{\partial r^2} + u^2 \frac{\partial^2 u}{\partial z^2} \right] &, \end{aligned} \quad (4.2)$$

$$\begin{aligned} \frac{\partial T}{\partial t} + u \frac{\partial T}{\partial z} + w \frac{\partial T}{\partial r} + \lambda_t \left[ \begin{aligned} &\frac{\partial^2 T}{\partial t^2} + \frac{\partial u}{\partial t} \frac{\partial T}{\partial z} + 2u \frac{\partial^2 T}{\partial t \partial z} + \frac{\partial w}{\partial t} \frac{\partial T}{\partial r} + 2w \frac{\partial^2 T}{\partial t \partial r} + 2uw \frac{\partial^2 T}{\partial r \partial z} \\ &+ w^2 \frac{\partial^2 T}{\partial r^2} + u^2 \frac{\partial^2 T}{\partial z^2} + u \frac{\partial u}{\partial z} \frac{\partial T}{\partial z} + w \frac{\partial u}{\partial r} \frac{\partial T}{\partial z} + u \frac{\partial w}{\partial z} \frac{\partial T}{\partial r} + w \frac{\partial w}{\partial r} \frac{\partial T}{\partial r} \end{aligned} \right] \\ &= \frac{1}{(\rho c_p)_f} \frac{1}{r} \frac{\partial}{\partial r} \left[ K(T) \left( r \frac{\partial T}{\partial r} \right) \right], \end{aligned} \quad (4.3)$$

$$\begin{aligned} \frac{\partial C}{\partial t} + u \frac{\partial C}{\partial z} + w \frac{\partial C}{\partial r} + \lambda_c \left[ \begin{aligned} & \frac{\partial^2 C}{\partial t^2} + \frac{\partial u}{\partial t} \frac{\partial C}{\partial z} + 2u \frac{\partial^2 C}{\partial t \partial z} + \frac{\partial w}{\partial t} \frac{\partial C}{\partial r} + 2w \frac{\partial^2 C}{\partial t \partial r} + 2uw \frac{\partial^2 C}{\partial r \partial z} \\ & + w^2 \frac{\partial^2 C}{\partial r^2} + u^2 \frac{\partial^2 C}{\partial z^2} + u \frac{\partial u}{\partial z} \frac{\partial C}{\partial z} + w \frac{\partial u}{\partial r} \frac{\partial C}{\partial z} + u \frac{\partial w}{\partial z} \frac{\partial C}{\partial r} + w \frac{\partial w}{\partial r} \frac{\partial C}{\partial r} \end{aligned} \right] \\ = D_B \frac{1}{r} \frac{\partial}{\partial r} \left[ \left( r \frac{\partial C}{\partial r} \right) \right]. \end{aligned} \quad (4.4)$$

The corresponding boundary conditions for given problems are

$$u(t, z, r) = u(t, z) = \frac{az}{1-\gamma t}, \quad w(t, z, r) = 0, \quad T = T_w, \quad C = C_w \quad \text{at } r = R_1, \quad (4.5)$$

$$u \rightarrow 0, \quad T \rightarrow T_\infty, \quad C \rightarrow C_\infty \quad \text{as } r \rightarrow \infty. \quad (4.6)$$

Here  $K(T) = k_\infty(1 + \epsilon\theta)$  is the variable thermal conductivity ( $k_\infty$  free stream conductivity,  $\epsilon$  small conductivity parameter and  $\theta$  the dimensionless temperature).

With the help of following conversion parameters

$$\begin{aligned} u &= -\frac{R_1}{r} \sqrt{\frac{a\nu}{1-\gamma t}} f(\eta), \quad w = \frac{az}{1-\gamma t} f'(\eta), \quad \theta(\eta) = \frac{T-T_\infty}{T_w-T_\infty} \\ \phi(\eta) &= \frac{C-C_\infty}{C_w-C_\infty}, \quad \eta = \sqrt{\frac{a}{\nu(1-\gamma t)}} \left( \frac{r^2-R_1^2}{2R_1} \right), \end{aligned} \quad (4.7)$$

Eqs. (4.2) – (4.6) are transformed into following system of ODEs

$$\begin{aligned} (1 + 2\alpha\eta)f'''' + 2\alpha f f'' - \frac{S}{2}\eta f'' - S f' - f'^2 + f f'' - \frac{7}{4}\beta_1 S^2 \eta f'' \\ - \frac{\beta_1}{4}\eta^2 S^2 f''' - 2\beta_1 S^2 f' - 2S\beta_1 f'^2 - \beta_1 \eta S f' f'' + S\beta_1 \eta f f''' \\ + 3S\beta_1 f f'' + 2\beta_1 f f' f'' - \frac{\alpha\beta_1}{1+2\alpha\eta} f^2 f'' - \beta_1 f^2 f''' = 0, \end{aligned} \quad (4.8)$$

$$\begin{aligned}
& (1 + 2\alpha\eta)\theta'' + \text{Pr}(f\theta' - \frac{S}{2}\eta\theta') + (1 + 2\alpha\eta)(\theta\theta'' + \theta'^2)\epsilon \\
& + 2\alpha\theta' + 2\alpha\epsilon\theta\theta' - \text{Pr}\beta_t(\frac{3}{4}S^2\eta\theta' - \frac{3S}{2}\theta'f - \frac{S}{2}\eta\theta'f' \\
& + \frac{1}{4}S^2\eta^2\theta'' - S\eta f\theta'' + \theta''f^2 - \theta'ff') = 0, \tag{4.9}
\end{aligned}$$

$$\begin{aligned}
& (1 + 2\alpha\eta)\phi'' + Le\text{Pr}(f\phi' - \frac{S}{2}\eta\phi') + 2\alpha\phi' \\
& - Le\text{Pr}\beta_c(\frac{3}{4}S^2\eta\phi' - \frac{3S}{2}\phi'f - \frac{S}{2}\eta\phi'f' \\
& + \frac{1}{4}S^2\eta^2\phi'' - S\eta f\phi'' + \phi''f^2 - \phi'ff') = 0, \tag{4.10}
\end{aligned}$$

$$f(0) = 0, \quad f'(0) = 1, \quad \theta(0) = 1, \quad \phi(0) = 1, \tag{4.11}$$

$$f'(\infty) = 0, \quad \theta(\infty) = 0, \quad \phi(\infty) = 0. \tag{4.12}$$

The dimensionless group of paramters in above equations are

$$\left\{ \begin{array}{l} S (= \frac{\gamma}{a}), \alpha \left( = \frac{1}{R_1} \sqrt{\frac{\nu(1-\gamma t)}{a}} \right), \beta_1 \left( = \frac{\lambda_1 a}{1-\gamma t} \right), \beta_t \left( = \frac{\lambda_t a}{1-\gamma t} \right) \\ , \beta_c \left( = \frac{\lambda_c a}{1-\gamma t} \right), \text{Pr} \left( = \frac{\nu}{\alpha_1} \right), Le \left( = \frac{\alpha_1}{D_B} \right) \end{array} \right\}$$

and these are termed as the unsteadiness parameter, the curvature parameter, the Maxwell parameter, the thermal relaxation time parameter, the mass relaxation time parameter, the Prandtl number and the Lewis number, respectively.



## 4.2 Computational Procedure

This section is proposed to evaluate the solutions of coupled ODEs for the flow of fluid and energy transport Eqs. (4.8), (4.9) and (4.10) with the specified boundary conditions given in Eqs. (4.11) and (4.12) the numerical method `bvp4c` built in MATLAB. The system of first order ordinary differential equations is needed to utilize this proposed technique. For this purpose the governing ODEs are transformed as follows:

$$f = y_1, f' = y_2, f'' = y_3, f''' = yy_1, \quad (4.13)$$

$$\theta = y_4, \theta' = y_5, \theta'' = yy_2, \quad (4.14)$$

$$\phi = y_6, \phi' = y_7, \phi'' = yy_3. \quad (4.15)$$

The resulting first order ODEs are as follows

$$yy_1 = \frac{y_2^2 - y_1y_3 + Sy_2 + \frac{S}{2}\eta y_3 - 2\alpha y_1y_3 + \frac{7}{4}\beta_1 S^2\eta y_3 + 2\beta_1 S^2 y_2 + 2\beta_1 S y_1^2 + \beta_1 S y_1y_3 - 3\beta_1 S y_1y_3 - 2\beta_1 y_1y_2y_3 + \frac{\alpha\beta_1}{1+2\alpha\eta} y_1^2 y_3}{a_1}, \quad (4.16)$$

$$yy_2 = \frac{\text{Pr} \beta_t (y_1y_2y_5 - \frac{3}{2}S y_5y_1 - \frac{S}{2}\eta y_2y_5 + \frac{3}{4}S^2\eta y_5) + \text{Pr}(\frac{S}{2}\eta y_5 - y_1y_5) - 2\alpha y_5}{a_2}, \quad (4.17)$$

$$yy_3 = \frac{Le \text{Pr} \beta_c (y_1y_2y_7 - \frac{3}{2}S y_1y_7 - \frac{S}{2}\eta y_2y_7 + \frac{3}{4}S^2\eta y_7) + Le \text{Pr}(\frac{S}{2}\eta y_7 - y_1y_7 - 2\alpha y_7)}{a_3}, \quad (4.18)$$

where

$$a_1 = 1 + 2\alpha\eta - \frac{\beta_1}{4}\eta^2 S^2 + S\beta_1\eta y_1 - \beta_1 y_1^2,$$

$$a_2 = 1 + 2\alpha\eta - \frac{\text{Pr}}{4}\beta_t S^2 \eta^2 + \beta_t S \text{Pr} \eta y_1 + (1 + 2\alpha\eta)\epsilon y_4 - \text{Pr} \beta_t y_1^2,$$

$$a_3 = 1 + 2\alpha\eta - \frac{Le \text{Pr}}{4}\beta_c S^2 \eta^2 + Le\beta_c S \text{Pr} \eta y_1 - Le \text{Pr} \beta_c y_1^2.$$

Boundary conditions for the above first order differential system are

$$y_1(0) = 0, \quad y_2(0) = 1, \quad y_4(0) = 1, \quad y_6(0) = 1, \quad (4.19)$$

$$y_2(\infty) = 0, \quad y_4(\infty) = 0, \quad y_6(\infty) = 0. \quad (4.20)$$

### 4.3 Analysis of Results

The flow velocity, temperature distribution and mass transport in Maxwell liquid are the key points of this physical problem. Impact of pertinent parameters with following fixed values  $S = \epsilon = 0.01$ ,  $\beta_1 = \beta_t = \beta_c = 0.5$ ,  $\text{Pr} = 6.5$ ,  $Le = 6.5$  on the flow field, thermal and concentration energy distribution is presented graphically with the comparison of cylinder and sheet. It is observed that there is higher energy transportation in case of cylinder than sheet. **Figs. 4.2(a–c)** explore the impact of curvature parameter on flow of fluid, temperature and concentration, respectively. For higher values of curvature parameter  $\alpha$  we noted an increasing trend in the velocity field, temperature and concentration distributions. Physically, the higher value of  $\alpha$  reduces the radius of the cylinder thus the influence of boundary in fluid motion decreases. Hence as a result velocity of fluid increases and corresponding heat and mass transportation in the fluid enhance. The increasing trend is observed for thermal and concentration fields in

the case of growing values of Maxwell parameter  $\beta_1$ . The adverse behavior is found for flow field as shown in **Fig. 4.3(a – c)**. Physically, the Maxwell parameter  $\beta_1$  describes the rheology of viscoelastic type material. The Maxwell parameter  $\beta_1$  is the dimensionless relaxation time. The relaxation time is used to depict the phenomenon of stress relaxation and stress relaxation (retain in deformation of a material after sudden relaxation in applied stress) observed due to the elasticity of the material. Therefore material for the higher value of  $\beta_1$  behaves like a solid. It means more time is required for the material to retain its deformation, thus, as result the decline in fluid velocity is observed due to the higher value of  $\beta_1$ . On the other hand, the energy transport phenomenon boost up for the same trend of  $\beta_1$  due to an increase in heat conduction rate.

Plots in **Figs. 4.4(a, b)** describe the effect of unsteadiness parameter  $S$  on heat and mass transportation mechanisms. Both the heat and solutal energy transport boost up for increasing values of  $S$ . **Figs. 4.5(a, b)** are sketched to depict the impact on thermal and solutal energy transfer rate of thermal and mass relaxation time parameters  $\beta_t$  and  $\beta_c$ . Increasing values of both thermal relaxation time and solutal relaxation time parameter declines the temperature and concentration fields, respectively. Physically, relaxation time parameter in the Cattaneo-Christov heat flux model due to increasing trend control the instant propagation of thermal energy waves in a given medium. Therefore the fluid with enlarging value of relaxation time parameters required more time for the transportation of heat and solutal energy. As a result, the decrease in temperature and solutal fields is noted. The relative importance of momentum, thermal and mass diffusivity is described by Prandtl number  $Pr$  and Lewis number  $Le$ . **Figs. 4.6(a, b)** are indicated the variation in temperature and concentration profiles via Prandtl and Lewis numbers, respectively. We conclude that both temperature and concentration fields

decrease for the enhanced values of  $Pr$  and  $Le$ , respectively. Physically, the Prandtl number with higher values reduce the thermal diffusivity of the fluid due to which the specific heat capacity ratio of fluid enhance and increasing values of  $Le$  decrease the mass diffusion coefficient. Thus, as a consequence, the transfer rate of heat and mass decreases in the fluid flow. The thermal conductivity parameter  $\varepsilon$  boosts up the heat transfer rate of the fluid due to this the temperature field enhances as shown in **Fig. 4.7**.

#### 4.4 Outcomes Validation and Surface Thermal and Solutal Gradients

A comparison is given in **Table 4.1** for reduced  $-f''(0)$  with varying values of  $\beta_1$  which assure the validation of present results. **Table 4.2** is provided for the numerical values of thermal and solutal gradients at cylinder surface with varying values of pertinent parameters. It is found that the both  $-\theta'(0)$  and  $-\phi'(0)$  are decreases with higher values of unsteadiness parameter  $S$  and increases for Prandtl number ( $Pr$ ) and Lewis number ( $Le$ ), respectively.

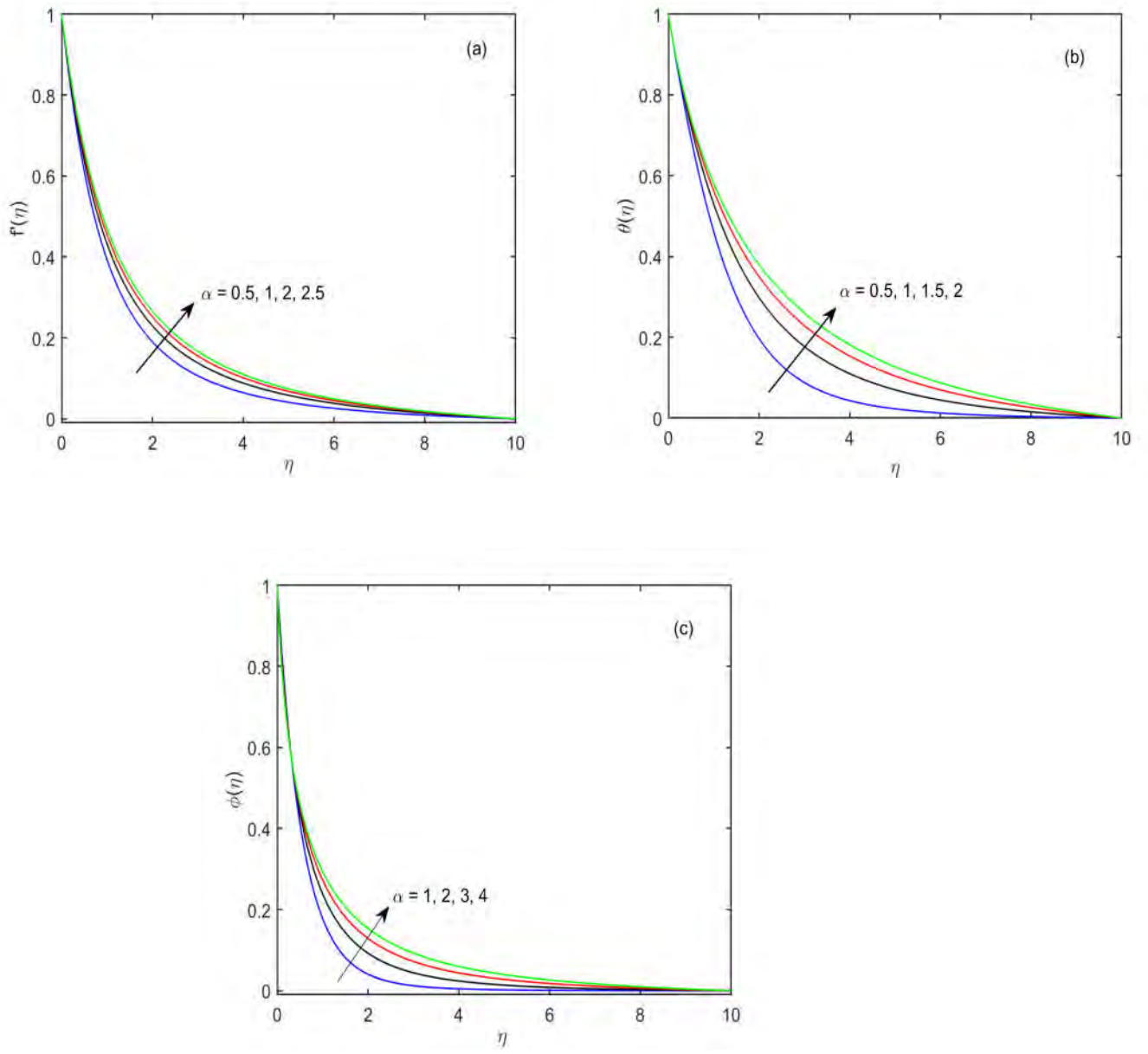


**Figure 4.2:** The velocity, temperature and concentration profiles via  $\alpha$ .

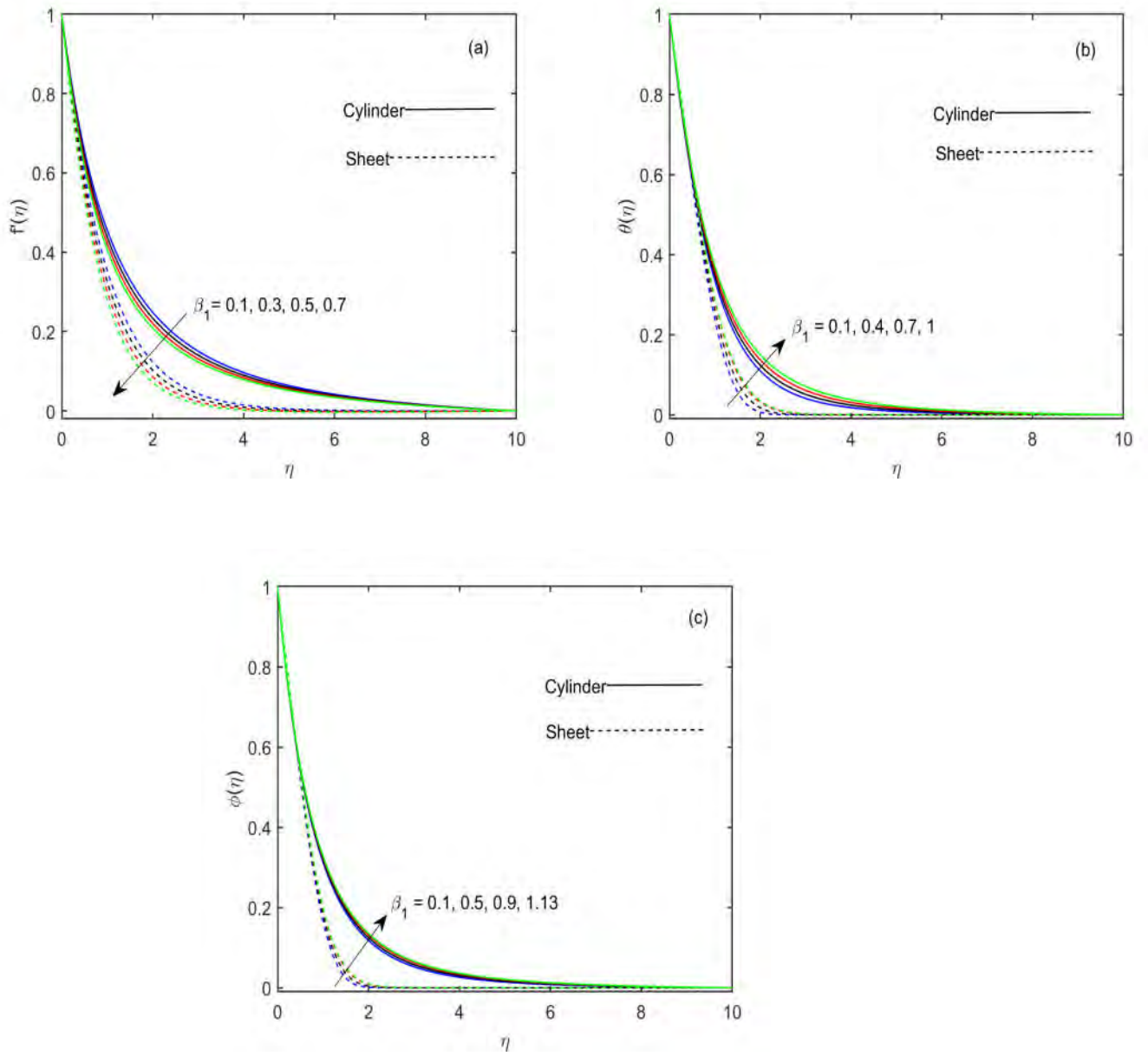


**Figure 4.3(a – c):** The velocity, temperature and concentration profiles via  $\beta_1$ .

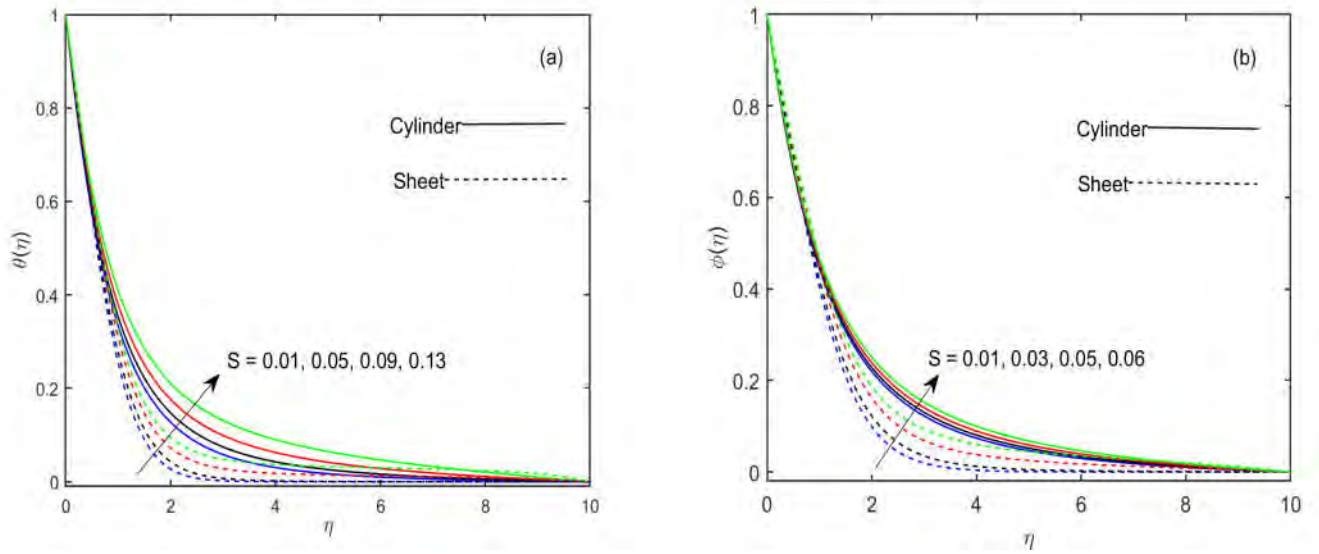


**Figure 4.4:** The temperature and concentration profiles via  $S$ .

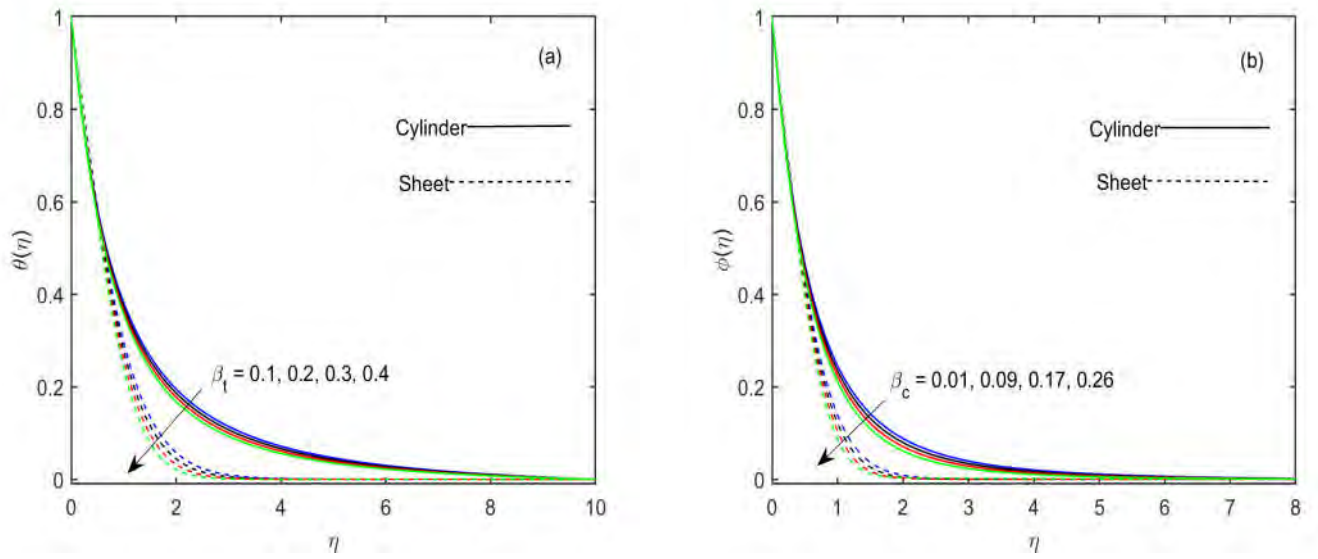


**Figure 4.5:** The temperature and concentration profiles via  $\beta_t$  and  $\beta_c$ , respectively.

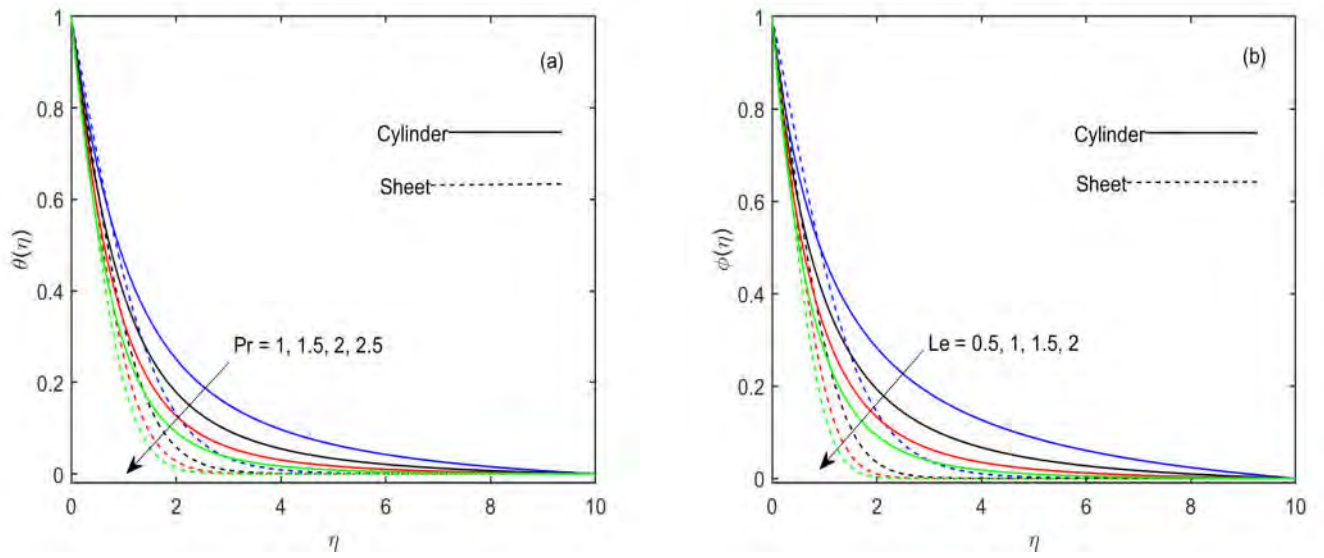


**Figure 4.6:** The temperature and concentration profiles via  $Pr$  and  $Le$ , respectively.

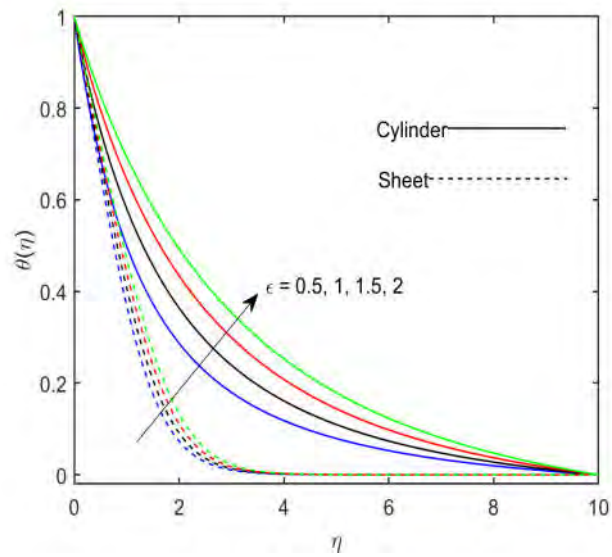


**Figure 4.7:** The temperature profile via  $\epsilon$ .



**Table 4.1:** Numerical values of  $-f''(0)$  for different values of  $\beta_1$  when  $\alpha = S = 0$ .

$\beta_1$	$-f''(0)$				
	Ref. [72]	Ref. [73]	Ref. [74]	Present (bvp4c)	Present (HAM)
0.0	1.000000	1.000000	1.000000	1.000000	1.000000
0.1			1.026183	1.026190	1.026166
0.2	1.051948	1.051889	1.051889	1.051892	1.051866
0.3			1.077125	1.077127	1.075466
0.4	1.101850	1.101903	1.101903	1.101903	1.101880
0.5			1.126235	1.126234	1.125678
0.6	1.150163	1.150137	1.150137	1.150136	1.150144
0.7			1.173624	1.173623	1.173629
0.8	1.196692	1.196711	1.196711	1.196709	1.196455
0.9			1.219414	1.219413	1.219419
1.0			1.241747	1.241741	1.124567

**Table 4.2:** Numerical values of  $-\theta'(0)$  and  $-\phi'(0)$  in the limiting case for  $\beta_t = \beta_c = 0$  and

$\alpha = 1$ .

$S$	$\beta_1$	$M$	$\epsilon$	Pr	$Le$	$-\theta'(0)$	$-\phi'(0)$
0.1	0.1	01	0.1	6.5	6.5	1.919590	5.034541
0.2						1.820360	4.858232
0.3						1.709981	4.671831
0.1	0.1	01	0.1	6.5	6.5	1.925401	5.034541
			0.3			1.922490	4.995886
			0.5			1.919592	4.958616
0.1	0.1	01	0.1	6.5	6.5	1.919501	
			02			1.856914	
			03			1.799712	
0.1	0.1	01	0.1	6.5	6.5	1.919591	5.043821
			0.2			1.825890	5.041512
			0.3			1.741672	5.039201
0.1	0.1	01	0.1	02	6.5	1.141467	
				04		1.508042	
				06		1.842103	
0.1	0.1	01	0.1	6.5	02		2.799817
					04		3.957422
					06		4.837691

## Chapter 5

# Buoyancy Driven Unsteady

# Stagnation Point Flow of Maxwell

# Fluid over a Stretchable Cylinder

This chapter is proposed to investigate the characteristics of stagnation point flow of Maxwell fluid generated by vertical stretchable cylinder under the influence of buoyancy force. The non-Fourier's heat conduction approach is considered here for the thermal energy transportation in flow. Moreover, analysis of two types of heating agents at surface namely prescribed surface temperature (PST) and constant wall temperature (CWT) is performed. The resulting partial differential equations for governing the flow and thermal energy transport problem are converted into the ordinary differential system through suitable flow ansatz. The acquired outcomes for the temperature field are presented graphically with the comparison of PST and CWT. The results of the present study revealed that a higher rate of thermal energy transfer is noted in the case of CWT. Moreover, it is observed that higher magnitude of the

buoyancy force enhances fluid flow velocity in assisting mode. The increasing values of the thermal relaxation time parameter decrease the heat transport in the fluid. A comparison is given of surface velocity gradient for magnetic parameter and Deborah number with existing literature.

## 5.1 Mathematical Formulation

Consider the unsteady, laminar and incompressible 2D flow of Maxwell fluid over vertical stretching cylinder of radius  $R_1$  with  $u$  and  $w$  are velocity components along  $z - axis$  (axis of cylinder) and  $r - axis$  (normal to  $z$ -axis), respectively. The stretching velocity of the cylinder and free stream velocity are assumed as  $u_w(t, z) = \frac{az}{1-\gamma t}$  and  $u_e(t, z) = \frac{cz}{1-\gamma t}$ , respectively, where  $a$ ,  $c$  and  $\gamma$  are positive constants. Suppose that a magnetic field  $\vec{B} = (0, 0, B_0)$  applied normal to the flow field and the force of gravity  $\mathbf{g} = [g, 0, 0]$  acts along the axis of cylinder. The whole flow scheme is presented in **Fig. 5.1**.

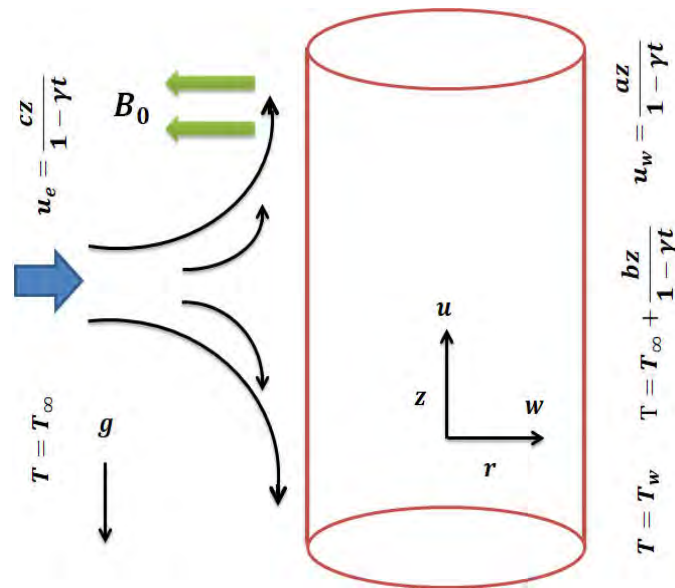


**Fig. 5.1:** A physical layout of the problem.

The constitutive equations for the flow of Maxwell fluid in addition to heat transport with all above assumptions are obtained by eliminating  $\mathbf{S}$  and  $\mathbf{q}$  in Eqs. (1.5, 1.12) and Eqs. (1.3, 1.10) (cf. Chapter 1) we acquired the following governing partial differential equations

$$\frac{\partial(ru)}{\partial z} + \frac{\partial(rw)}{\partial r} = 0, \quad (5.1)$$

$$\begin{aligned} & \frac{\partial u}{\partial t} + u \frac{\partial u}{\partial z} + w \frac{\partial u}{\partial r} + \lambda_1 \left[ \begin{aligned} & \frac{\partial^2 u}{\partial t^2} + \frac{\partial^2 u_e}{\partial t^2} + 2u \frac{\partial^2 u}{\partial t \partial z} + 2u_e \frac{\partial^2 u_e}{\partial t \partial z} \\ & + 2w \frac{\partial^2 u}{\partial r \partial t} + 2uw \frac{\partial^2 u}{\partial r \partial z} + w^2 \frac{\partial^2 u}{\partial r^2} + u^2 \frac{\partial^2 u}{\partial z^2} \end{aligned} \right] \\ = & \nu \left[ \frac{\partial^2 u}{\partial r^2} + \frac{1}{r} \frac{\partial u}{\partial r} \right] + gB_T [(T - T_\infty) + \lambda_1 \left\{ \frac{\partial T}{\partial t} + u \frac{\partial T}{\partial z} + w \frac{\partial T}{\partial r} - (T - T_\infty) \frac{\partial u}{\partial z} \right\}] \\ & + \frac{\partial u_e}{\partial t} + u_e \frac{\partial u_e}{\partial z} - \frac{\sigma B_0^2}{\rho} [(u - u_e) + \lambda_1 \left\{ \frac{\partial u}{\partial t} - \frac{\partial u_e}{\partial t} + w \frac{\partial u}{\partial r} \right\}], \end{aligned} \quad (5.2)$$

$$\begin{aligned} & \frac{\partial T}{\partial t} + u \frac{\partial T}{\partial z} + w \frac{\partial T}{\partial r} + \lambda_t \left[ \begin{aligned} & \frac{\partial^2 T}{\partial t^2} + \frac{\partial u}{\partial t} \frac{\partial T}{\partial z} + 2u \frac{\partial^2 T}{\partial t \partial z} + \frac{\partial w}{\partial t} \frac{\partial T}{\partial r} + 2w \frac{\partial^2 T}{\partial t \partial r} + 2uw \frac{\partial^2 T}{\partial r \partial z} \\ & + w^2 \frac{\partial^2 T}{\partial r^2} + u^2 \frac{\partial^2 T}{\partial z^2} + u \frac{\partial u}{\partial z} \frac{\partial T}{\partial z} + w \frac{\partial u}{\partial r} \frac{\partial T}{\partial z} + u \frac{\partial w}{\partial z} \frac{\partial T}{\partial r} + w \frac{\partial w}{\partial r} \frac{\partial T}{\partial r} \end{aligned} \right] \\ & = \frac{k}{(\rho c_p)} \frac{1}{r} \frac{\partial}{\partial r} \left[ r \frac{\partial T}{\partial r} \right], \end{aligned} \quad (5.3)$$

with the corresponding boundary conditions for given problems are

$$u(t, z, r) = u_w(t, z) = \frac{az}{1-\gamma t}, \quad w(t, z, r) = 0, \quad \text{at } r = R_1$$

$$T = T_w \text{ (CWT)}, \quad T = T_\infty + \frac{bz}{1-\gamma t} \text{ (PST)} \quad \text{at } r = R_1, \quad (5.4)$$

$$u \rightarrow u_e = \frac{cz}{1-\gamma t}, \quad T \rightarrow T_\infty, \quad \text{as } r \rightarrow \infty. \quad (5.5)$$

Introducing the following conversion parameters

$$\begin{aligned}
u &= \frac{az}{1-\gamma t} f'(\eta), \quad w = -\frac{R_1}{r} \sqrt{\frac{a\nu}{1-\gamma t}} f(\eta), \\
T &= T_\infty + (T_w - T_\infty) \theta(\eta) \text{ (CWT)}, \quad T = T_\infty + \frac{bz}{1-\gamma t} \theta(\eta) \text{ (PST)} \\
\eta &= \sqrt{\frac{a}{\nu(1-\gamma t)}} \left( \frac{r^2 - R_1^2}{2R_1} \right). \tag{5.6}
\end{aligned}$$

After substituting the overhead conversions Eq. (5.1) is satisfied automatically and Eqs. (5.2)–(5.5) yield

$$\begin{aligned}
&(1 + 2\alpha\eta) f''' + 2\alpha f f'' - \frac{S}{2} \eta f'' - S f' - f'^2 + f f'' - \frac{7}{4} \beta_1 S^2 \eta f'' \\
&- \frac{\beta_1}{4} \eta^2 S^2 f''' - 2\beta_1 S^2 f' - 2S\beta_1 f'^2 - \beta_1 \eta S f' f'' + S\beta_1 \eta f f''' \\
&+ 3S\beta_1 f f'' + 2\beta_1 f f' f'' - \frac{\alpha\beta_1}{1+2\alpha\eta} f^2 f'' - \beta_1 f^2 f''' \\
&+ AS + A^2 + \lambda(\theta + \beta_1 \frac{S}{2} \eta \theta' - \beta_1 \theta' f) - M f' + MA \\
&+ \beta_1 (2A^2 S + 2AS^2) - M\beta_1 (\frac{S}{2} \eta f'' - AS + S f' - f f'') = 0, \tag{5.7}
\end{aligned}$$

$$\begin{aligned}
&(1 + 2\alpha\eta) \theta'' + \text{Pr}(f \theta' - \frac{S}{2} \eta \theta') + 2\alpha \theta' \\
&- \text{Pr} \beta_t (\frac{3}{4} S^2 \eta \theta' - \frac{3S}{2} \theta' f - \frac{S}{2} \eta \theta' f' + \frac{1}{4} S^2 \eta^2 \theta'' \\
&- S \eta f \theta'' + \theta'' f^2 + \theta' f f') = 0, \quad \text{(CWT)} \tag{5.8}
\end{aligned}$$

$$\begin{aligned}
& (1 + 2\alpha\eta)\theta'' + \text{Pr}(f\theta' - \frac{S}{2}\eta\theta') + 2\alpha\theta' \\
& - \text{Pr} \beta_t (\frac{7S^2}{4}\eta\theta' + \frac{S^2}{4}\eta^2\theta'' + 2S^2\theta + \frac{S}{2}\eta\theta f'' + 3Sf'\theta + \frac{S}{2}\eta f'\theta' \\
& - \frac{7}{2}Sf\theta' - S\eta f\theta'' + f'^2\theta - ff''\theta + \theta''f^2 - \theta'ff') = 0, \quad \text{(PST)} \quad (5.9)
\end{aligned}$$

$$f = 0, \quad f' = 1, \quad \theta = 1, \quad \text{at } r = R_1 \quad (5.10)$$

$$f' \rightarrow A, \quad \theta \rightarrow 0. \quad \text{as } r \rightarrow \infty. \quad (5.11)$$

In the above equations,  $S$  ( $= \frac{\gamma}{a}$ ) is the unsteadiness parameter,  $\alpha$  ( $= \frac{1}{R_1} \sqrt{\frac{\nu(1-\gamma t)}{a}}$ ) the curvature parameter,  $\beta_1$  ( $= \frac{\lambda_1 a}{1-\gamma t}$ ) the Maxwell number,  $\text{Pr}$  ( $= \frac{\nu}{\alpha_1}$ ) the Prandtl number and  $\alpha_1 = \frac{k}{(\rho c_p)_f}$  the thermal diffusivity of fluid,  $\beta_t$  ( $= \frac{\lambda_t a}{1-\gamma t}$ ) the thermal relaxation time parameter,  $\lambda$  ( $= \frac{Gr}{\text{Re}_z^2}$ ) the buoyancy parameter in which  $Gr$  ( $= \frac{gB_T(T_w - T_\infty)z^3}{\nu^2}$ ) the Grashof number where  $\lambda > 0$  and  $\lambda < 0$  corresponds to the assisting and opposing modes of flow, respectively,  $A$  ( $= \frac{c}{a}$ ) the velocity ratio and  $M$  ( $= \frac{\sigma B_0^2(1-\gamma t)}{(\rho_f)a}$ ) the magnetic parameter.

## 5.2 Numerical Methodology

In this part, the numerical computation is performed of governing Eqs. (5.7) – (5.9) with corresponding boundary conditions in Eqs. (5.10) and (5.11). The bvp4c technique is utilized for the numerical results. By making the use of substitutions  $f = y_1$ ,  $f' = y_2$ ,  $f'' = y_3$ ,

$f''' = yy_1, \theta = y_4, \theta' = y_5, \theta'' = yy_2$ , the system first order ODEs are obtained as follows

$$\begin{aligned}
& y_2^2 - y_1y_3 + Sy_2 + \frac{S}{2}\eta y_3 - 2\alpha y_1 + \frac{7}{4}\beta_1 S^2\eta y_3 + \frac{\beta_1}{4}\eta^2 S^2 y_1 + 2\beta_1 S^2 y_2^2 \\
& + \beta_1 S\eta y_1 y_3 - S\beta_1 y_3 - 2S\beta_1 y_1 y_3 - 2\beta_1 y_1 y_2 y_3 + \frac{\alpha\beta_1}{1+2\alpha\eta} y_1^2 y_3 \\
& - AS - A^2 - \lambda(y_4 + \beta_1 \frac{S}{2}\eta y_5 - \beta_1 y_1 y_5 - \beta_1 y_2 y_4) \\
& + My_2 - MA + M\beta_1(\frac{S}{2}\eta y_3 + Sy_2 - AS - y_1 y_3)
\end{aligned}$$

$$yy_1 = \frac{\quad}{a_1}, \quad (5.12)$$

$$\begin{aligned}
& \Pr \beta_t(\frac{3}{4}S^2\eta y_5 - \frac{3}{2}Sy_5 y_1 - \frac{S}{2}\eta y_2 y_5 - y_1 y_2 y_5) \\
& + \Pr(\frac{S}{2}\eta y_5 - y_1 y_5) - 2\alpha y_5
\end{aligned}$$

$$yy_2 = \frac{\quad}{a_2}, \quad (5.13)$$

$$\begin{aligned}
& \Pr \beta_t(\frac{7}{4}S^2\eta y_5 + 2S^2 y_4 + \frac{S}{2}\eta y_4 y_3 + 3Sy_2 y_5) \\
& + \frac{S}{2}\eta y_2 y_5 - \frac{7S}{2}y_1 y_5 + y_2 y_2 y_4 - y_1 y_4 y_3 - y_1 y_2 y_5) \\
& + \Pr(\frac{S}{2}\eta y_5 - y_1 y_5) - 2\alpha y_5
\end{aligned}$$

$$yy_2 = \frac{\quad}{a_3}, \quad (5.14)$$

with

$$\begin{aligned}
a_1 &= 1 + 2\alpha\eta - \frac{\beta_1}{4}\eta^2 S^2 + S\beta_1\eta y_1 - \beta_1 y_1^2, \\
a_2 &= 1 + 2\alpha\eta - \frac{\Pr}{4}\beta_t S^2 \eta^2 + \beta_t S \Pr \eta y_1 - \Pr \beta_t y_1^2, \\
a_3 &= 1 + 2\alpha\eta - \frac{\Pr}{4}\beta_t S^2 \eta^2 + \beta_t S \Pr \eta y_1 - \Pr \beta_t y_1^2.
\end{aligned}$$



The boundary conditions for the above non-linear first order differential system are

$$y_1(0) = 0, y_2(0) = 1, y_4(0) = 1,$$

$$y_2(\infty) = A, y_4(\infty) = 0.$$

### 5.3 Physical Interpretation of Outcomes

In this section, numerical outcomes for the velocity and temperature fields are presented graphically. The results are compared for both Newtonian and non-Newtonian fluids in case of the flow field. The temperature profile plotted for both types of wall heating agents CWT and PST. It is noted that in the comparison of CWT and PST there is a higher rate of heat transfer in the fluid flow for CWT. The results are acquired with the following fixed values of physical parameters  $S = 0.01$ ,  $A = 0.05$ ,  $\lambda = \beta_t = 0.5$ ,  $\alpha = \beta_1 = 1$ ,  $\text{Pr} = 6.5$ .

The impact of curvature parameter  $\alpha$  on the flow and thermal fields presented in **Figures 5.2(a, b)**. It is noted that a higher value of  $\alpha$  enhances the fluid velocity and heat transport in the fluid away from the cylinder surface. Physically, for the increasing value of  $\alpha$  the radius of the cylinder decreases thus, the momentum boundary layer thickness reduces due to less influence of boundary in the fluid flow which leads to a rise in fluid flow velocity. **Figures 5.3(a, b)** enlisted to shows the influence of relaxation time parameter  $\beta_1$  on the velocity and temperature fields. The higher values of  $\beta_1$  fluid flow velocity decline and temperature profile enhance. Physically, the fluid behaves like a solid with an increase in time relaxation parameter  $\beta_1$  and fluidity of material reduces, thus, the fluid motion decrease. On the other hand, the temperature field boost up due to an increase in thermal conduction of fluid. **Figures 5.4(a, b)**

illustrate that velocity of the fluid reduces and the temperature field enhance with the increasing values of magnetic parameter  $M$ . Physically, the normally applied magnetic field to the fluid flow velocity produce Lorentz force which creates the resistance to the fluid motion in the boundary layer thus, results in the velocity field declines. Furthermore, in the case of thermal energy transportation, the conduction of heat energy in the fluid flow is increased by Lorentz force which enhances the fluid particles interaction.

The dimensionless parameter  $A$  corresponds to the velocities ratio of stretching cylinder to free stream velocity. **Figures 5.5(a, b)** depict that the velocity field enhances and the temperature field reduces due to the increment in velocity ratio parameter  $A$ . As  $A < 1$  means stretching cylinder velocity greater than free stream velocity and the converse is true for  $A > 1$ . So, for the case of  $A < 1$  the fluid velocity enhances with the rising value of  $A$  because a higher stretching velocity boost up the fluid motion. On the other hand, temperature profile decline for increasing values of  $A$ . Physically, the main mechanism for the transport of thermal energy in the fluid is forced convection. Thus, for higher values of  $A$ , the forced convection is diminished. Therefore the temperature field falls down in this situation. The buoyancy parameter  $\lambda$ , characterize the convection flow into forced and free convection with the regime of mixed convection in both aiding and opposing mode. The mixed convection region is defined as  $\lambda_{\min} < \lambda < \lambda_{\max}$  outside this region the flow is purely free or forced convection. In the present study of the heat transport phenomenon the mixed convection region is  $[0, 8]$  and  $[-8, 0]$  for aiding and opposing mode, respectively. The variation in velocity and temperature fields versus buoyancy parameter  $\lambda > 0$  (assisting mode) and  $\lambda < 0$  (opposing mode) is reported in plots of **Figures 5.6(a, b)** and **Figures 5.7(a, b)**, respectively. **Figures 5.6(a, b)** depict that in assisting mode the fluid motion boost up due to the same direction of forced and buoyant motion but

the thermal energy transport in the fluid flow declines. The converse results are observed in the opposing mode that is clear by **Figures 5.7(a, b)**. The velocity and temperature fields via unsteadiness parameter  $S$  are presented in **Figures 5.8(a, b)**. It is observed that the velocity of the fluid reduces for higher values of  $S$  and the temperature field declines in the case of PST because dimensionless temperature  $\theta$  has an inverse relation with the unsteady stretching rate of the cylinder. Moreover, the temperature field boost up in the case of CWT. Physically, more values of  $S$  decreases the stretching rate thus, in results velocity of the fluid reduces. To picture the impact of dimensionless time relaxation parameter  $\beta_t$  on the temperature field the **Figure 5.9** is delineated. It is observed that higher  $\beta_t$  decrease the fluid temperature in rising trend. Physically, the dimensionless time relaxation parameter  $\beta_t$  in the non-Fourier's heat flux model is the controlling parameter for the propagation of heat waves in the fluid. Thus, increment in  $\beta_t$  declines the heat transport in the fluid.

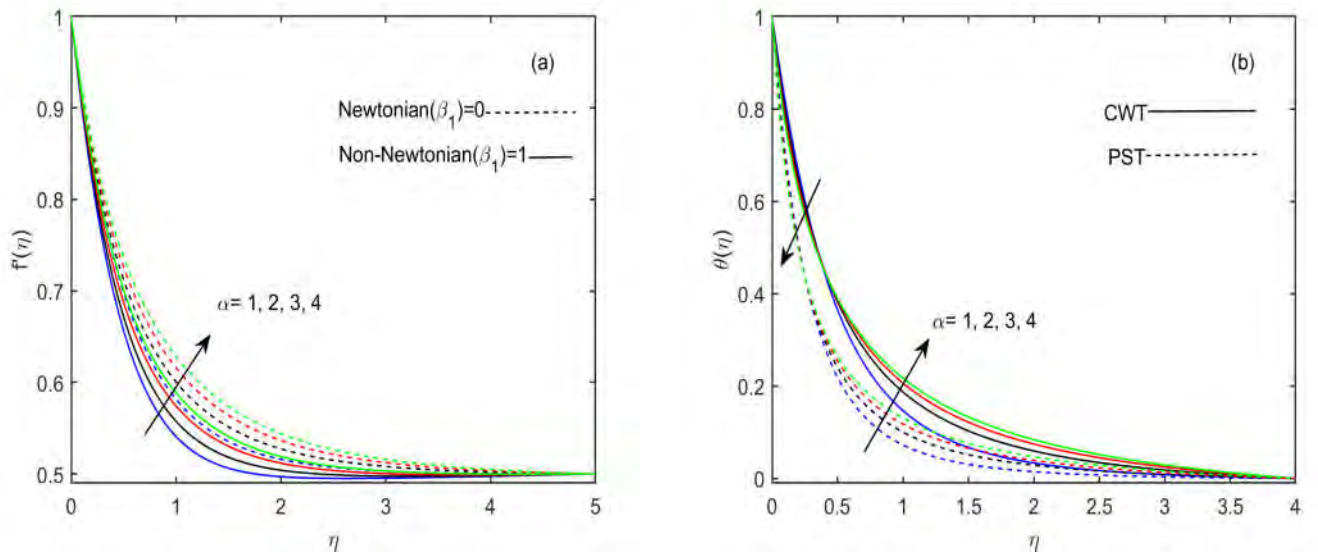


**Figure 5.2:** Plots of velocity and temperature fields via curvature parameter  $\alpha$ .

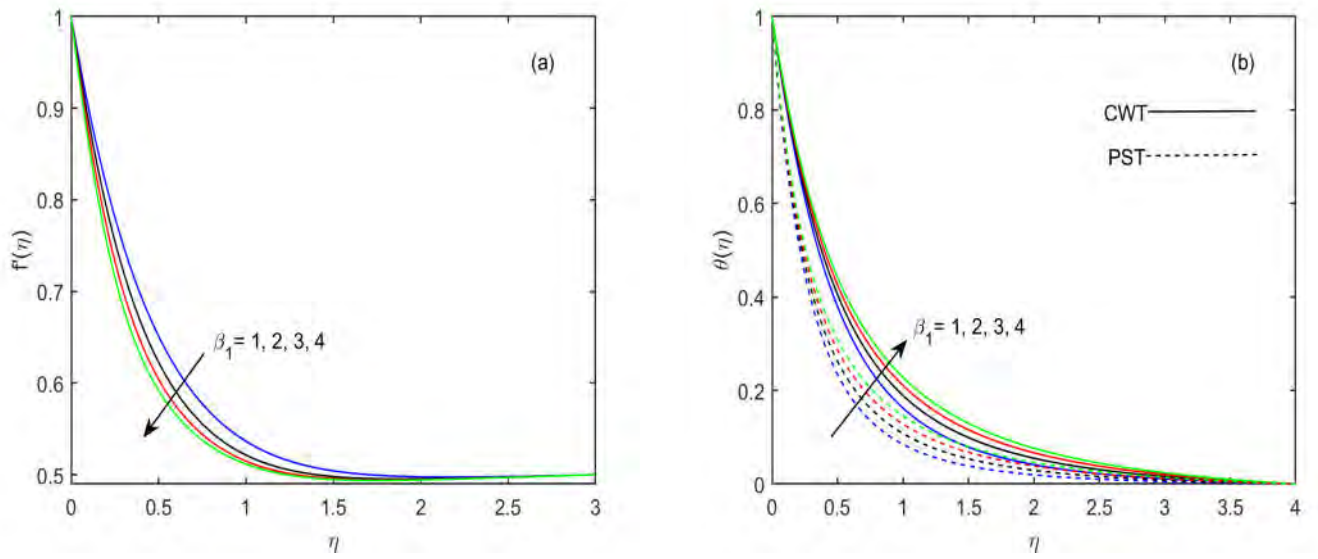


**Figure 5.3:** Plots of velocity and temperature fields via Deborah number  $\beta_1$ .

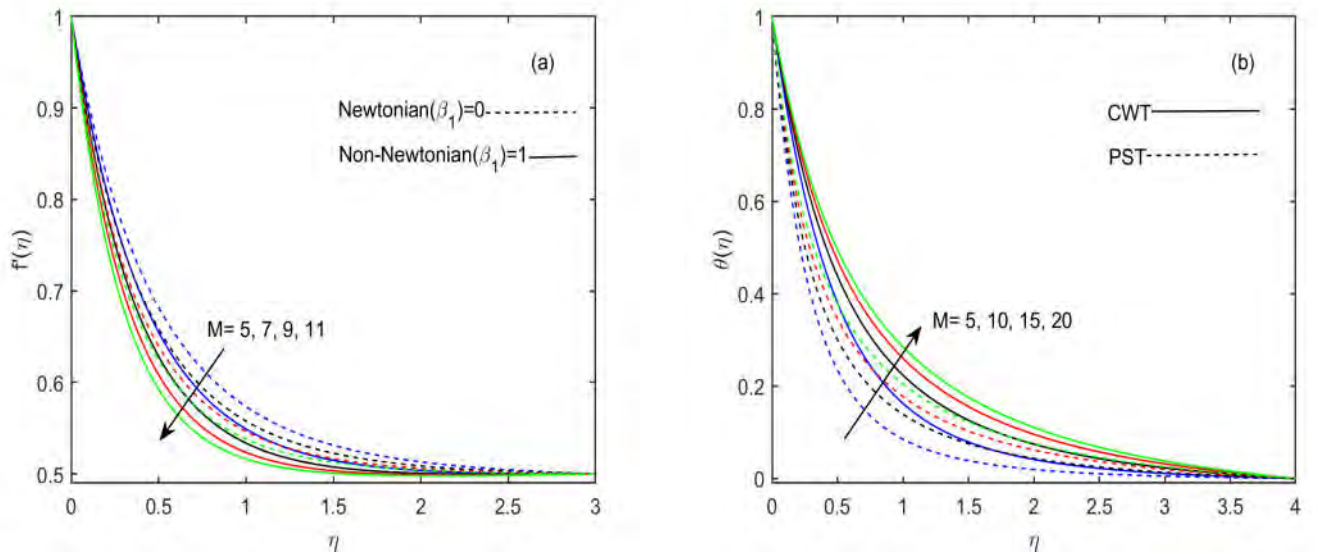


**Figure 5.4:** Plots of velocity and temperature fields via magnetic parameter  $M$ .

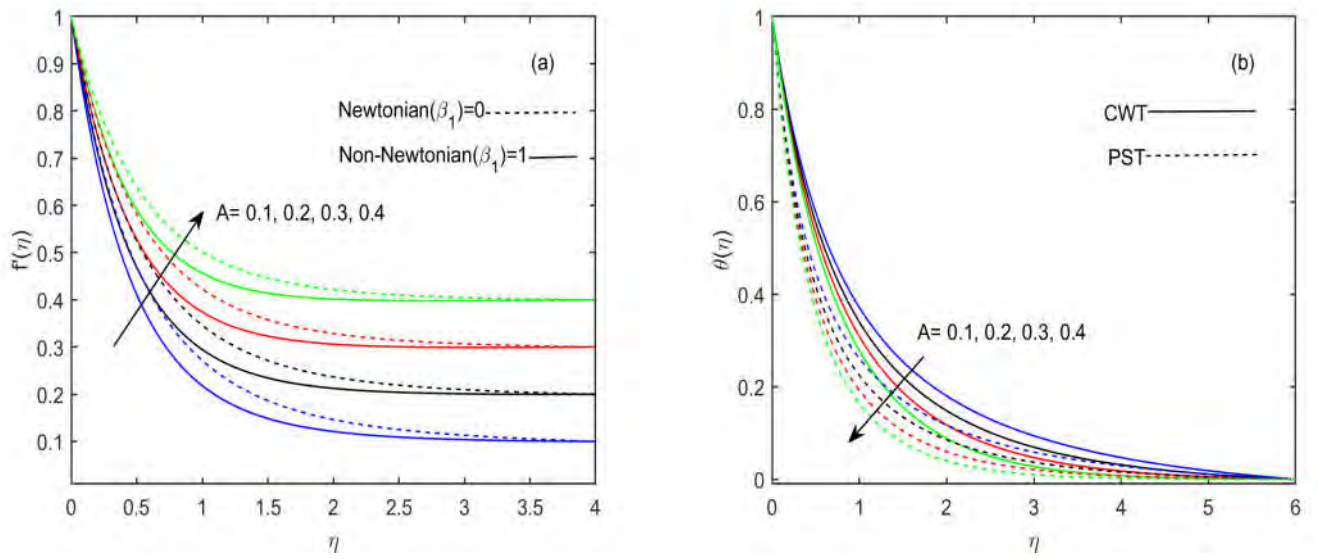


**Figure 5.5:** Plots of velocity and temperature fields via stagnation point  $A$ .

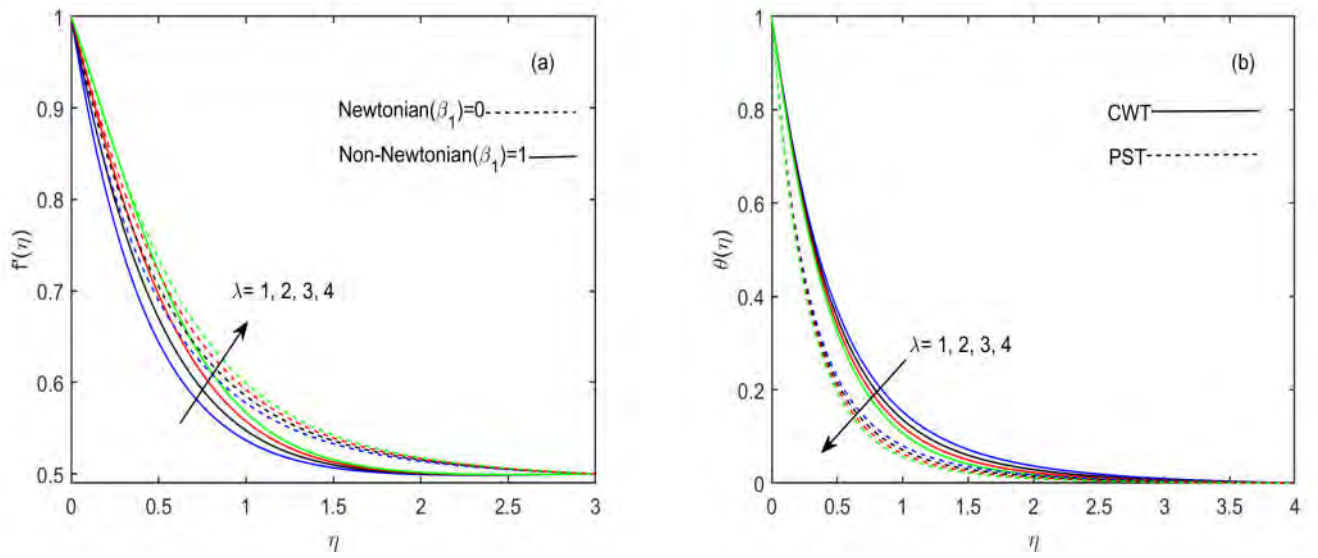


**Figure 5.6:** Plots of velocity and temperature fields via buoyancy parameter  $\lambda > 0$ .

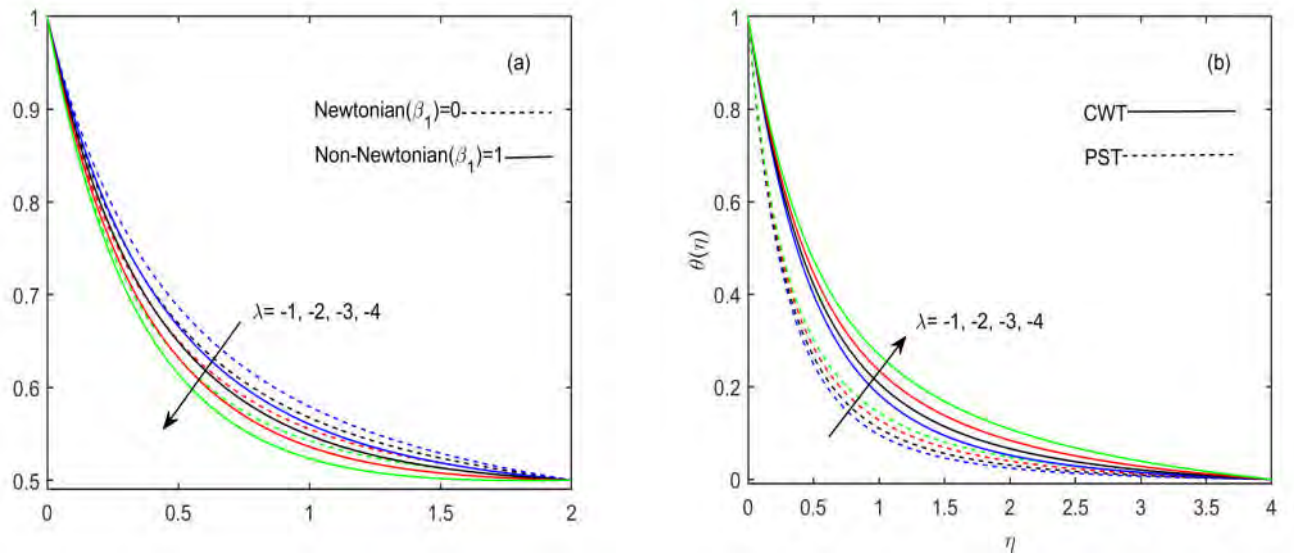


**Figure 5.7:** Plots of velocity and temperature fields via buoyancy parameter  $\lambda < 0$ .

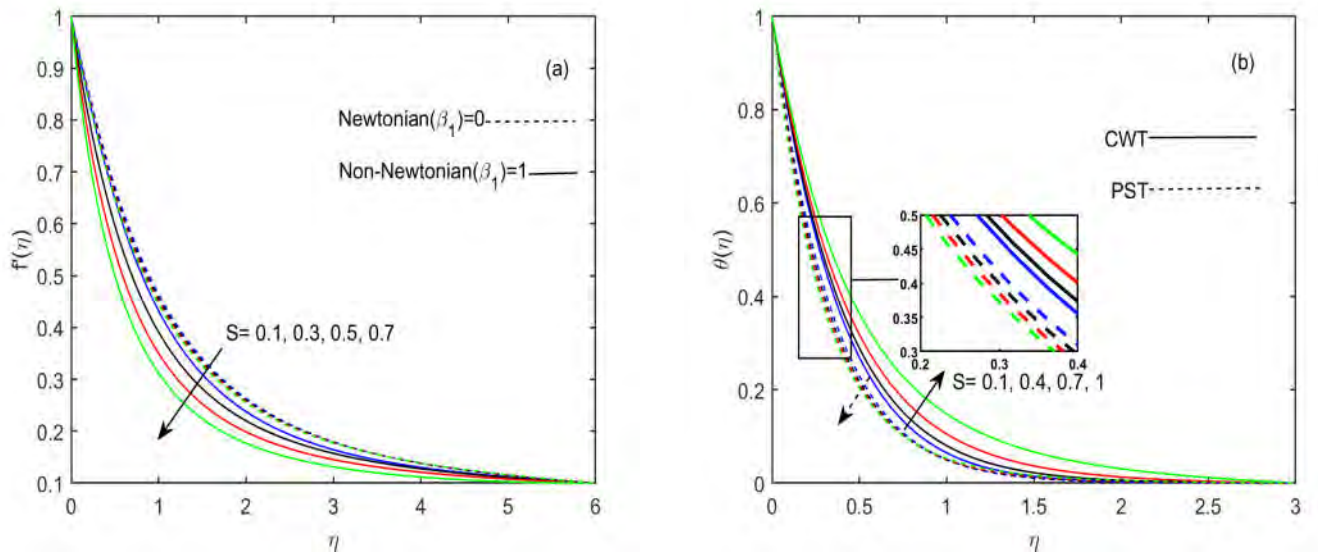


**Figure 5.8:** Plots of velocity and temperature fields via  $S$ .

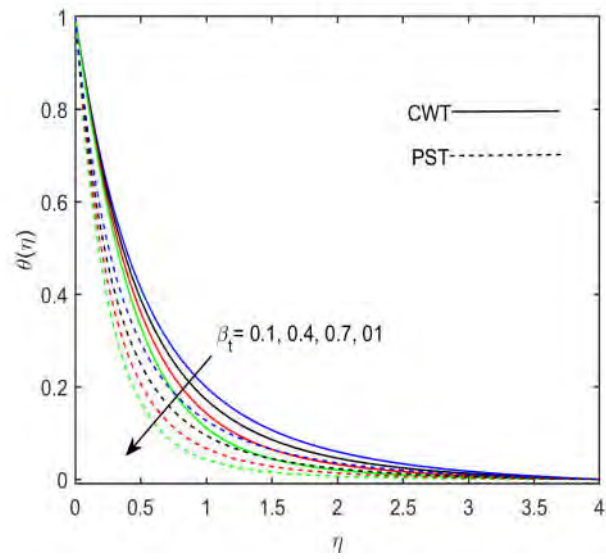


**Figure 5.9:** Plots of temperature field via  $\beta_t$ .

## 5.4 Validation of Present Outcomes

**Table 5.1** is constructed for  $-f''(0)$  for different values of  $\beta_1$  in limiting case. Moreover, **Table 5.2** shows the comparison of surface velocity gradient in the limiting case for with various values of  $M$  with previously published outcomes. These numerical results also are confirmed the validation of our analysis.

**Table 5.2:** Numerical values of surface velocity gradient  $-f''(0)$  for different values of  $\beta_1$  when  $\alpha = M = \lambda = S = 0$  and  $A = 2$ .

$\beta_1$	$-f''(0)$			
	Ref. [77]	Ref. [78]	Ref. [79]	Present results
0.0	0.99996	0.99997	1.000000	1.000000
0.2	1.05194	1.05194	1.051921	1.056190
0.4	1.10185	1.10184	1.101789	1.101792
0.6	1.15016	1.15016	1.150168	1.156027
0.8	1.19669	1.19669	1.196682	1.191509
1.2	1.28525	1.28525	1.285324	1.280354
1.6	1.36864	1.36864	1.368715	1.360341
2.0	1.44761	1.44761	1.447639	1.442810



**Table 5.1:** Numerical values of surface velocity gradient  $-f''(0)$  for different values of  $M$  when  $\alpha = \beta_1 = \lambda = S = 0$  and  $A = 2$ .

$M$	$-f''(0)$		
	Ref. [75]	Ref. [76]	Present results
0.0	2.0175	2.01750	2.017659
0.5	2.1363	2.13632	2.136319
1.0	2.2491	2.24910	2.249104
2.0	2.4597	2.35667	2.459660
3.0	2.6540	2.45967	2.653976
4.0			2.835224
5.0	3.0058	3.00578	3.005775
10	3.7447	3.74472	3.744716
20	4.9004	4.90037	4.900367
40	6.6339	6.63381	6.633770
60	8.0002	8.00032	8.000323
80	9.1642	9.16537	9.165366
100	10.1934	10.19819	10.19817

## Chapter 6

# Boundary Layer Flow of Maxwell Fluid Due to Stretchable Rotating Cylinder

The three-dimensional boundary layer flow of Maxwell fluid induced by stretchable rotating cylinder under the impact of a transverse magnetic field is investigated in this chapter. The constitutive flow equations for the current physical problem have been modeled and analyzed for the first time in literature. The cylinder swirl motion is kept constant in order to avoid the secondary axial flow. The concept of the boundary layer is employed to simplify the partial differential equations (PDEs) that govern the swirling flow of Maxwell fluid together with energy. The Reynolds number plays the role of flow controlling parameter here and a certain range of positive Reynolds number is acceptable for the current analysis. Thus, for the analysis of large Reynolds number the governing similar equations are simplified through suitable constitutive mathematical relations. The numerically computed outcomes for the flow, heat

and mass transport mechanisms are expressed graphically. The results proved that the velocity field and energy transport declines due to rise in Reynolds number and flow penetrates shallower into free stream fluid. Furthermore, it decays exponentially faster. An excellent validation of numerical results is assured through tabular data with existing literature.

## 6.1 Mathematical Modelling

Consider an elastic stretchable cylinder of radius  $R_1$  immersed into infinite viscoelastic Maxwell fluid and flow is produced due to swirling motion of the cylinder. The swirl motion of the cylinder is assumed as  $u_w = 2az$  (cylinder stretching velocity and  $a > 0$  having dimension  $T^{-1}$ ) and  $v_w = E$  (constant cylinder rotation and  $E$  has dimensions same as the velocity). Suppose that velocity field for flow is  $\mathbf{V} = [u, v, w]$  where  $u, v$ , and  $w$  are components along  $(z, \theta, r) - axes$ , respectively, and  $\mathbf{B} = [0, 0, B_0]$  the magnetic field applied normal to the flow in the direction of  $r - axis$ . (see **Fig. 6.1**).

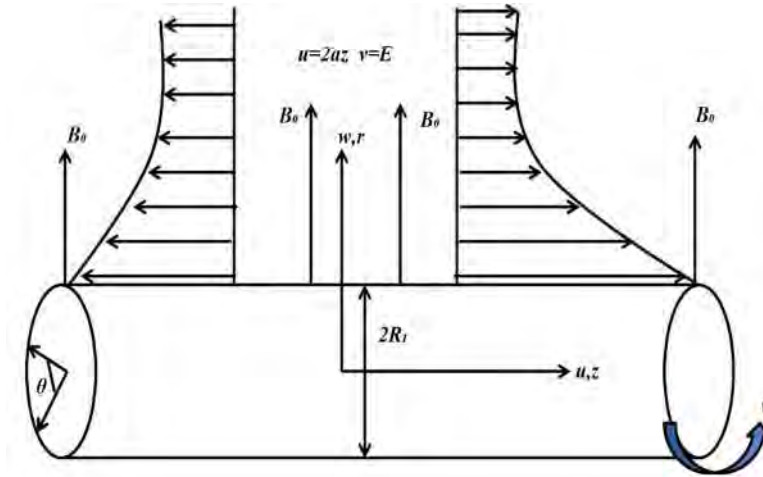


**Figure 6.1:** Schematic diagram for flow configuration.

Based on the assumptions of axisymmetric, steady, incompressible and by using Eqs. (1.1)–(1.4) with (1.7), (1.8) and (1.12) (cf. Chapter 1) we obtain the governing boundary layer PDEs for the present flow and energy transport problem as:

$$\frac{\partial u}{\partial z} + \frac{w}{r} + \frac{\partial w}{\partial r} = 0, \quad (6.1)$$

$$u \frac{\partial u}{\partial z} + w \frac{\partial u}{\partial r} + \lambda_1 \left[ u^2 \frac{\partial^2 u}{\partial z^2} + 2uw \frac{\partial^2 u}{\partial r \partial z} + w^2 \frac{\partial^2 u}{\partial r^2} \right] = \nu \left[ \frac{\partial^2 u}{\partial r^2} + \frac{1}{r} \frac{\partial u}{\partial r} \right] - \frac{\sigma B_0^2}{\rho} \left( u + \lambda_1 w \frac{\partial u}{\partial r} \right), \quad (6.2)$$

$$\begin{aligned} u \frac{\partial v}{\partial z} + w \frac{\partial v}{\partial r} + \frac{wv}{r} + \lambda_1 \left[ u^2 \frac{\partial^2 v}{\partial z^2} + 2uw \frac{\partial^2 v}{\partial r \partial z} + w^2 \frac{\partial^2 v}{\partial r^2} + \frac{2wv}{r} \frac{\partial w}{\partial r} + \frac{2uv}{r} \frac{\partial w}{\partial z} - \frac{2w^2 v}{r^2} \right] \\ = \nu \left[ \frac{\partial^2 v}{\partial r^2} - \frac{v}{r^2} + \frac{1}{r} \frac{\partial v}{\partial r} \right] - \frac{\sigma B_0^2}{\rho} \left( v + \lambda_1 w \frac{\partial v}{\partial r} - \lambda_1 \frac{wv}{r} \right), \end{aligned} \quad (6.3)$$

$$u \frac{\partial T}{\partial z} + w \frac{\partial T}{\partial r} = \alpha_1 \frac{1}{r} \frac{\partial}{\partial r} \left[ r \frac{\partial T}{\partial r} \right], \quad (6.4)$$

$$u \frac{\partial C}{\partial z} + w \frac{\partial C}{\partial r} = D_B \frac{1}{r} \frac{\partial}{\partial r} \left[ r \frac{\partial C}{\partial r} \right], \quad (6.5)$$

with the corresponding boundary conditions for given flow problem are

$$\begin{aligned} u(z, r) = 2az, \quad v(z, r) = E, \quad w(z, r) = 0, \quad T = T_w, \quad C = C_w \quad \text{at } r = R_1, \\ u \rightarrow 0, \quad T \rightarrow T_\infty, \quad C \rightarrow C_\infty \quad \text{as } r \rightarrow \infty. \end{aligned} \quad (6.6)$$

The governing equations can be reduced to ordinary differential equations with the help of

following transformations group

$$\begin{aligned}
u &= 2azf'(\eta), \quad v = Eg(\eta), \quad w = -aR_1 \frac{f(\eta)}{\eta^{1/2}}, \\
\theta(\eta) &= \frac{T-T_\infty}{T_w-T_\infty}, \quad \phi(\eta) = \frac{C-C_\infty}{C_w-C_\infty}, \quad \eta = \frac{r^2}{R_1^2}.
\end{aligned} \tag{6.7}$$

After substituting the overhead ansatz, Eq. (6.1) is satisfied automatically and Eqs. (6.2)–(6.6)

reduce to

$$\begin{aligned}
&\eta f''' + f'' + \operatorname{Re} f f'' - \operatorname{Re} f'^2 \\
&-\beta_1 \operatorname{Re} \left( \frac{f^2 f''}{\eta} + 2f^2 f''' - 4f f' f'' \right) - M \operatorname{Re} \left( \frac{f'}{2} - \beta_1 f f'' \right) = 0,
\end{aligned} \tag{6.8}$$

$$\begin{aligned}
&2\eta^2 g'' + 2\eta g' - \frac{g}{2} + 2\operatorname{Re} \eta f g' + \operatorname{Re} f g \\
&-\beta_1 \operatorname{Re} \left( 2f^2 g' + 4\eta f^2 g'' + 4f f' g - \frac{4f^2 g}{\eta} \right) - M \operatorname{Re} \left( g - 2\beta_1 f g' - \beta_1 \frac{f g}{\eta} \right) = 0,
\end{aligned} \tag{6.9}$$

$$\eta \theta'' + \theta' + \operatorname{Re} \operatorname{Pr} f \theta' = 0, \tag{6.10}$$

$$\eta \phi'' + \phi' + \operatorname{Re} \operatorname{Pr} \operatorname{Le} f \phi' = 0, \tag{6.11}$$

with BCs as

$$f(1) = 0, \quad f'(1) = 1, \quad g(1) = 1, \quad \theta(1) = 1, \quad \phi(1) = 1 \tag{6.12}$$

$$f'(\infty) = 0, \quad g(\infty) = 0, \quad \theta(\infty) = 0, \quad \phi(\infty) = 0. \tag{6.13}$$

In the above equations,  $\beta_1$  ( $= \lambda_1 a$ ) is the Maxwell number,  $\text{Re}$  ( $= \frac{aR_1^2}{2\nu}$ ) the Reynolds number,  $M$  ( $= \frac{\sigma B_0^2}{\rho a}$ ) the magnetic parameter,  $\text{Pr}$  ( $= \frac{\nu}{\alpha_1}$ ) the Prandtl number and  $Le$  ( $= \frac{\alpha_1}{D_B}$ ) the Lewis number.

The above similar equations for flow and energy transport phenomena holds for  $\text{Re} > 0$ . As reported by Fang *et al.* [20] in the investigation of viscous flow due to stretchable rotating cylinder, the convergence of solution for flow equations is too slow especially for lessing values of  $\text{Re}$ . Thus, following the Fang to make convergence fast the variable  $\eta$  transformed as  $\eta = e^x$ . Hence, Eqs. (6.8) – (6.13) become

$$\begin{aligned}
& f_{xxx} - 2f_{xx} + f_x - \text{Re} (f_x^2 - ff_{xx} + ff_x) \\
& -\beta_1 \text{Re} e^{-x} (2f^2 f_{xxx} - 5f^2 f_{xx} + 3f^2 f_x - 4ff_x f_{xx} + 4ff_x^2) \\
& -M \text{Re} \left( e^x \frac{f_x}{2} - \beta_1 ff_{xx} + \beta_1 ff_x \right) = 0, \tag{6.14}
\end{aligned}$$

$$\begin{aligned}
& 2g_{xx} - \frac{g}{2} + \text{Re}(2fg_x + fg) \\
& -\beta_1 \text{Re} e^{-x} (2f^2 g_x + 4f^2 g_{xx} + 4f^2 g_x + 4ff_x g - 4f^2 g) \\
& -M \text{Re} (g - 2\beta_1 e^{-x} fg_x - \beta_1 e^{-x} fg) = 0, \tag{6.15}
\end{aligned}$$

$$\theta_{xx} + \text{Re Pr } f\theta_x = 0, \tag{6.16}$$

$$\phi_{xx} + \text{Re Pr } Le\phi_x = 0, \tag{6.17}$$

with transformed BCs as

$$f(0) = 0, \quad f_x(0) = 1, \quad g(0) = 1, \quad \theta(0) = 1, \quad \phi(0) = 1 \quad (6.18)$$

$$\lim_{x \rightarrow \infty} e^{-x} f_x = 0, \quad g(\infty) = 0, \quad \theta(\infty) = 0, \quad \phi(\infty) = 0. \quad (6.19)$$

Where the subscript  $x$  represents the derivative with respect to  $x$ .

### 6.1.1 Analysis for Large Re

Before finding the numerical solution of the above ordinary differential system, we define the certain transformations for the simplification of above equations to find the results for large Reynolds number. Thus, the following transformations  $\xi = \sqrt{\text{Re}}(\eta-1)$ ,  $f(\eta) = \frac{1}{\sqrt{\text{Re}}}F(\xi)$ ,  $g(\eta) = G(\xi)$ ,  $\theta(\eta) = \Theta(\xi)$  and  $\phi(\eta) = \Phi(\xi)$  substituted into Eqs. (6.14) – (6.17) and employe the limit  $\text{Re} \rightarrow \infty$ , we get

$$F'' - F'^2 + FF'' - \beta_1(2F^2F''' - 4FF'F'') - M(F' - \beta_1FF'') = 0, \quad (6.20)$$

$$G'' + 2FG' - \beta_1FG' - M\left(\frac{G}{2} - \beta_1FG'\right) = 0, \quad (6.21)$$

$$\Theta'' + \text{Pr} F\Theta' = 0, \quad (6.22)$$

$$\Phi'' + \text{Pr} LeF\Phi' = 0, \quad (6.23)$$

with BCs

$$F(0) = 0, \quad F'(0) = 1, \quad G(0) = 1, \quad \Theta(0) = 1, \quad \Phi(0) = 1 \quad , \quad (6.24)$$

$$F(\infty) = 0, \quad G(\infty) = 0, \quad \Theta(\infty) = 0, \quad \Phi(\infty) = 0. \quad (6.25)$$

Here in overhead equations, the prime denotes the derivative with respect to  $\xi$ . Thus Eq. (6.21) corresponds to the flow problem for Maxwell fluid over stretching surface. This result is not unexpected, physically justified, because for very large value of Reynolds number  $Re$  the curvature of cylinder becomes very small and occupy the whole space and it look like sheet. Moreover for  $\beta_1 = M = 0$ , Eq. (25) reduces to the viscous fluid flow problem over stretching sheet which discussed by Wang [17].

## 6.2 Quantities of Interest

The Nusselt and Sherwood numbers ( $Nu, Sh$ ) are defined as

$$Nu = \frac{R_1 q_s}{k(T_w - T_\infty)}, \quad Sh = \frac{R_1 j_s}{D_B(C_w - C_\infty)}, \quad (6.26)$$

where  $q_s$  and  $j_s$  are the heat and mass fluxes, respectively,

$$q_s = -k \left( \frac{\partial T}{\partial r} \right)_{r=R_1}, \quad j_s = -D_B \left( \frac{\partial C}{\partial r} \right)_{r=R_1}. \quad (6.27)$$

The non-dimensionl form of Eq. (6.27) is given by

$$Nu = -2\theta'(1), \quad Sh = -2\phi'(1). \quad (6.28)$$



### 6.3 Numerical Solution

The flow mechanism, solutal and thermal energy distributions are expressed through the similar differential Eqs. (6.14)– (6.17) along with corresponding boundary conditions given in Eqs. (6.18) and (6.19). The solutions to these equations are obtained using a built-in MATLAB technique known as `bvp4c`. Furthermore, the numerical scheme is also employed for the solution of resulting Eqs. (6.20) – (6.23) in the analysis of large Reynolds number with boundary conditions given in Eqs. (6.24) and(6.25). For this the governing ODEs are transformed to the system of first order ordinary differential equations. Thus, the suitable transformation variables for Eqs. (6.14) – (6.17) as

$$f = y_1, f_x = y_2, f_{xx} = y_3, f_{xxx} = yy_1, \quad (6.29)$$

$$g = y_4, g_x = y_5, g_{xx} = yy_2 \quad (6.30)$$

$$\theta = y_6, \theta_x = y_7, \theta_{xx} = yy_3, \quad (6.31)$$

$$\phi = y_8, \phi_x = y_9, \phi_{xx} = yy_4, \quad (6.32)$$

and for Eqs. (6.20) – (6.23) as

$$F = x_1, F' = x_2, F'' = x_3, F''' = xx_1, \quad (6.33)$$

$$G = x_4, G' = x_5, G'' = xx_2 \quad (6.34)$$

$$\Theta = x_6, \Theta' = x_7, \Theta'' = xx_3, \quad (6.35)$$

$$\Phi = x_8, \Phi' = x_9, \Phi'' = x x_4. \quad (6.36)$$

The resulting first order ODEs are as follows

$$yy_1 = \frac{2y_3 - y_2 + \operatorname{Re}(y_2^2 - y_1y_3 + y_1y_2) + \beta_1 \operatorname{Re} e^{-x}(3y_1^2 - 5y_1^2y_3 - 4y_1y_2y_3 + 4y_1y_2^2) + M \operatorname{Re}(e^x y_2 - \beta_1 y_1y_3)}{a_1}, \quad (6.37)$$

$$yy_2 = \frac{\frac{y_4}{2} - 2 \operatorname{Re} y_1y_5 - \operatorname{Re} y_1y_4 + \beta_1 \operatorname{Re} e^{-x}(6y_1^2y_5 + 4y_1^2y_2y_4 - 4y_1^2y_4) + M \operatorname{Re}(y_4 - 2\beta_1 e^{-x}y_1y_5 + y_1y_4)}{a_2}, \quad (6.38)$$

$$yy_3 = -\frac{\operatorname{Re} \operatorname{Pr}}{2} y_1y_5, \quad (6.39)$$

$$yy_4 = -\frac{\operatorname{Re} \operatorname{Le} \operatorname{Pr}}{2} y_1y_7, \quad (6.40)$$

where

$$a_1 = 1 - 2\beta_1 \operatorname{Re} e^{-x} y_1^2 \text{ and } a_2 = 2 - 4\beta_1 \operatorname{Re} e^{-x} y_1^2,$$

and BCs for above first order differential system are

$$y_1(0) = 0, y_2(0) = 1, y_4(0) = 1, y_6(0) = 1, y_8(0) = 1 \quad (6.41)$$

$$\lim_{x \rightarrow \infty} e^{-x} y_2 = 0, y_4(\infty) = 0, y_6(\infty) = 0, y_8(\infty) = 1. \quad (6.42)$$

The conversion of Eqs.(6.20) – (6.24) into first order ODEs obtain as

$$xx_1 = \frac{x_2^2 - x_1x_3 - 4\beta_1 x_1x_2x_3 + M(x_2 - \beta_1 x_1x_3)}{b_1}, \quad (6.43)$$

$$xx_2 = \frac{M(\frac{x_4}{2} - \beta_1 x_1 x_5) - x_1 x_5}{b_1}, \quad (6.44)$$

$$xx_3 = -\text{Pr } x_1 x_5, \quad (6.45)$$

$$xx_4 = -Le \text{Pr } x_1 x_7, \quad (6.46)$$

where  $b_1 = 1 - \beta_1 x_1^2$  and boundary conditions for the above non-linear first order differential system are

$$x_1(0) = 0, \quad x_2(0) = 1, \quad x_4(0) = 1, \quad x_6(0) = 1, \quad x_8(0) = 1, \quad (6.47)$$

$$x_2(\infty) = 0, \quad x_4(\infty) = 0, \quad x_6(\infty) = 0, \quad x_8(\infty) = 1. \quad (6.48)$$

## 6.4 Presentation of Results

The physical analysis of graphical outcomes for flow velocity, thermal and solutal energy transport is presented in this part of the chapter. Impact of physical constraint parameters on the velocity field, temperature and solutal distribution is expressed graphically with the comparison of  $Re = 1$  and  $Re = 3$ . The values of non-dimensional physical parameters are taken to be fixed as  $\beta_1 = 0.5$ ,  $M = 1$ ,  $Pr = 6.5$ , and  $Le = 6.5$ . It is found that the velocity of the fluid decays quickly to free stream for Newtonian fluid and large Reynolds number thus, the flow produces only near to the surface of the cylinder. Furthermore, heat and mass transport is higher in non-Newtonian fluid and at a low Reynolds number. One thing should be noted here for  $Re = 0$  the swirl velocity independent from axial velocity. Thus, from Eq. (6.3) we obtained swirl velocity as  $g(\eta) = \eta^{-1/2}$ . Physically, for zero Reynolds number, the stretching of the cylinder is diminished and the flow around the cylinder is due to pure rotational constant

motion. Moreover, constant swirling motion of cylinder does not induce a secondary axial flow of fluid. The Reynolds number is the controlling parameter for the flow of Maxwell fluid. Basically is the ratio of inertial force due to the surface stretching to viscous force. Thus, the higher values of increase the inertial force in the system which opposes the fluid accelerating force. In consequence of this argument the flow field decreases. The axial velocity field for increasing values of Maxwell parameter  $\beta_1$  and magnetic parameter  $M$  illustrated in **Figs. 6.2(a, b)**. The results reveal that axial velocity declines and decays exponentially for all of these three parameters. Plots in **Figs. 6.3(a, b)** show that the swirl velocity decreases for higher values of  $\beta_1$  and  $M$  and the same result is true for radial velocity which is portrayed in **Figs. 6.4(a, b)**. The above results are physically valid, because higher values of magnetic parameter  $M$  boost up the Lorentz force that occurs in fluid flow due to transverse applied magnetic field and this force provides the resistance to the flow velocity. Hence, in results velocity of fluid decreases. In the case of higher values of Maxwell parameter  $\beta_1$  the stress relaxation phenomenon increases in viscoelastic fluid and the liquid becomes more solid like with less fluidity (ability of material to flow) due to which the fluid motion declines.

The transportation of thermal and solutal energy in the given swirling flow mechanism is visualized in the graphs of **Figs. 6.5(a – d)**. These graphical results for the temperature field prove that increasing values of Maxwell parameter  $\beta_1$ , enhance the heat and mass transport rate in the flow. As mention above for the more values of  $\beta_1$  the fluid behavior is solid like thus particles of fluids are close to each other, so in consequence, the thermal and solutal energy conduction boost up in the fluid flow. The impact of Reynolds number  $Re$  on temperature and concentration profile is found in decreasing trend. Physically, the Reynolds number controls the flow of fluid and it is clear for higher values of  $Re$  reduce the flow field thus, the main

forced convection mechanism for the transport of energy is reduced. Therefore, the temperature and concentration fields decline. Moreover, Prandtl number  $Pr$  and Lewis number  $Le$  describe the relative importance of thermal and solutal energy transport in the fluid to the momentum transport. The higher values of both dimensionless numbers  $Pr$  and  $Le$  lower down the temperature and concentration fields due to the reduction in thermal and mass diffusivity of the fluid, respectively.

In flow analysis for very large Reynolds number  $Re$ , **Figs. 6.6(a, b)** express the graphical results for axial and swirl velocity field, respectively, for increasing values magnetic parameter  $M$ . These findings reveal to us that the axial and swirl flow velocity declines. There is the same physical justification for this reduction in axial and swirl velocity which is given above in the case of higher values of  $M$ . The physical mechanism for the transport of energy in the swirling flow of Maxwell fluid for very large Reynolds can be analyzed through the graphical outcomes given in **Figs. 6.7(a, b)**. It can be seen that both thermal and solutal energy transport boost up for increasing values of  $M$ . Physically, in case of higher magnetic parameter  $M$  the conduction of energy increases between the fluid particles due to the enhancement in Lorentz force. Furthermore, in the comparison of Newtonian and non-Newtonian fluids for higher values of magnetic parameter  $M$ , higher fluid flow velocity and less energy transport is observed for Newtonian fluids and the opposite trend noted is noted for non-Newtonian fluids.

The comparison of numerical values of initial axial and swirl velocity gradient with existing article for various values of  $Re$  is presented in **Table 6.1**. It is noted that the magnitude of these velocities gradient increases with the higher trend in  $Re$ . Moreover, **Table 6.1** also validates the current analysis. The numerical values of the Nusselt and Sherwood number is given in **Table 6.2** for different pertinent parameters and fixed  $M = 0$ .

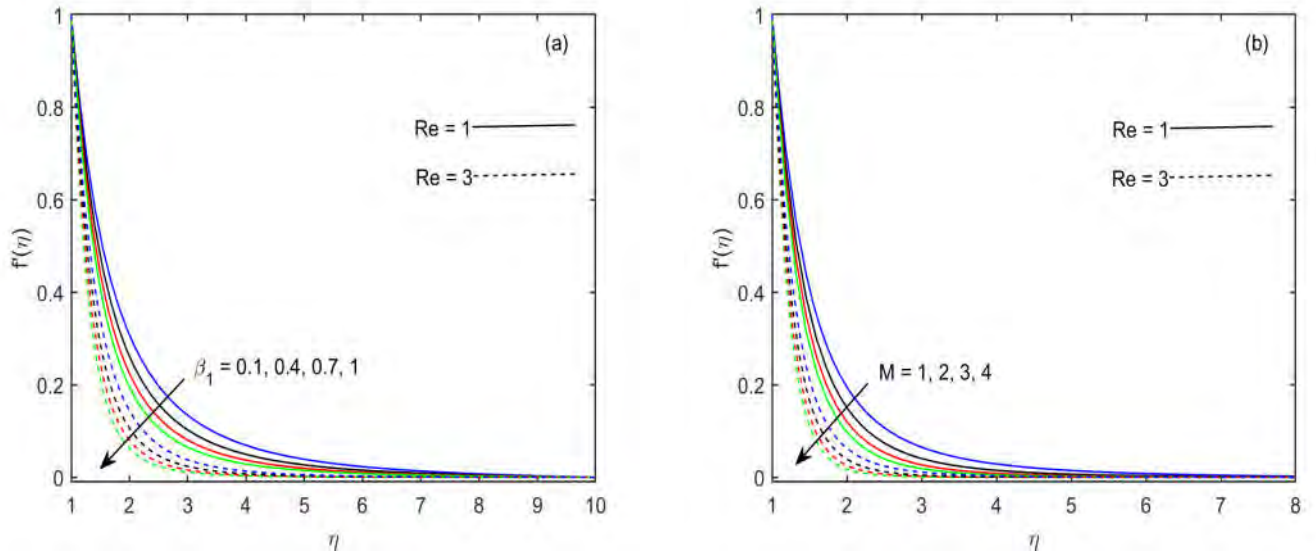


**Figure 6.2:** Axial velocity profiles via  $\beta_1$  and  $M$ .

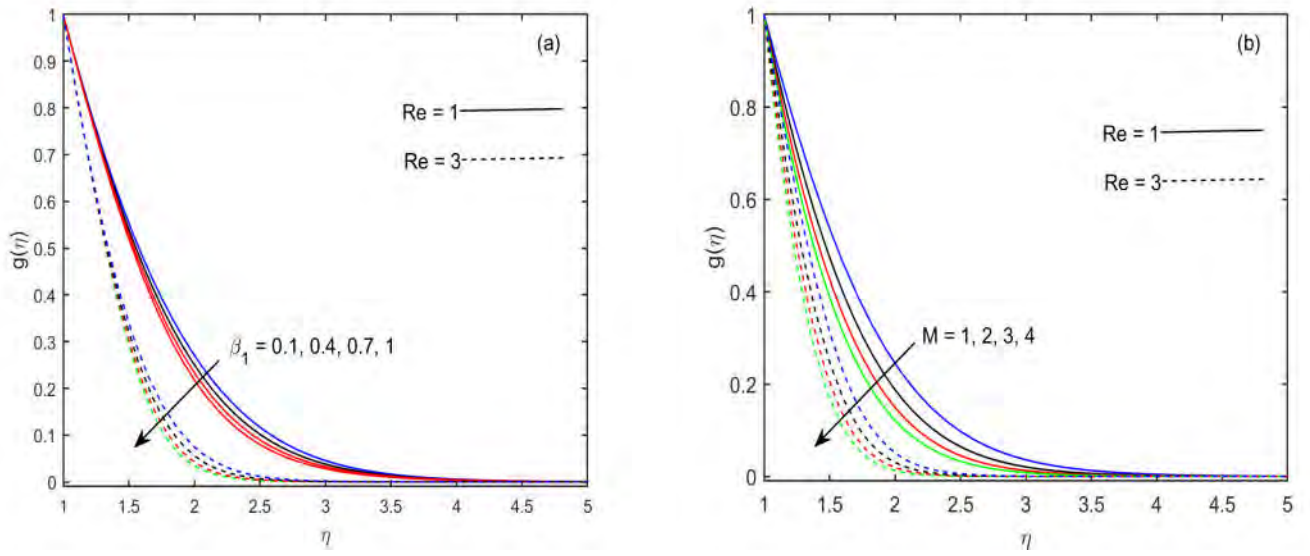


**Figure 6.3:** Swirl velocity profiles via  $\beta_1$  and  $M$ .

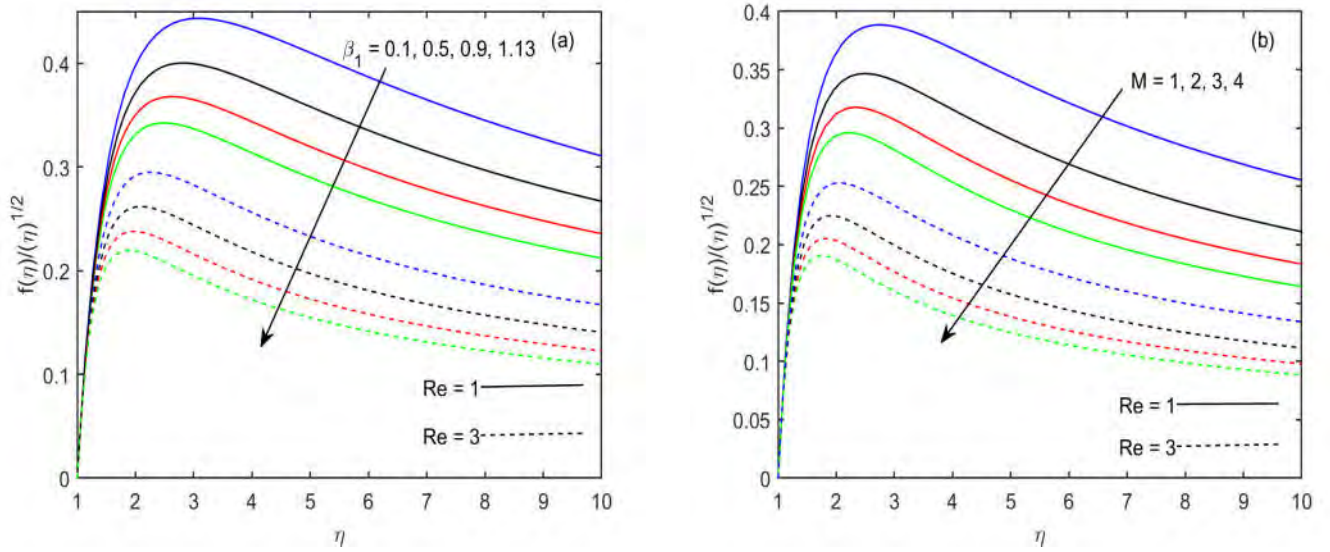


**Figure 6.4:** Radial velocity profiles via  $\beta_1$  and  $M$ .

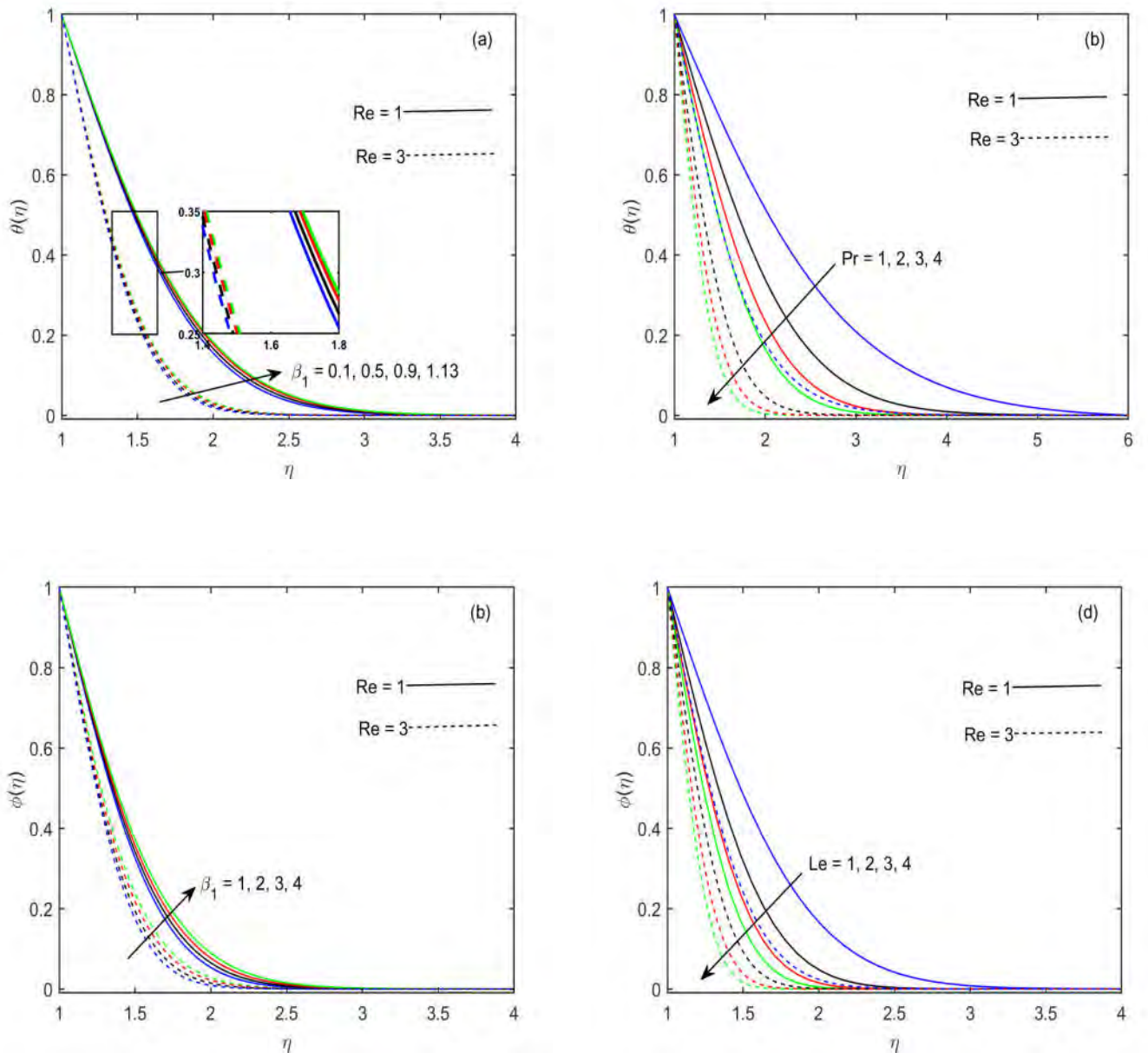


**Figure 6.5:** Temperature and concentration profiles via  $\beta_1$ ,  $Pr$  and  $Le$ .



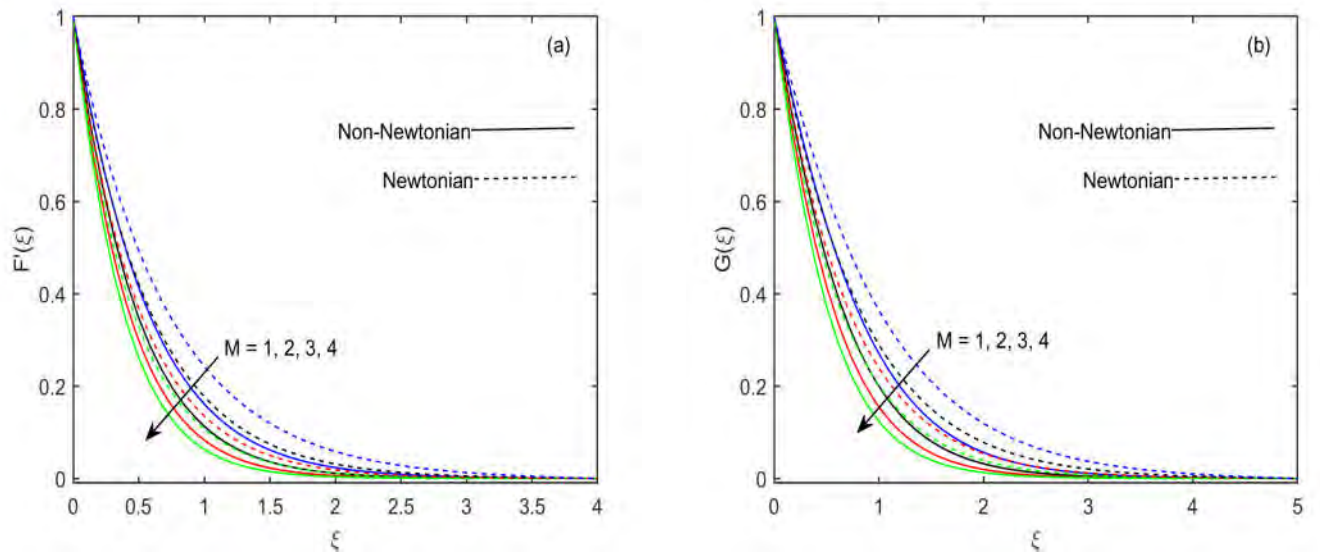


**Figure 6.6:** Axial and swirl velocity profiles via  $M$  for  $Re \rightarrow \infty$ .

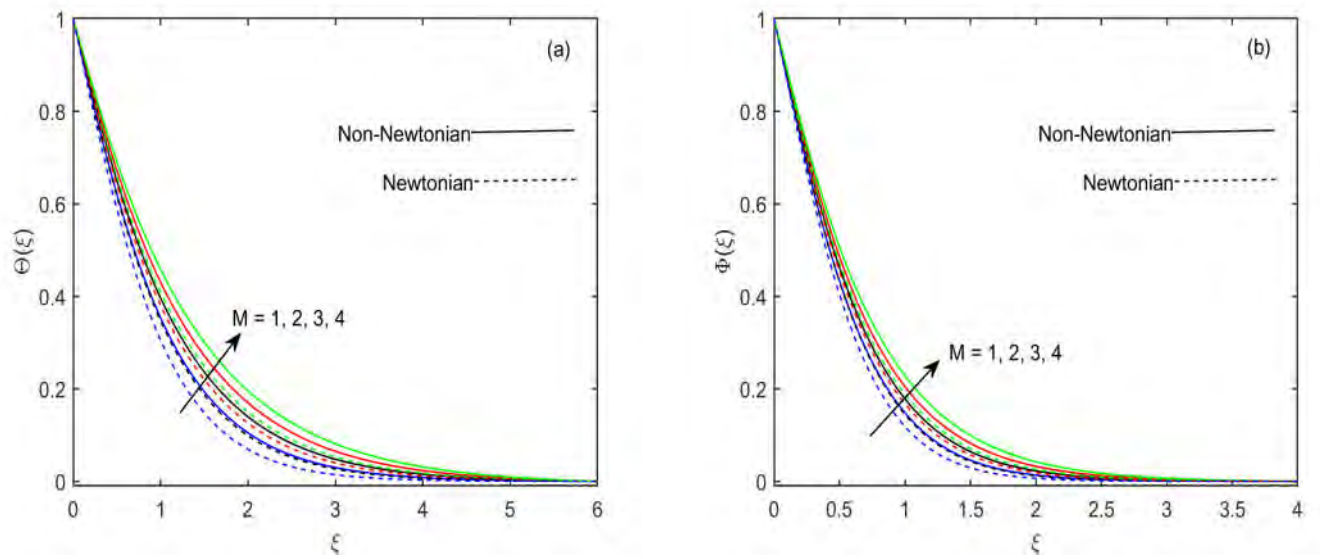


**Figure 6.7:** Temperature and concentration profiles via  $M$  for  $Re \rightarrow \infty$ .

**Table 6.1:** Comparison values of velocity gradients in axial and swirl directions for various Re in limiting case when  $\beta_1 = M = \text{Pr} = Le = 0$ .

Re	$f''(1)$	$g'(1)$	$f''(1)$	$g'(1)$
	Ref. [20]	Ref. [20]	Present outcomes	Present outcomes
0.1	-0.48180	-0.51019	-0.489603	-0.510233
0.2	-0.61748	-0.52605	-0.614250	-0.527509
0.3			-0.729469	-0.545828
0.4			-0.812939	-0.565435
0.5	-0.88220	-0.58488	-0.887010	-0.585714
01	-1.17775	-0.68772	-1.179549	-0.687943
02	-1.59389	-0.87263	-1.597000	-0.872647
03			-1.914139	-1.031356
04			-2.181917	-1.171360
05	-2.41743	-1.29788	-2.417984	-1.297884
10	-3.34446	-1.81006	-3.344542	-1.810074

**Table 6.2:** Numerical values of  $-\theta'(1)$  and  $-\phi'(1)$  for various values of  $Re$ ,  $\beta_1$ ,  $Pr$ ,  $Le$  and

$M = 0$ .

$Re$	$\beta_1$	$Pr$	$Le$	$-\theta'(1)$	$-\phi'(1)$
01	0.1	4.5	02	1.122190	1.624961
				1.110453	1.613206
				1.098944	1.601671
				1.087626	1.590307
01	0.1	4.5	02	0.474278	
		0.2		0.718912	
		0.3		0.904159	
		04		1.059115	
01	0.1	01	02		1.221940
		02			1.624961
		03			2.008637
		04			2.331290
01	0.1	4.5	01	1.129003	1.624961
			02	1.533036	2.219778
			03	1.842840	2.667455
			04	2.103945	3.037788

## Chapter 7

# Thermal Analysis in Swirl Motion of Maxwell Nanofluid over a Rotating Cylinder

In this chapter, the transport mechanisms of thermal and solutal energy in the swirling flow of Maxwell nanofluid generated by a stretchable rotating cylinder are investigated. The novel features of heat generation/absorption, thermal radiation, and Joule heating have been studied to control the rate of heat transport. The temperature at the surface of the cylinder is assumed as constant (CWT) and axially varying (PST). The influence of thermophoretic and Brownian forces in Maxwell nanofluid for convective energy transport is studied by utilizing an effective model for nanofluid proposed by Buongiorno. The whole physical problem of fluid flow and energy transport is modeled in the form of partial differential equations (PDEs) and transformed into nonlinear ordinary differential equations (ODEs) with help of a suitable flow ansatz. Numerically acquired results through the scheme `bvp4c` are reported graphically

with the physical explanation. Graphical analysis reveals that there is higher transport of heat energy in Maxwell nanoliquid for constant wall temperature (CWT) as compared to the prescribed surface temperature (PST). Moreover, the temperature distribution increases with increasing values of radiation parameter and Eckert number. It is also noted that a rise in Reynolds number reduces the penetration depth and as a result, the flow and transport of energy occur only near the surface of a cylinder.

## 7.1 Problem Development

Consider an electrically conducting axisymmetric, steady and incompressible swirling flow of Maxwell nanofluid engendered by stretchable rotating cylinder of radius  $R_1$  in the presence of transverse magnetic field. The velocity field for flow is assumed as  $\mathbf{V} = [u, v, w]$ , where  $u, v$ , and  $w$  are velocity components along  $(z, \varphi, r)$ -axes, respectively, and  $\mathbf{B} = [0, 0, B_0]$  the uniform magnetic field which is applied in the direction  $r$ -axis. It is assumed that the cylinder rotation is constant around its axis and stretching is axially varying. Thermal analysis is investigated by considering the temperatures at surface of the cylinder as  $T(z, R_1) = T_w$  (constant wall temperature) and  $T(z, R_1) = T_\infty + bz$  (prescribed surface temperature). The flow mechanism is presented in **Fig. 6.1** (cf. Chapter 6).

In view of above assumptions the governing boundary layer equations of the present flow and energy transport problem by utilizing Cattneo-Christov theory (see Eqs. 1.10, 1.11) and conservation laws (cf. Chapter 1) are obtained as:

$$\frac{\partial u}{\partial z} + \frac{w}{r} + \frac{\partial w}{\partial r} = 0, \quad (7.1)$$

$$u \frac{\partial u}{\partial z} + w \frac{\partial u}{\partial r} + \lambda_1 \left[ u^2 \frac{\partial^2 u}{\partial z^2} + 2uw \frac{\partial^2 u}{\partial r \partial z} + w^2 \frac{\partial^2 u}{\partial r^2} \right] = \nu \left[ \frac{\partial^2 u}{\partial r^2} + \frac{1}{r} \frac{\partial u}{\partial r} \right] - \frac{\sigma B_0^2}{\rho} \left( u + \lambda_1 w \frac{\partial u}{\partial r} \right), \quad (7.2)$$

$$u \frac{\partial v}{\partial z} + w \frac{\partial v}{\partial r} + \frac{wv}{r} + \lambda_1 \left[ u^2 \frac{\partial^2 v}{\partial z^2} + 2uw \frac{\partial^2 v}{\partial r \partial z} + w^2 \frac{\partial^2 v}{\partial r^2} + \frac{2wv}{r} \frac{\partial w}{\partial r} + \frac{2uv}{r} \frac{\partial w}{\partial z} - \frac{2w^2 v}{r^2} \right] = \nu \left[ \frac{\partial^2 v}{\partial r^2} - \frac{v}{r^2} + \frac{1}{r} \frac{\partial v}{\partial r} \right] - \frac{\sigma B_0^2}{\rho} \left( v + \lambda_1 w \frac{\partial v}{\partial r} - \lambda_1 \frac{wv}{r} \right), \quad (7.3)$$

$$u \frac{\partial T}{\partial z} + w \frac{\partial T}{\partial r} = \alpha_1 \left[ \frac{\partial^2 T}{\partial r^2} + \frac{1}{r} \frac{\partial T}{\partial r} \right] + \tau \left[ D_B \frac{\partial C}{\partial r} \frac{\partial T}{\partial r} + \frac{D_T}{T_\infty} \left( \frac{\partial T}{\partial r} \right)^2 \right] - \frac{1}{\rho c_p} \frac{1}{r} \frac{\partial}{\partial r} (r q_r) + \frac{\sigma B_0^2}{\rho c_p} (u^2 + v^2) + \frac{Q_0}{\rho c_p} (T - T_\infty), \quad (7.4)$$

$$u \frac{\partial C}{\partial z} + w \frac{\partial C}{\partial r} = D_B \left[ \frac{\partial^2 C}{\partial r^2} + \frac{1}{r} \frac{\partial C}{\partial r} \right] + \frac{D_T}{T_\infty} \left[ \frac{\partial^2 T}{\partial r^2} + \frac{1}{r} \frac{\partial T}{\partial r} \right], \quad (7.5)$$

with the corresponding boundary conditions (BCs) are

$$u_s(z, r) = 2az, \quad v_s(z, r) = E, \quad w(z, r) = 0$$

$$-k \frac{\partial T}{\partial z} = h_T (T_w - T), \quad C = C_w \text{ at } r = R_1, \quad (7.6)$$

$$u \rightarrow 0, \quad v \rightarrow 0, \quad T \rightarrow T_\infty, \quad C \rightarrow C_\infty \text{ as } r \rightarrow \infty. \quad (7.7)$$

Here  $h_T$  is the heat transfer coefficient and  $q_r = \frac{-16\sigma^*}{3k^*} T_\infty^3 \frac{\partial T}{\partial r}$  the radiative heat flux, where  $(\sigma^*, k^*)$  the Stefan-Boltzmann constant and mean absorption coefficient, respectively.

Introducing the following transformation group (Fang *et al.* [20])

$$\begin{aligned}
u &= 2azf'(\eta), \quad v = Eg(\eta), \quad w = -aR_1 \frac{f(\eta)}{\eta^{1/2}}, \\
\theta(\eta) &= \frac{T-T_\infty}{T_w-T_\infty} \text{ (CWT)}, \quad \theta(\eta) = \frac{T-T_\infty}{bz} \text{ (PST)}, \\
\phi(\eta) &= \frac{C-C_\infty}{C_w-C_\infty}, \quad \eta = \frac{r^2}{R_1^2}.
\end{aligned} \tag{7.8}$$

These flow ansatz, satisfied the Eq. (7.1) automatically and Eqs. (7.2) – (7.7) yield

$$\begin{aligned}
&\eta f''' + f'' + \operatorname{Re} f f'' - \operatorname{Re} f'^2 \\
&-\beta_1 \operatorname{Re} \left( \frac{f^2 f''}{\eta} + 2f^2 f''' - 4f f' f'' \right) - M \operatorname{Re} \left( \frac{f'}{2} - \beta_1 f f'' \right) = 0 \quad ,
\end{aligned} \tag{7.9}$$

$$\begin{aligned}
&2\eta^2 g'' + 2\eta g' - \frac{g}{2} + 2 \operatorname{Re} \eta f g' + \operatorname{Re} f g \\
&-\beta_1 \operatorname{Re} \left( 2f^2 g' + 4\eta f^2 g'' + 4f f' g - \frac{4f^2 g}{\eta} \right) - M \operatorname{Re} \left( g - 2\beta_1 f g' - \beta_1 \frac{f g}{\eta} \right) = 0,
\end{aligned} \tag{7.10}$$

$$\begin{aligned}
&(1 + R_d)(\eta\theta'' + \theta') + \operatorname{Re} \operatorname{Pr} f\theta' + \operatorname{Pr} N_b \eta \theta' \phi' + \operatorname{Pr} N_t \eta \theta'^2 \\
&+ \operatorname{Pr} \delta \operatorname{Re} \theta + \operatorname{Pr} \operatorname{Re} M(Ec_1 f'^2 + Ec_2 g^2) = 0, \text{ (CWT)}
\end{aligned} \tag{7.11}$$

$$\begin{aligned}
&(1 + R_d)(\eta\theta'' + \theta') + \operatorname{Re} \operatorname{Pr} f\theta' - \operatorname{Pr} \operatorname{Re} \theta f' + \operatorname{Pr} N_b \eta \theta' \phi' \\
&+ \operatorname{Pr} N_t \eta \theta'^2 + \operatorname{Pr} \delta \operatorname{Re} \theta + \operatorname{Pr} \operatorname{Re} M(Ec_1 f'^2 + Ec_2 g^2) = 0, \text{ (PST)}
\end{aligned} \tag{7.12}$$

$$\eta\phi'' + \phi' + \operatorname{Re} \operatorname{Pr} Le f \phi' + Le \operatorname{Pr} \frac{N_t}{N_b} \theta' + Le \operatorname{Pr} \frac{N_t}{N_b} \eta \theta'' = 0, \tag{7.13}$$

with BCs as

$$f(1) = 0, \quad f'(1) = 1, \quad g(1) = 1, \quad \theta'(1) = -\gamma_1(1 - \theta(1)), \quad \phi(1) = 1, \quad (7.14)$$

$$f'(\infty) = 0, \quad g(\infty) = 0, \quad \theta(\infty) = 0, \quad \phi(\infty) = 0. \quad (7.15)$$

Here the physical parameters are defined as  $\beta_1$  ( $= \lambda_1 a$ ) is the Maxwell number,  $Re$  ( $= \frac{aR^2}{2\nu}$ ) the Reynolds number,  $M$  ( $= \frac{\sigma B_0^2}{\rho a}$ ) the magnetic number,  $N_b$  ( $= \frac{\tau D_B \Delta C}{\nu}$ ) the Brownian motion parameter,  $N_t$  ( $= \frac{\tau D_T \Delta T}{\nu T_\infty}$ ) the thermophoresis parameter,  $R_d$  ( $= \frac{16\sigma^* T_\infty^3}{3kk^*}$ ) the radiation parameter,  $\delta$  ( $= \frac{Q_0}{\rho c_p a}$ ) the heat generation/absorption parameter,  $Ec_1$  ( $= \frac{u_s^2}{c_p \Delta T}$ ) and  $Ec_2$  ( $= \frac{v_s^2}{c_p \Delta T}$ ) are the Eckert numbers due to stretching and rotation of cylinder, respectively,  $\gamma_1$  ( $= \frac{h_T}{k} \sqrt{\frac{\nu}{a}}$ ) the Biot number,  $Pr$  ( $= \frac{\nu}{\alpha_1}$ ) the Prandtl number and  $Le$  ( $= \frac{\alpha_1}{D_B}$ ) the Lewis number.

In the study of Newtonian fluid flow caused by stretching and rotating cylinder as analyzed by Fang *et al.* [20], for lower values of  $Re$  the solution convergence of similar flow equations is too slow. Thus, following Fang to make convergence fast, the variable  $\eta$  is transformed as  $\eta = e^x$ . Hence, Eqs. (7.9) – (7.15) become

$$\begin{aligned} & f_{xxx} - 2f_{xx} + f_x - Re(f_x^2 - ff_{xx} + ff_x) \\ & -\beta_1 Re e^{-x} (2f^2 f_{xxx} - 5f^2 f_{xx} + 3f^2 f_x - 4ff_x f_{xx} + 4ff_x^2) \\ & -M Re \left( e^x \frac{f_x}{2} - \beta_1 ff_{xx} + \beta_1 ff_x \right) = 0, \end{aligned} \quad (7.16)$$



$$\begin{aligned}
& 2g_{xx} - \frac{g}{2} + \operatorname{Re}(2fg_x + fg) \\
& -\beta_1 \operatorname{Re} e^{-x} (2f^2 g_x + 4f^2 g_{xx} + 4f^2 g_x + 4ff_x g - 4f^2 g) \\
& -M \operatorname{Re} (g - 2\beta_1 e^{-x} f g_x - \beta_1 e^{-x} f g) = 0, \tag{7.17}
\end{aligned}$$

$$\begin{aligned}
& (1 + R_d)\theta_{xx} + \operatorname{Re} \operatorname{Pr} f\theta_x + N_b\theta_x\phi_x + N_t\theta_x^2 + \operatorname{Pr} \delta \operatorname{Re} e^x\theta \\
& + \operatorname{Pr} \operatorname{Re} M(Ec_1 e^{-x} f_x^2 + Ec_2 e^x g^2) = 0, \quad \text{(CWT)} \tag{7.18}
\end{aligned}$$

$$\begin{aligned}
& (1 + R_d)\theta_{xx} + \operatorname{Re} \operatorname{Pr} f\theta_x - \operatorname{Pr} \operatorname{Re} \theta f_x + N_b\theta_x\phi_x + N_t\theta_x^2 \\
& + \operatorname{Pr} \delta \operatorname{Re} e^x\theta + \operatorname{Pr} \operatorname{Re} M(Ec_1 e^{-x} f_x^2 + Ec_2 e^x g^2) = 0, \quad \text{(PST)} \tag{7.19}
\end{aligned}$$

$$\phi_{xx} + \operatorname{Re} \operatorname{Pr} Lef\phi_x + Le \operatorname{Pr} \frac{N_t}{N_b} \theta_{xx} = 0, \tag{7.20}$$

with transformed BCs as

$$f(0) = 0, \quad f_x(0) = 1, \quad g(0) = 1, \quad \theta_x(0) = -\gamma_1(1 - \theta(0)), \quad \phi(0) = 1 \tag{7.21}$$

$$\lim_{x \rightarrow \infty} e^{-x} f_x = 0, \quad g(\infty) = 0, \quad \theta(\infty) = 0, \quad \phi(\infty) = 0. \tag{7.22}$$

The derivative with respect to  $x$  is represented by the subscript  $x$  in the above equations.

## 7.2 Physical Quantities

The Nusselt and Sherwood numbers ( $Nu, Sh$ ) are defined as

$$Nu = \frac{R_1 q_s}{k(T_w - T_\infty)}, \quad Sh = \frac{R_1 j_s}{D_B(C_w - C_\infty)}, \quad (7.23)$$

where  $q_s$  and  $j_s$  are the heat and mass fluxes, respectively, defined as

$$q_s = -k \left( \frac{\partial T}{\partial r} \right)_{r=R_1}, \quad j_s = -D_B \left( \frac{\partial C}{\partial r} \right)_{r=R_1}. \quad (7.24)$$

The dimensionless form of Eq. (7.23) is given by

$$Nu = -2\theta'(1), \quad Sh = -2\phi'(1). \quad (7.25)$$

## 7.3 Numerical Solution

In this section the numerical solutions of established similar ODEs representing the flow and energy transport given in Eqs. (7.16)–(7.20) along with boundary conditions in Eqs. (7.21) and (7.22) acquired with the help of `bvp4c` function. In order to employ the `bvp4c` scheme the governing ODEs are transformed into the system of first-order ordinary differential equations by using the transformed variables as  $f = y_1, f_x = y_2, f_{xx} = y_3, f_{xxx} = yy_1, g = y_4, g_x = y_5, g_{xx} = yy_2, \theta = y_6, \theta_x = y_7, \theta_{xx} = yy_3, \phi = y_8, \phi_x = y_9, \phi_{xx} = yy_4$  for Eqs. (7.16) – (7.20).

The resulting first order ODEs are as follows

$$\begin{aligned}
& 2y_3 - y_2 + \text{Re}(y_2^2 - y_1y_3 + y_1y_2) \\
& + \beta_1 \text{Re} e^{-x} (3y_1^2y_2 - 5y_1^2y_3 - 4y_1y_2y_3 + 4y_1y_2^2) \\
& + M \text{Re}(e^{x\frac{y_2}{2}} - \beta_1y_1y_3 + \beta_1y_1y_2) \\
yy_1 = & \frac{\hspace{10em}}{a_1}, \tag{7.26}
\end{aligned}$$

$$\begin{aligned}
& \frac{y_4}{2} - 2 \text{Re} y_1y_5 - \text{Re} y_1y_4 + \beta_1 \text{Re} e^{-x} (6y_1^2y_5 + 4y_1^2y_2y_4 - 4y_1^2y_4) \\
& + M \text{Re}(y_4 - 2\beta_1e^{-x}y_1y_5 - \beta_1e^{-x}y_1y_4) \\
yy_2 = & \frac{\hspace{10em}}{a_2}, \tag{7.27}
\end{aligned}$$

$$\begin{aligned}
& - \text{Re} \text{Pr} y_1y_7 - \text{Pr} N_b y_7y_9 - \text{Pr} N_t y_7^2 - \text{Pr} \delta \text{Re} e^x y_6 \\
& - \text{Pr} \text{Re} M(Ec_1e^{-x}y_2^2 + Ec_2e^x y_4^2) \\
yy_3 = & \frac{\hspace{10em}}{b_1} \text{(CWT)}, \tag{7.28}
\end{aligned}$$

$$\begin{aligned}
& - \text{Re} \text{Pr} y_1y_7 - \text{Pr} N_b y_7y_9 - \text{Pr} N_t y_7^2 - \text{Pr} \delta \text{Re} e^x y_6 \\
& + \text{Pr} \text{Re} y_2y_6 - \text{Pr} \text{Re} M(Ec_1e^{-x}y_2^2 + Ec_2e^x y_4^2) \\
yy_3 = & \frac{\hspace{10em}}{b_1} \text{(PST)}, \tag{7.29}
\end{aligned}$$

$$yy_4 = - \text{Re} Le \text{Pr} y_1y_9 - Le \text{Pr} \frac{N_t}{N_b} yy_3, \tag{7.30}$$

where

$$a_1 = 1 - 2\beta_1 \text{Re} e^{-x} y_1^2, \quad a_2 = 2 - 4\beta_1 \text{Re} e^{-x} y_1^2, \quad b_1 = 1 + R_d,$$

and corresponding BCs are

$$y_1(0) = 0, \quad y_2(0) = 1, \quad y_4(0) = 1, \quad y_6(0) = 1, \quad y_8(0) = 1 \tag{7.31}$$

$$\lim_{x \rightarrow \infty} e^{-x} y_2 = 0, \quad y_4(\infty) = 0, \quad y_6(\infty) = 0, \quad y_8(\infty) = 1. \tag{7.32}$$

## 7.4 Discussion of Results

The analysis of thermal energy transport in the swirling flow of Maxwell nanofluid with the impact of heat generation/absorption, thermal radiation and resistive heating is the basic theme of our study. In this section of the study, we demonstrate the numerical results with physical description for flow and heat transport under the influence of involved physical parameters, such as Reynolds number  $Re$ , Maxwell parameter  $\beta_1$ , magnetic parameter  $M$ , thermophoretic parameter  $N_t$ , Brownian motion parameter  $N_b$ , radiation parameter  $R_d$ , Eckert numbers ( $Ec_1$ ,  $Ec_2$ ), heat source/sink  $\delta$ , Biot number  $\gamma_1$ , Prandtl number  $Pr$  and Lewis number  $Le$ . Throughout the numerical computation, we have fixed the values of pertinent parameters for thermal analysis as  $Re = 3$ ,  $M = 1$ ,  $\beta_1 = N_t = N_b = \gamma_1 = R_d = 0.5$ ,  $Ec_1 = Ec_2 = \delta = 0.01$ ,  $Pr = Le = 6.5$ . In the case of flow analysis, we just change the values of  $Pr = Le = 2.5$  for appropriate results.

The impacts of Reynolds number  $Re$  and Maxwell number  $\beta_1$  on temperature distribution are envisioned in **Figs. 7.2(a, b)**. The results reveal that higher estimation in  $Re$  decreases the temperature field but a converse trend is found for  $\beta_1$ . Physically, due to the solid like response of viscoelastic material in case of higher stress relaxation phenomenon, the conduction of thermal energy enhances between the particles of the material and as a result, the temperature distribution increases. As we know that the higher value of  $Re$  reduces the forced convection mechanism in the flow, which causes to decline in the temperature field. The thermo-migration and haphazard motions of nano-size particles in the flow of Maxwell fluid are described by the dimensionless parameters  $N_t$  and  $N_b$ . The heat transport in the flow is significantly enhanced with the higher values of thermophoretic and Brownian motion parameters  $N_t$  and  $N_b$ . Physically, higher values of thermophoretic parameter  $N_t$  enhance the thermal gradient in fluid

particles, which results in the enhancement of heat transport. Furthermore, due to the increasing trend of Brownian diffusion parameter  $N_b$ , the particle collisions and nano-convection are enhanced. Therefore, as a result, thermal energy transport increases. These results are explored through **Figs. 7.3(a, b)**.

The heat source  $\delta > 0$  in the system produces the extra heat which increases the heat transport in the fluid flow and converse is true for the heat sink  $\delta < 0$ . The results for  $\delta > 0$  and  $\delta < 0$  are presented in **Figs. 7.4(a, b)**. **Figs. 7.5(a, b)** depict the influence of Eckert numbers  $Ec_1$  and  $Ec_2$  on temperature distribution in the Maxwell fluid flow. It is observed that there is higher transport in the thermal energy due to augmentation in  $Ec_1$  and  $Ec_2$ . Physically, the Eckert number describes the Joule heating effect in the system which is the ratio of the kinetic energy of the flow to the thermal energy transport driving force. The higher values of  $Ec_1$  and  $Ec_2$  increase the temperature field because the advection mechanism for heat transport in the flow enhances and heat dissipation reduces. Moreover, it is noted that the influence of  $Ec_2$  is more prominent on the temperature field as compared to  $Ec_1$ . **Figs. 7.6(a, b)** show that both the radiative parameter  $R_d$  and Biot number  $\gamma_1$  boost up the temperature field. Physically, the Biot number increases the thermal gradient at the surface of the cylinder due to a decrease in the resistance for energy transport inside to the outside of the body. In view of this physical justification, the temperature field enhances. The thermal energy transportation in the fluid flow is the decreasing function of Prandtl number  $Pr$  for higher values as given in **Fig. 7.7**. In the whole thermal analysis, we conclude that there is higher transport of thermal energy in fluid flow for CWT as compared to PST. Physically, in the case of PST, the axial varying temperature of the surface of the cylinder declines the heat transport in the Maxwell fluid flow. The outcomes acquired through numerical computation are validated through **Table 7.1**. The

numerical values of thermal gradient against various pertinent parameters at the surface of the cylinder for both surface heating agents CWT and PST are shown in **Table 7.2**. It is observed that there is a higher value of thermal gradient in case PST than CWT. Moreover,  $E_{c2}$  has more influence on the thermal gradient at the surface as compared to  $E_{c1}$ .

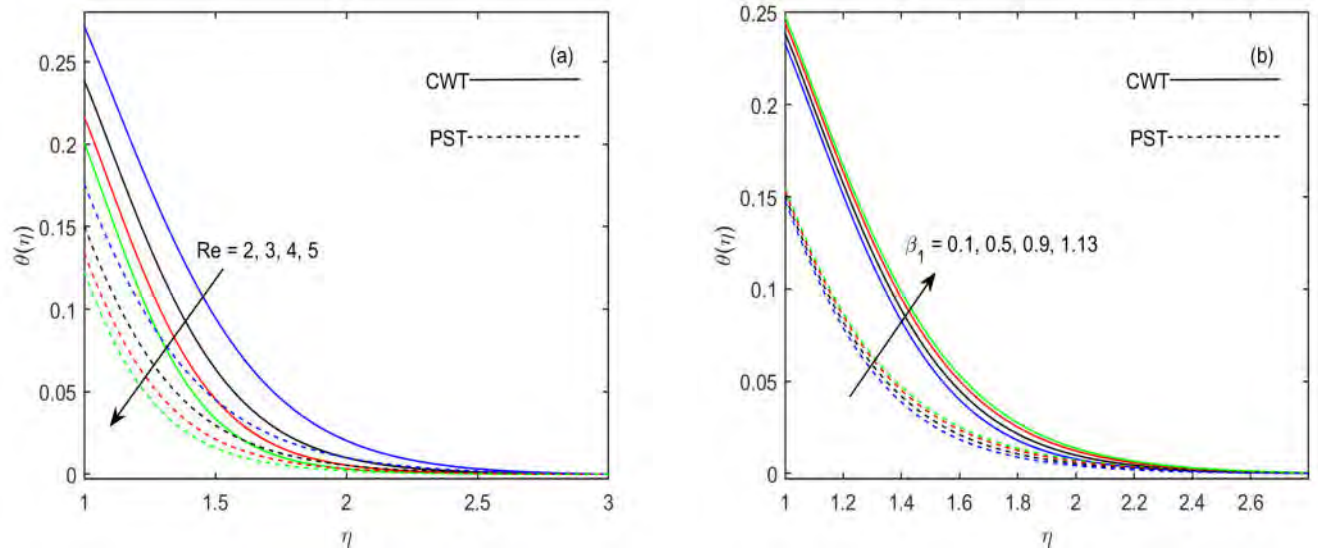


**Figure 7.2:** Temperature profile via  $Re$  and  $\beta_1$ .

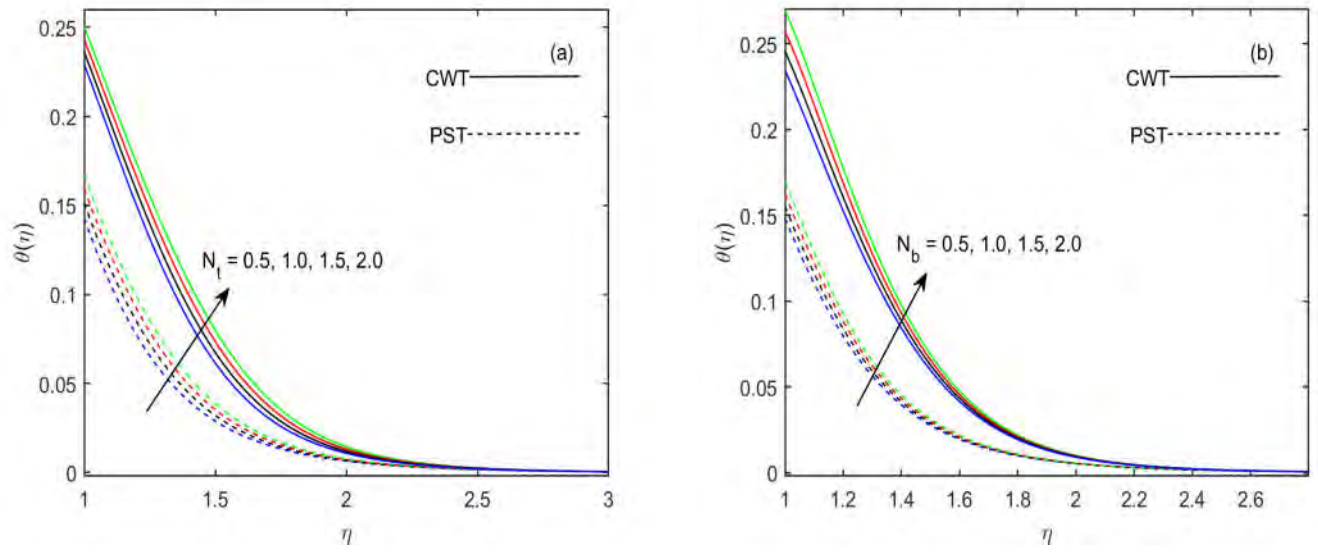


**Figure 7.3:** Temperature profile via  $N_t$  and  $N_b$ .

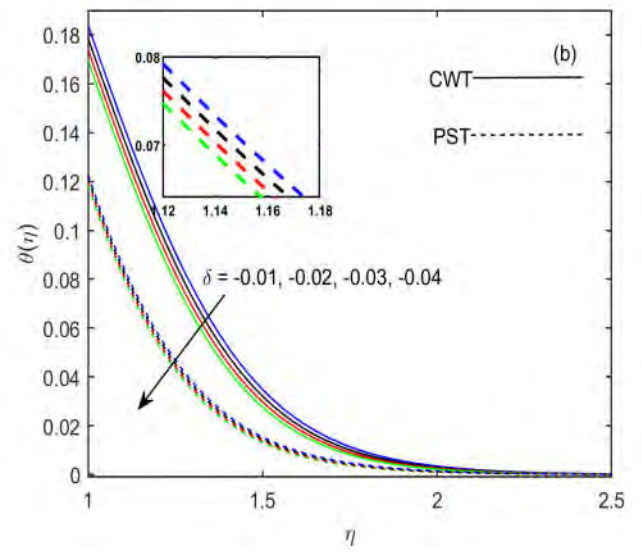
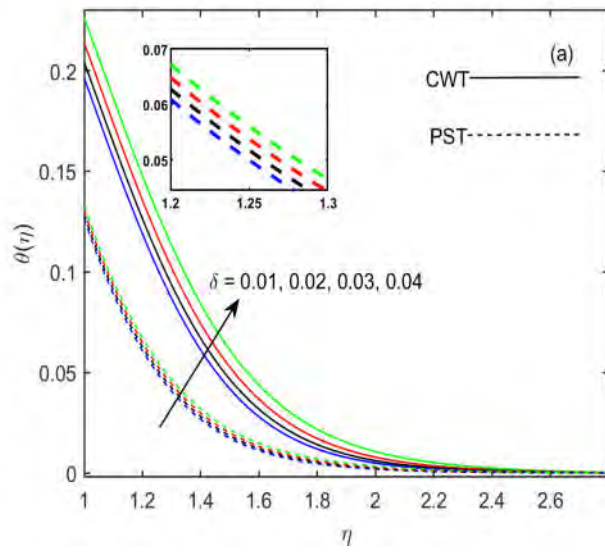


Figure 7.4: Temperature profile via  $\delta$ .

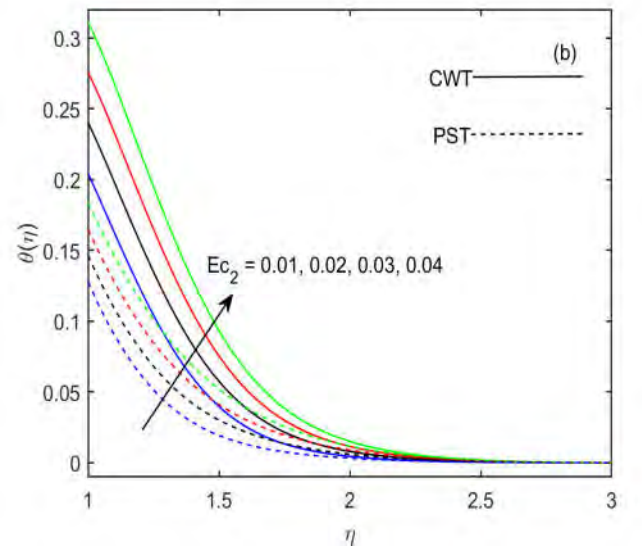
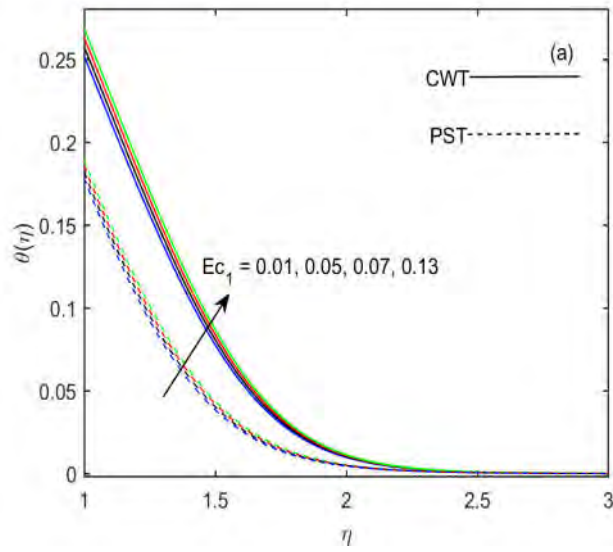
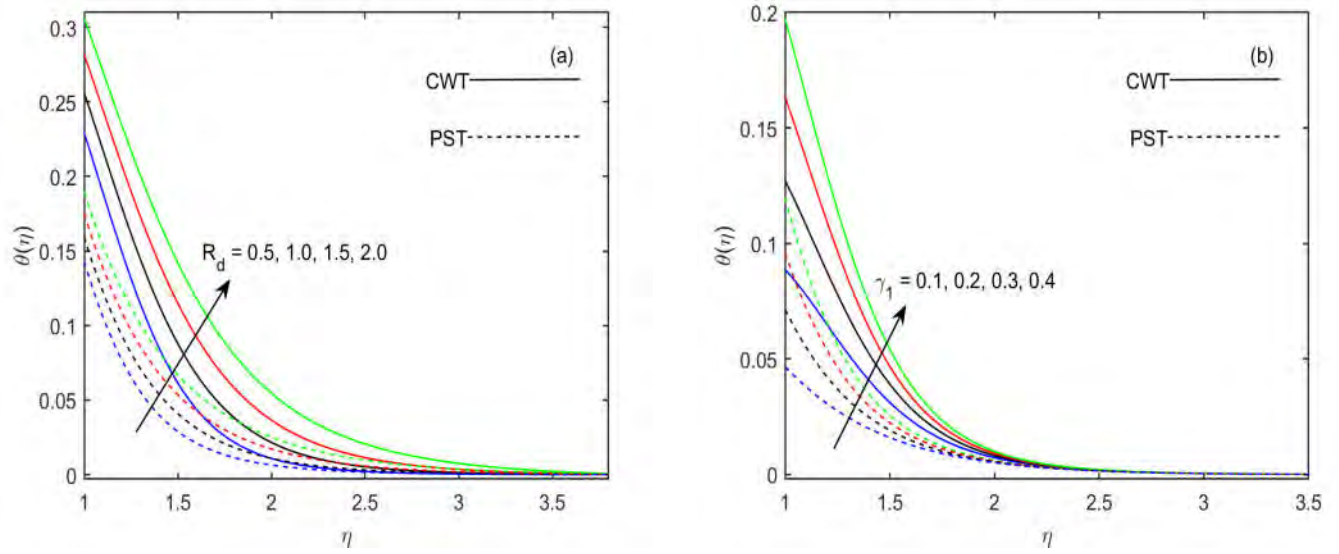
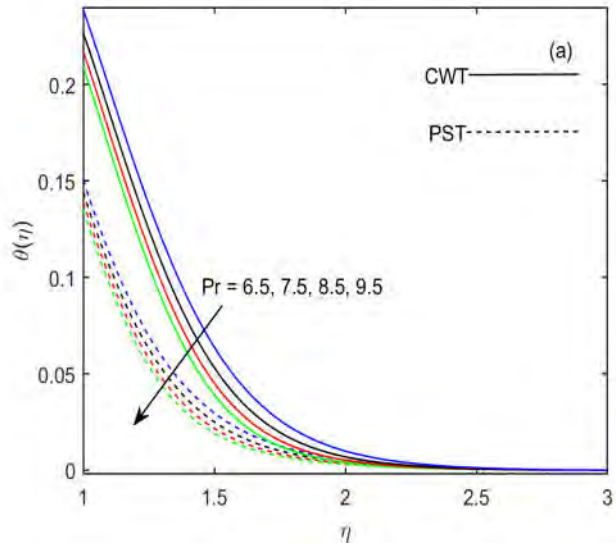


Figure 7.5: Temperature profile via  $Ec_1$  and  $Ec_2$ .





**Figure 7.6:** Temperature profile via  $R_d$  and  $\gamma_1$ .



**Figure 7.6:** Temperature profile via  $Pr$ .

**Table 7.1:** Comparison values of axial  $f'(1)$  and swirl  $g'(1)$  velocities gradient for various Re in limiting case when  $\beta_1 = M = 0$ .

Re	$f''(1)$	$g'(1)$	$f''(1)$	$g'(1)$
	Ref. [20]	Ref. [20]	Present results	Present results
0.1	-0.48180	-0.51019	-0.488907	-0.501542
0.2	-0.61748	-0.52605	-0.610423	-0.528809
0.3			-0.711562	-0.563363
0.4			-0.797618	-0.585919
0.5	-0.88220	-0.58488	-0.809541	-0.608461
01	-1.17775	-0.68772	-1.177669	-0.697671
02	-1.59389	-0.87263	-1.596640	-0.869605
03			-1.911086	-1.038214
04			-2.178536	-1.178690
05	-2.41743	-1.29788	-2.417865	-1.297590
10	-3.34446	-1.81006	-3.340094	-1.800194

**Table 7.2:** Numerical values of thermal gradient  $\theta'(1)$  at the surface of cylinder for different values of  $Re$ ,  $R_d$ ,  $\gamma_1$ ,  $Ec_1$  and  $Ec_2$  with fixed  $\beta_1 = 0.5$ ,  $M = 1$ ,  $Pr = Le = 6.5$ .

Re	$R_d$	$\gamma_1$	$Ec_1$	$Ec_2$	$-\theta'(1)$ (CWT)	$-\theta'(1)$ (PST)
01	0.5	0.5	0.01	0.01	0.3337021	0.3732276
02					0.3605406	0.3982065
03					0.3740732	0.4108923
03	0.5	0.5	0.01	0.01	0.3744063	0.4108923
	1.0				0.3646504	0.4051505
	1.5				0.3558449	0.3997259
03	0.5	0.5	0.01	0.01	0.3741061	0.4108923
		1.0			0.5807860	0.6734085
		1.5			0.7007817	0.8421188
03	0.5	0.5	0.01	0.01	0.3741061	0.4108923
			0.05		0.3713700	0.4090617
			0.09		0.3686487	0.4072392
03	0.5	0.5	0.1	0.01	0.3741061	0.4108923
				0.03	0.3539136	0.3988376
				0.05	0.3338697	0.3868411

## Chapter 8

# Von Kármán Flow of Maxwell

# Nanofluid Featuring the

# Cattaneo-Christov Theory with

# Buongiorno Model

This chapter analyzes the transport of thermal and solutal energy in Maxwell nanofluid flow induced above the constant rotating disk. The significant features of fluid thermal and solutal relaxation times are studied by using the Cattaneo-Christov double diffusion theory rather than classical Fourier's and Fick's approaches. A novel idea of the Buongiorno nanofluid model together with Cattaneo-Christov theory is introduced for the Maxwell fluid flow over a rotating disk. Additionally, the thermal and solutal distributions have been controlled with the impacts of the heat source and chemical reaction. The classical von Karman similarities are used to acquire the non-linear system of ordinary equations (ODEs).

The analytical series solution of governing ODEs is obtained by employing the well-known homotopy analysis method. The validation of results is provided with published results by making the comparison tables. The graphically presented outcomes for the physical problem reveal that the higher values of stretching strength parameter enhance the radial velocity and decline the circumferential velocity. The increasing trend is noted for axial velocity profile in a downward direction with the higher values of stretching strength parameter. The higher values of relaxation time parameters in Cattaneo-Christov theory decrease the thermal and solutal energy transportation in the flow of Maxwell nanoliquid.

## 8.1 Mathematical Formulation

Consider the laminar incompressible flow of Maxwell nanofluid above the stretchable rotating disk. The stretching velocity of the disk is assumed as  $u_s = cr$  and rotating velocity is  $v_s = \Omega r$ , where  $c$  and  $\Omega$  are stretching and rotating rates, respectively. A transverse uniform magnetic field  $\mathbf{B} = (0, 0, B_0)$  is applied to the flow velocity in  $z$ -direction. The whole flow analysis is performed into cylindrical coordinates by assuming that the velocity field as  $\mathbf{V} = [u, v, w]$  in the directions of  $(r, \varphi, z)$ , respectively, where  $(r, \varphi, z)$  are (radial, azimuthal, axial) directions, respectively and physical interpretation of the phenomenon given in **Fig. 8.1**.

By utilizing the conservation laws, Eqs. (1.1, 1.2, 1.6, 1.7) and material relations given in Eqs. (1.10 – 1.12) (cf. Chapter 1) we arrived at following set of governing boundary layer

partial differential equations

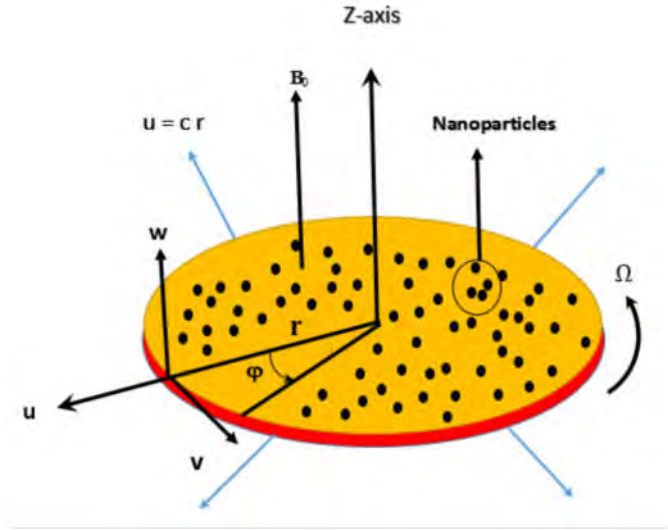


**Figure 8.1:** Geomertic presentation of problem.

$$\frac{\partial u}{\partial r} + \frac{u}{r} + \frac{\partial w}{\partial z} = 0, \quad (8.1)$$

$$\begin{aligned} u \frac{\partial u}{\partial r} + w \frac{\partial u}{\partial z} - \frac{v^2}{r} &= \nu \left[ \frac{\partial^2 u}{\partial z^2} \right] - \frac{\sigma B_0^2}{\rho} \left( u + \lambda_1 w \frac{\partial u}{\partial z} \right) \\ -\lambda_1 \left[ u^2 \frac{\partial^2 u}{\partial r^2} + 2uw \frac{\partial^2 u}{\partial r \partial z} + w^2 \frac{\partial^2 u}{\partial z^2} - \frac{2uv}{r} \frac{\partial v}{\partial r} - \frac{2vw}{r} \frac{\partial v}{\partial z} + \frac{v^2}{r} \frac{\partial u}{\partial r} + \frac{uw^2}{r^2} \right], \end{aligned} \quad (8.2)$$

$$\begin{aligned} u \frac{\partial v}{\partial r} + w \frac{\partial v}{\partial z} + \frac{uw}{r} &= \nu \left[ \frac{\partial^2 v}{\partial z^2} \right] - \frac{\sigma B_0^2}{\rho} \left( v + \lambda_1 w \frac{\partial v}{\partial z} \right) \\ -\lambda_1 \left[ u^2 \frac{\partial^2 v}{\partial r^2} + 2uw \frac{\partial^2 v}{\partial r \partial z} + w^2 \frac{\partial^2 v}{\partial z^2} + \frac{2uv}{r} \frac{\partial u}{\partial r} + \frac{2vw}{r} \frac{\partial u}{\partial z} - \frac{2u^2}{r^2} - \frac{v^3}{r^2} + \frac{v^2}{r^2} \frac{\partial v}{\partial r} \right], \end{aligned} \quad (8.3)$$

$$\begin{aligned}
& u \frac{\partial T}{\partial r} + w \frac{\partial T}{\partial z} - \tau \left[ D_B \left( \frac{\partial C}{\partial z} \frac{\partial T}{\partial z} \right) + \frac{D_T}{T_\infty} \left( \frac{\partial T}{\partial z} \right)^2 \right] \\
& + \lambda_t \left[ u^2 \frac{\partial^2 T}{\partial r^2} + 2uw \frac{\partial^2 T}{\partial r \partial z} + w^2 \frac{\partial^2 T}{\partial z^2} + u \frac{\partial u}{\partial r} \frac{\partial T}{\partial r} + w \frac{\partial u}{\partial z} \frac{\partial T}{\partial r} + u \frac{\partial w}{\partial r} \frac{\partial T}{\partial z} + w \frac{\partial w}{\partial z} \frac{\partial T}{\partial z} \right] \\
& - \lambda_t \tau D_B \left[ u \frac{\partial^2 C}{\partial r \partial z} \frac{\partial T}{\partial z} + u \frac{\partial C}{\partial z} \frac{\partial^2 T}{\partial r \partial z} + w \frac{\partial^2 C}{\partial z^2} \frac{\partial T}{\partial r} + w \frac{\partial C}{\partial z} \frac{\partial^2 T}{\partial z^2} \right] \\
& - 2\lambda_t \tau \frac{D_T}{T_\infty} \left[ u \frac{\partial T}{\partial z} \frac{\partial^2 T}{\partial r \partial z} + w \frac{\partial T}{\partial z} \frac{\partial^2 T}{\partial z^2} \right] = \frac{k}{\rho c_p} \left[ \frac{\partial^2 T}{\partial z^2} \right] \\
& + \frac{Q_\infty}{\rho c_p} (T - T_\infty) + \lambda_t \frac{Q_\infty}{\rho c_p} \left( u \frac{\partial T}{\partial r} + w \frac{\partial T}{\partial z} \right), \tag{8.4}
\end{aligned}$$

$$\begin{aligned}
& u \frac{\partial C}{\partial r} + w \frac{\partial C}{\partial z} + \lambda_c \left[ \begin{array}{c} u^2 \frac{\partial^2 C}{\partial r^2} + 2uw \frac{\partial^2 C}{\partial r \partial z} + w^2 \frac{\partial^2 C}{\partial z^2} \\ u \frac{\partial u}{\partial r} \frac{\partial C}{\partial r} + w \frac{\partial u}{\partial z} \frac{\partial C}{\partial r} + u \frac{\partial w}{\partial r} \frac{\partial C}{\partial z} + w \frac{\partial w}{\partial z} \frac{\partial C}{\partial z} \end{array} \right] \\
& - \lambda_c \frac{D_T}{T_\infty} \left[ u \frac{\partial^3 T}{\partial r \partial z^2} + w \frac{\partial^3 T}{\partial z^3} \right] = D_B \left[ \frac{\partial^2 C}{\partial z^2} \right] + \frac{D_T}{T_\infty} \left( \frac{\partial^2 T}{\partial z^2} \right) \\
& - k_1 (C - C_\infty) - \lambda_c k_1 \left( u \frac{\partial C}{\partial r} + w \frac{\partial C}{\partial z} \right). \tag{8.5}
\end{aligned}$$

The corresponding boundary conditions for given problems are

$$u(r, z) = cr, \quad v(r, z) = \Omega r, \quad w(r, z) = 0, \quad T = T_w, \quad C = C_w \quad \text{at } z = 0, \tag{8.6}$$

$$u \rightarrow 0, \quad v \rightarrow 0, \quad T \rightarrow T_\infty, \quad C \rightarrow C_\infty \quad \text{as } z \rightarrow \infty. \tag{8.7}$$

In the view of von Karman flow similities

$$\begin{aligned}
& u = \Omega r F, \quad v = \Omega r G, \quad w = \sqrt{\Omega \nu} H, \quad \eta = \sqrt{\frac{\Omega}{\nu}} z \\
& \phi(\eta) = \frac{C - C_\infty}{C_w - C_\infty}, \quad \theta(\eta) = \frac{T - T_\infty}{T_w - T_\infty}. \tag{8.8}
\end{aligned}$$

The overhead Eqs. (8.1) – (8.7) yield

$$H' + 2F = 0, \quad (8.9)$$

$$\begin{aligned} F^2 - G^2 + F'H - F'' + \beta_1(F''H^2 + 2FF'H - 2GG'H) \\ + M(F + \beta_1F'H) = 0, \end{aligned} \quad (8.10)$$

$$\begin{aligned} 2FG + G'H - G'' + \beta_1(G''H^2 + 2FG' + 2F'G) \\ + M(G + \beta_1G'H) = 0, \end{aligned} \quad (8.11)$$

$$\begin{aligned} \theta'' - \text{Pr } H\theta' + \text{Pr } N_b\beta_t(H\theta'\phi'' + H\theta''\phi') + \text{Pr } N_t(\theta'^2 + 2\beta_tH\theta'\theta'') \\ + \text{Pr } N_b\theta'\phi' - \text{Pr } \beta_t(H^2\theta'' + HH'\theta') + \text{Pr } \delta\theta + \text{Pr } \beta_t\delta H\theta' = 0, \end{aligned} \quad (8.12)$$

$$\begin{aligned} \phi'' - \text{Le } \text{Pr } H\phi' - \text{Le } \text{Pr } \beta_c(H^2\phi'' + HH'\phi') \\ + \frac{N_t}{N_b}(\theta'' + \beta_cH\theta''') - \text{Le } \text{Pr } K_1\phi - \text{Le } \text{Pr } \beta_cK_1H\phi' = 0, \end{aligned} \quad (8.13)$$

with corresponding boundary conditions

$$F(0) = R, \quad G(0) = 1, \quad H(0) = 1, \quad \theta(0) = 1, \quad \phi(0) = 1, \quad (8.14)$$

$$F(\infty) = 0, \quad G(\infty) = 0, \quad \theta(\infty) = 0, \quad \phi(\infty) = 0, \quad (8.15)$$



with  $R$  ( $= \frac{c}{\Omega}$ ) as the stretching strength parameter,  $\beta_1$  ( $= \lambda_1 \Omega$ ) the Maxwell number,  $M$  ( $= \frac{\sigma B_0^2}{\rho \Omega}$ ) the magnetic parameter,  $\beta_t$  ( $= \lambda_t \Omega$ ) the thermal relaxation parameter,  $\beta_c$  ( $= \lambda_c \Omega$ ) the mass relaxation time,  $\delta$  ( $= \frac{Q_0}{(\rho c_p) \Omega}$ ) heat generation parameter,  $K_1$  ( $= \frac{k_1}{\Omega}$ ) the chemical reaction parameter,  $N_b$  ( $= \frac{\tau D_B (C_w - C_\infty)}{\nu}$ ) the Brownian diffusion coefficient,  $N_t$  ( $= \frac{\tau D_T (T_w - T_\infty)}{\nu T_\infty}$ ) the thermophoresis parameter,  $Pr$  ( $= \frac{\nu (\rho c_p)}{k}$ ) the Prandtl number and  $Le$  ( $= \frac{\alpha_1}{D_B}$ ) the Lewis number.

## 8.2 Solution Procedure

The solution of governing ODEs which are given in Eqs. (8.9) – (8.13) for flow field, temperature and concentration distributions is acquired by adopting the well known semi-analytical technique namely as homotopy analysis method (HAM) along with corresponding boundary conditions given in Eqs. (8.14) and (8.15). For the construction of homotopic series solution via homotopy approach we choose the following initial guesses ( $H_0, G_0, \theta_0, \phi_0$ ) auxiliary linear operators ( $\mathcal{L}_H, \mathcal{L}_G, \mathcal{L}_\theta, \mathcal{L}_\phi$ ) as

$$H_0(\eta) = -2R(1 + e^{-\eta}), \quad G_0(\eta) = e^{-\eta}, \quad \theta_0(\eta) = e^{-\eta}, \quad \phi_0(\eta) = e^{-\eta}, \quad (8.16)$$

$$\begin{aligned} \mathcal{L}_H[H(\eta)] &= H''' - H', \quad \mathcal{L}_G[G(\eta)] = G'' - G, \\ \mathcal{L}_\theta[\theta(\eta)] &= \theta'' - \theta, \quad \mathcal{L}_\phi[\phi(\eta)] = \phi'' - \phi. \end{aligned} \quad (8.17)$$

### 8.3 Convergence of Solution

In order to get the convergent series solution the optimal value of convergence control parameters  $\hbar_H$ ,  $\hbar_G$ ,  $\hbar_\theta$  and  $\hbar_\phi$  for the velocity field, temperature and concentration distributions, respectively, must be found. By employing the following exact square residual error formula for any function  $\hat{F}$  the appropriate value of these parameters are obtained:

$$\hat{F}_{f,m} = \frac{1}{N+1} \sum_{j=0}^N \left[ N_f \sum_{i=0}^m \hat{F}_j(i\Delta\eta) \right]^2. \quad (8.18)$$

Series solution convergence for velocity field achieved at 20<sup>th</sup>–order of estimate while 30<sup>th</sup>–order of estimate is noted for temperature and concentration fields.

**Table 8.1:** Convergence of homotopic solutions of velocity field, temperature and concentration distributions for fixed  $R = \beta_1 = N_t = N_b = \beta_t = \beta_c = K_1 = 0.1$ ,  $M = 1$ ,  $\delta = 0.05$ ,  $Pr = Le = 2.5$ .

Order of approximation	$-H'(0)$	$-G'(0)$	$-\theta'(0)$	$-\phi'(0)$
1	0.098180	1.031300	0.805625	0.914583
5	0.187226	1.135630	0.463267	1.167764
10	0.179973	1.157462	0.327401	1.444659
15	0.179393	1.160232	0.300465	1.424335
20	0.179323	1.160626	0.281796	1.454769
25	0.179323	1.160626	0.276891	1.450788
30	0.179323	1.160626	0.283497	1.522378
35	0.179323	1.160626	0.283497	1.522378

## 8.4 Discussion of Results

The flow field, temperature and concentration distributions with the impact of pertinent parameters are presented graphically. An extensive discussion of acquired graphical results for the current physical problem is presented in this section. Moreover, a physical justification is given for each result. The fix values of all physical parameters are taken as  $R = 0.5$ ,  $\beta_1 = 0.1$ ,  $M = 1$  for velocity field and  $R = \beta_1 = \beta_t = \beta_c = N_t = N_b = 0.1$ ,  $M = 1$ ,  $\delta = K_1 = 0.05$ ,  $Pr = Le = 6.5$  for temperature and concentration distributions.

It is observed from **Figs. 8.2(a–c)** that for higher values of stretching strength parameter  $R$  the velocity field increases in radial direction and decreases in the azimuthal direction. Because for higher values of  $R$  the stretching rate enhance in the radial direction and swirl rate declines in angular direction thus, corresponding components of velocity field increase and decrease, respectively. In the case of the axial component of the velocity field, we noted that the axial velocity increases in the negative direction. Physically, the rotating disk acts as a centrifugal pump which throws the fluid in an outward direction thus, the axial velocity enhances in a downward direction from the free stream. **Figs. 8.3(a – c)** depict the impact of Maxwell parameter  $\beta_1$  on the velocity field. The results reveal that both radial and azimuthal velocities decline and axial velocity increases in the upward direction. These outcomes are physically justified because for the higher values of  $\beta_1$  we observe the large value of relaxation time in the fluid which means the fluidity of material significantly decreases the fluid becomes more solid like. Thus, in result the fluid motion decreases in all directions. The axial velocity in downward direction decreases because disk is required larger centrifugal force to throw fluid outward which is more solid like. **Figs. 8.4(a – c)** explore that rise in magnetic parameter  $M$

decreases the velocity of the fluid motion. Physically, the magnetic parameter corresponds to the Lorentz force which acts as a resistive force to the fluid motion thus, the flow field declines.

There is a higher transport rate of thermal and solutal energy in the flow of Maxwell fluid induced above the rotating disk with the enlargement of  $\beta_1$ . This result is explored through **Figs. 8.5(a, b)**. Physically, the conduction of heat and mass transport increases with a large value of relaxation time in the viscoelastic fluid. The consequence of Cattaneo-Christov theory to the transport of thermal and solutal is depicted through the relaxation time parameter  $\beta_t$  and  $\beta_c$ , respectively. **Figs. 8.6(a, b)** show that there is a decrease in thermal and solutal energy with higher values of  $\beta_t$  and  $\beta_c$ , respectively. Physically, increase in relaxation time the instant propagation of energy waves in the fluid is controlled thus, transport of energy decreases. The impact of stretching strength parameter  $R$  and magnetic parameter  $M$  on the temperature and concentration fields is reported in **Figs. 8.7(a, b)** and **Figs. 8.8(a, b)**, respectively. It is noted that the temperature and concentration fields boost up and decline with the increasing trend in  $M$  and  $R$ , respectively. Physically, the forced mechanism for the transport of thermal and solutal energy from the surface of a disk to the free stream fluid mainly depends upon the axial velocity component thus, the rise in  $R$  the axial component of the velocity field increases in downward direction. So, in result the temperature and concentration fields decline. On the other hand, the rise in magnetic parameter  $M$  enhances the Lorentz force in the axial direction. Thus, the conduction of energy between the fluid particles rise due to the large Lorentz force, which causes to boost up the temperature and concentration distribution.

In the nanofluid flow, the thermophoretic and Brownian forces contribute to the enhancement of heat and mass transport. The effect of these two forces on the temperature and concentration distributions is studying through two dimensionless parameters  $N_t$  and  $N_b$ . The plots in

**Figs. 8.9(a, b)** explored that higher values of  $N_t$  enhance both temperature and concentration distributions. Physically, rise in  $N_t$  the thermal gradient in the nanofluid increases due to which the tiny solid particles move away from higher temperature point to lower temperature point. So, as a result, the conduction of energy rises in a nanofluid. The converse trend is observed in the case of a higher value of  $N_b$  for temperature and concentration distributions which is cleared by **Figs. 8.10(a, b)**. The temperature field enhances but concentration declines. Physically, the Brownian motion increases due to a rise in  $N_b$  that produce the resistance to mass transport. So, concentration distribution falls down but thermal transport enhances the due increase in effective heat capacity of nanoparticles. Plots in **Figs. 8.11(a, b)** envision the results for heat generation source  $\delta$  to the thermal distribution and constructive chemical reaction  $K_1$  to the concentration distribution. It is noted that temperature profile rises due to increment in  $\delta$  and concentration profile boost up for higher values of  $K_1$ . Physically, the heat source  $\delta$  generate the extra heat in the fluid due to which the temperature field increases. In the case of higher values of  $K_1$ , the constructive reaction in the fluid increases the mass transport. The validation of results is proved with help of comparison **Tables 8.2, 8.3** and **8.4** with excellent agreement.

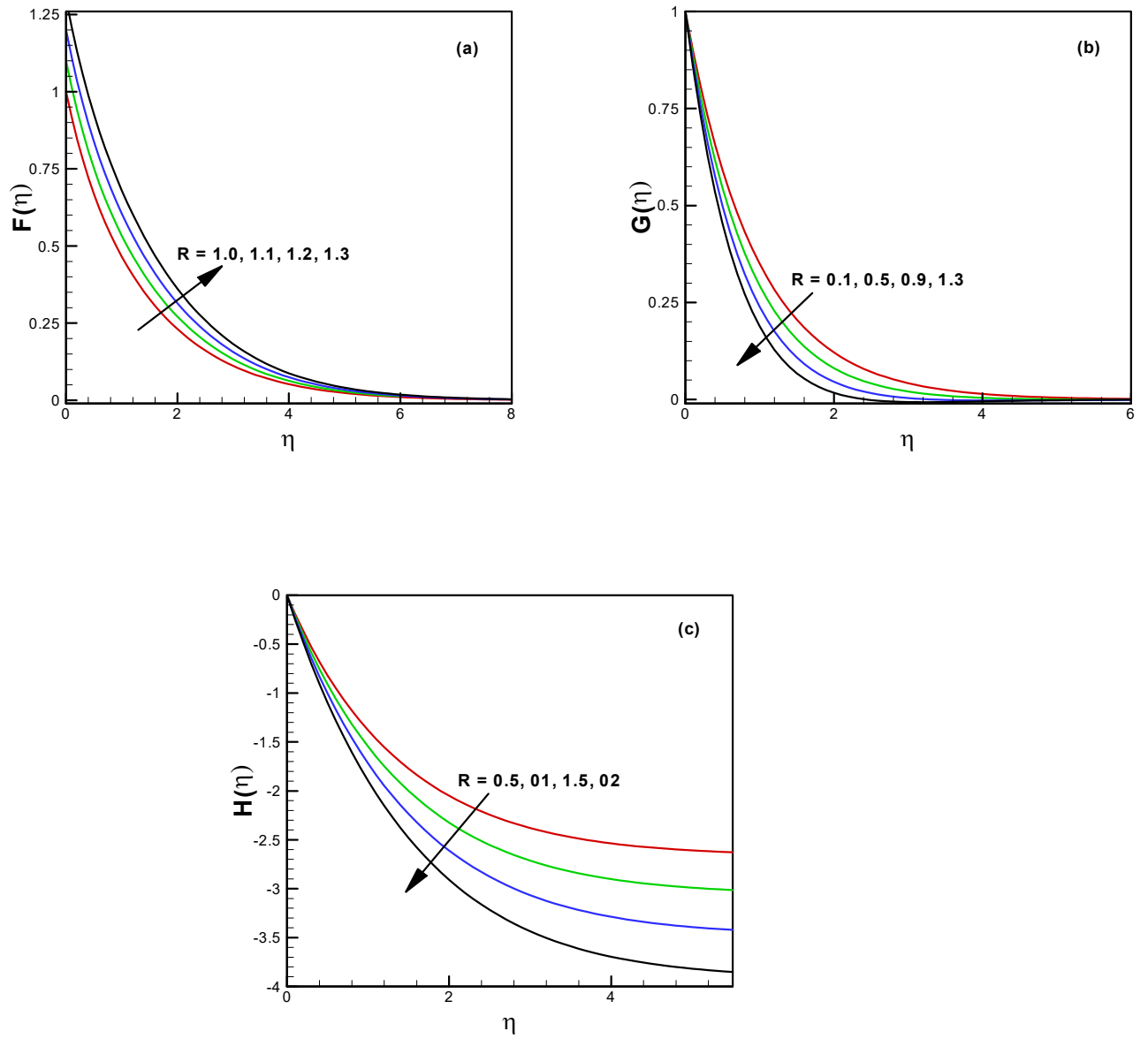


**Figure 8.2:** Velocity field via rotation parameter  $R$ .

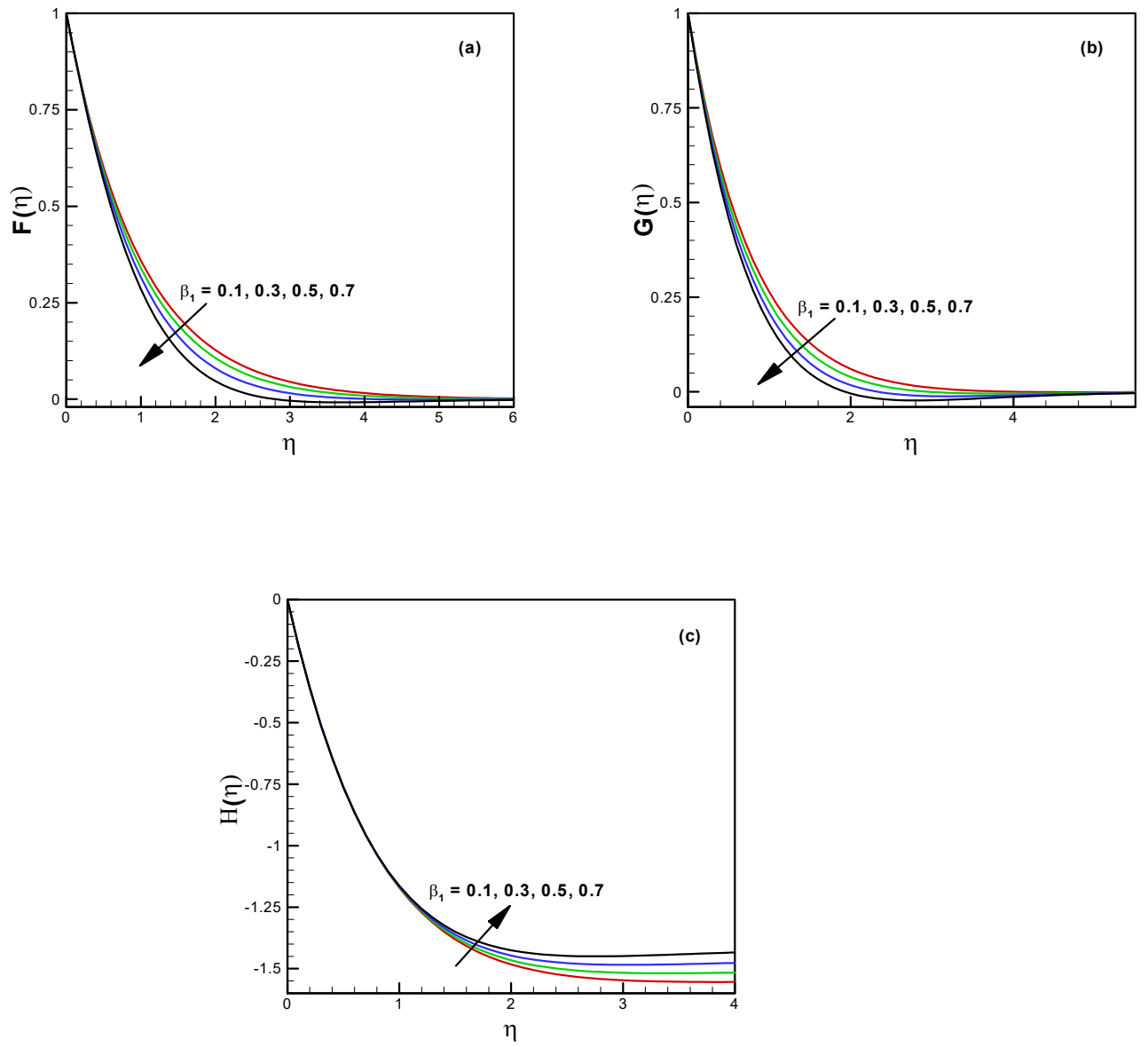


**Figure 8.3:** Velocity field via Maxwell parameter  $\beta_1$ .

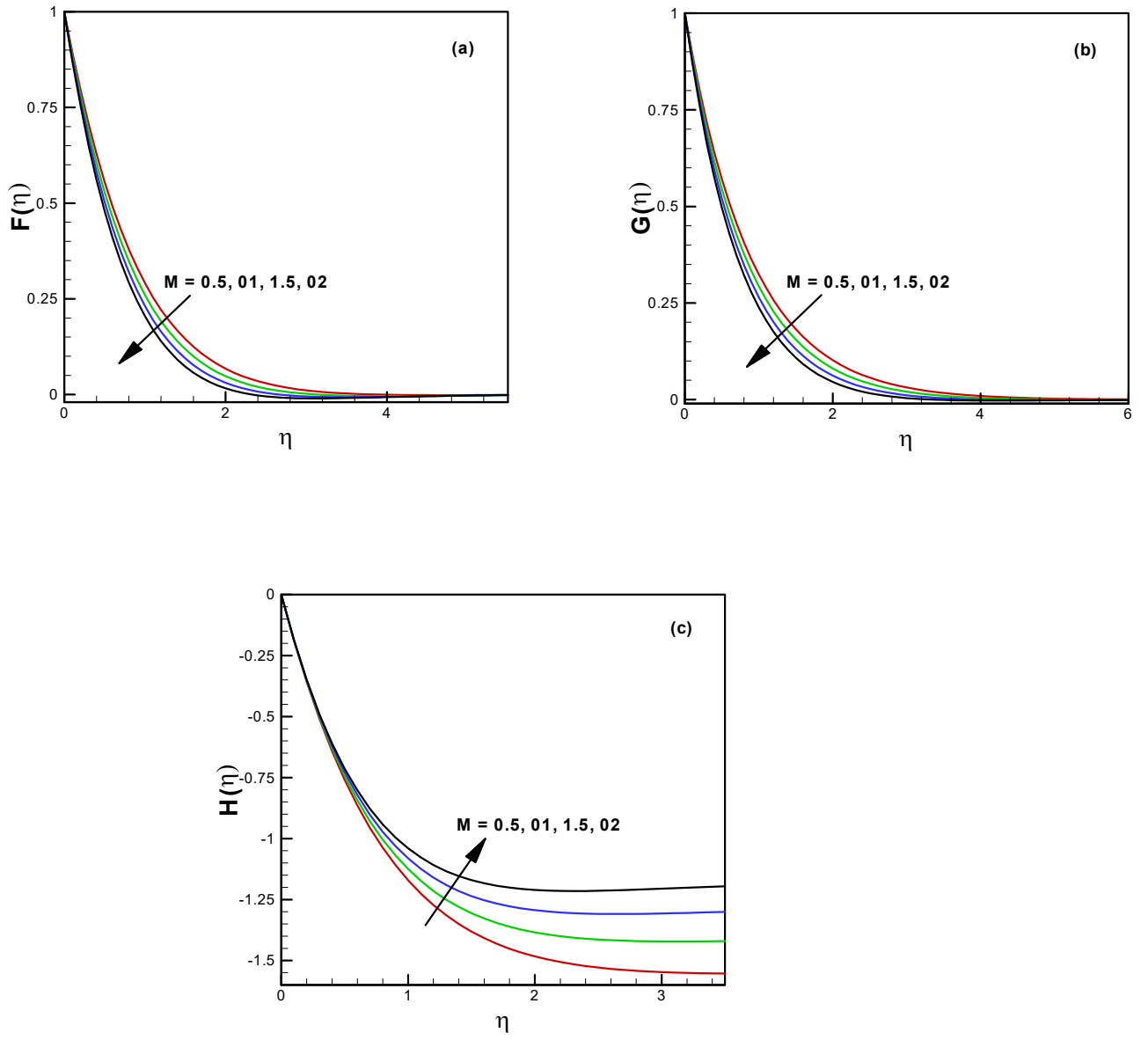


**Figure 8.4:** Velocity field via magnetic parameter  $M$ .



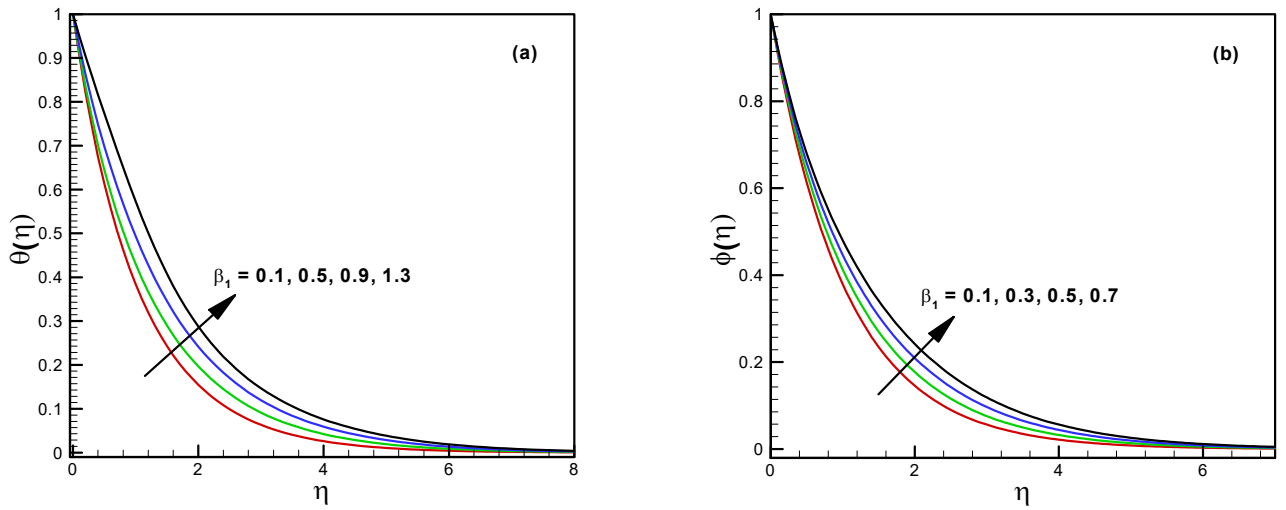


**Figure 8.5:** Temperature and concentration profiles via  $\beta_1$ .

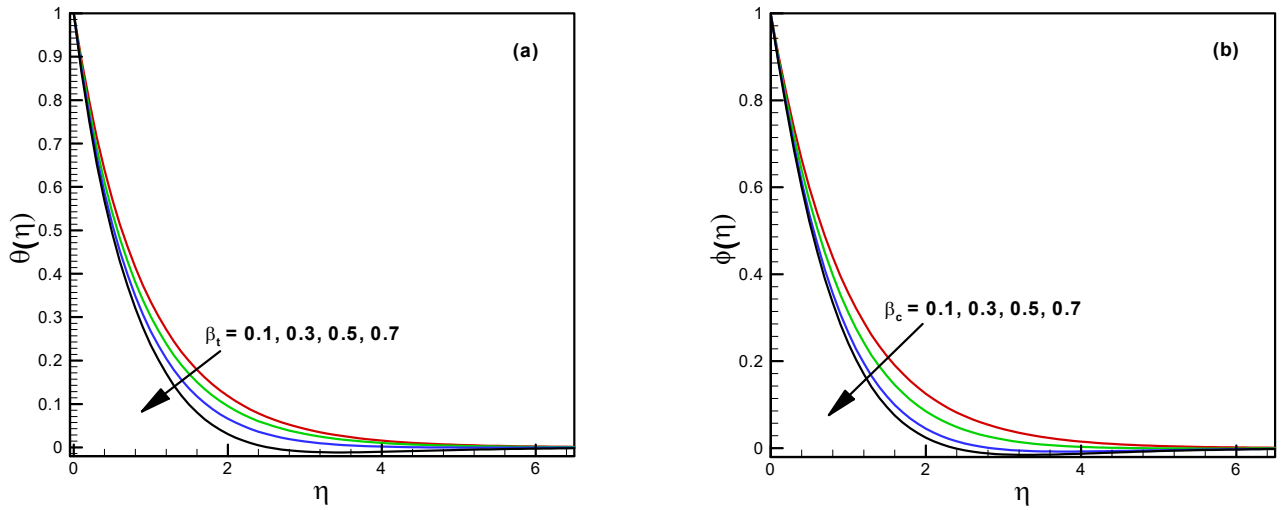


**Figure 8.6:** Temperature and concentration profiles via  $\beta_t$  and  $\beta_c$ .

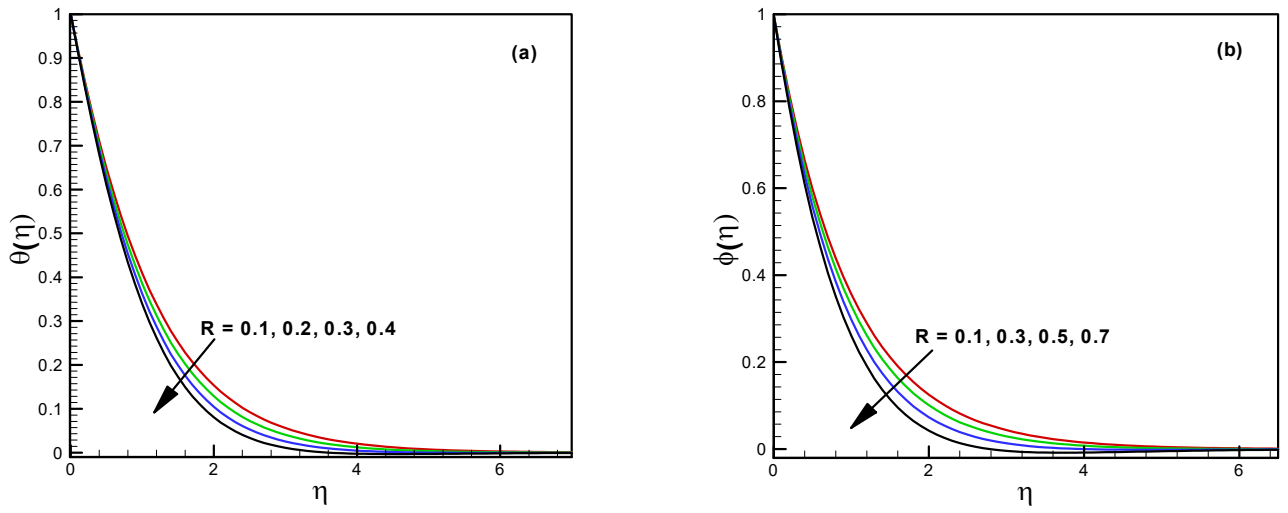


**Figure 8.7:** Temperature and concentration profiles via  $R$ .

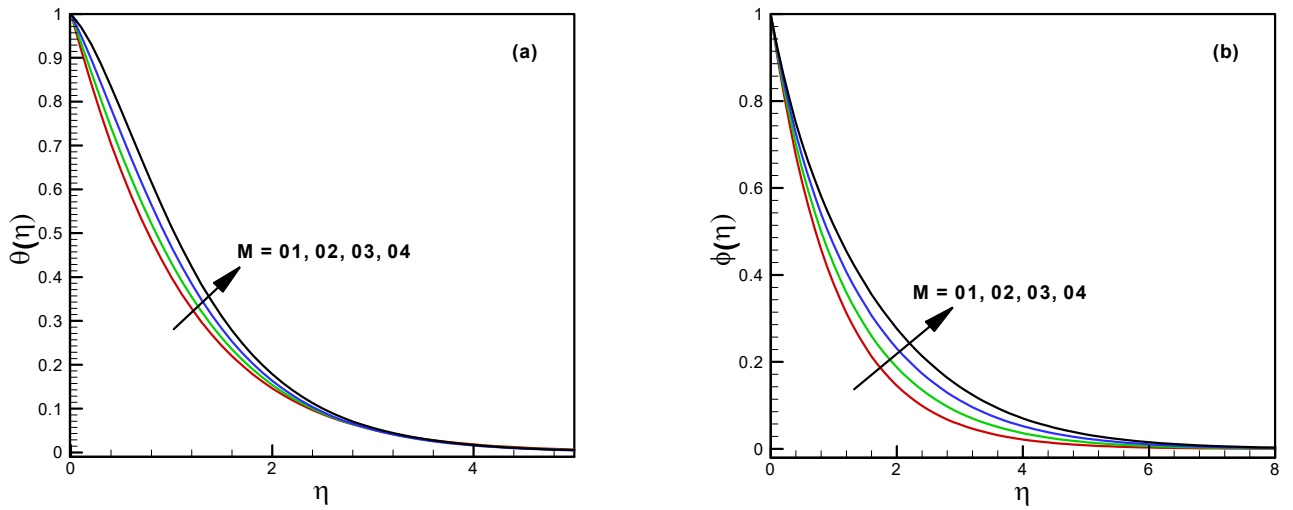


**Figure 8.8:** Temperature and concentration profiles via  $M$ .

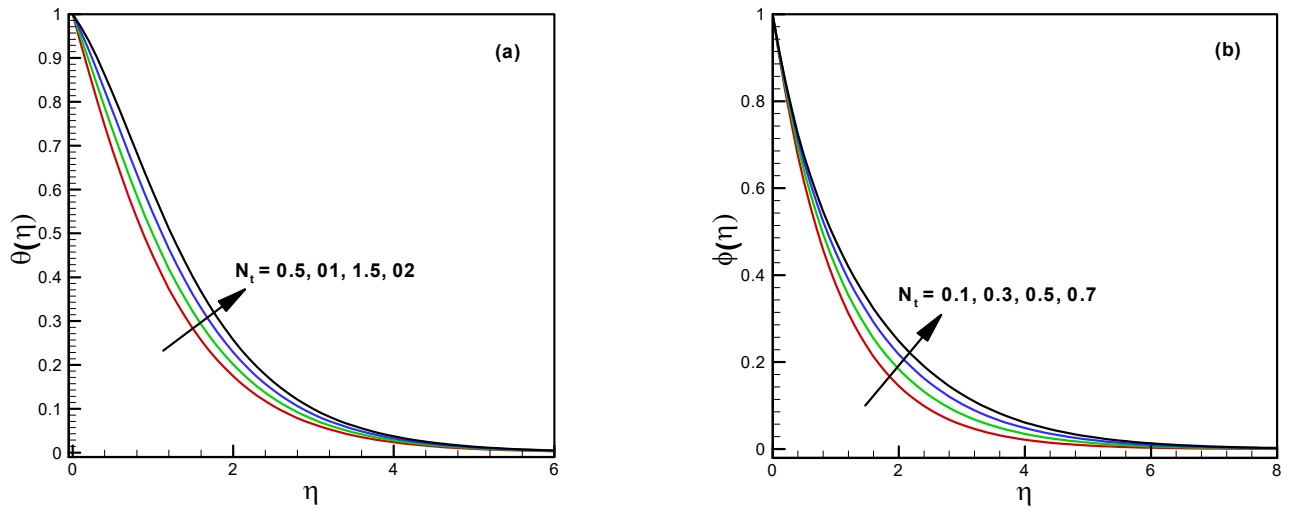


**Figure 8.9:** Temperature and concentration profiles via  $N_t$ .

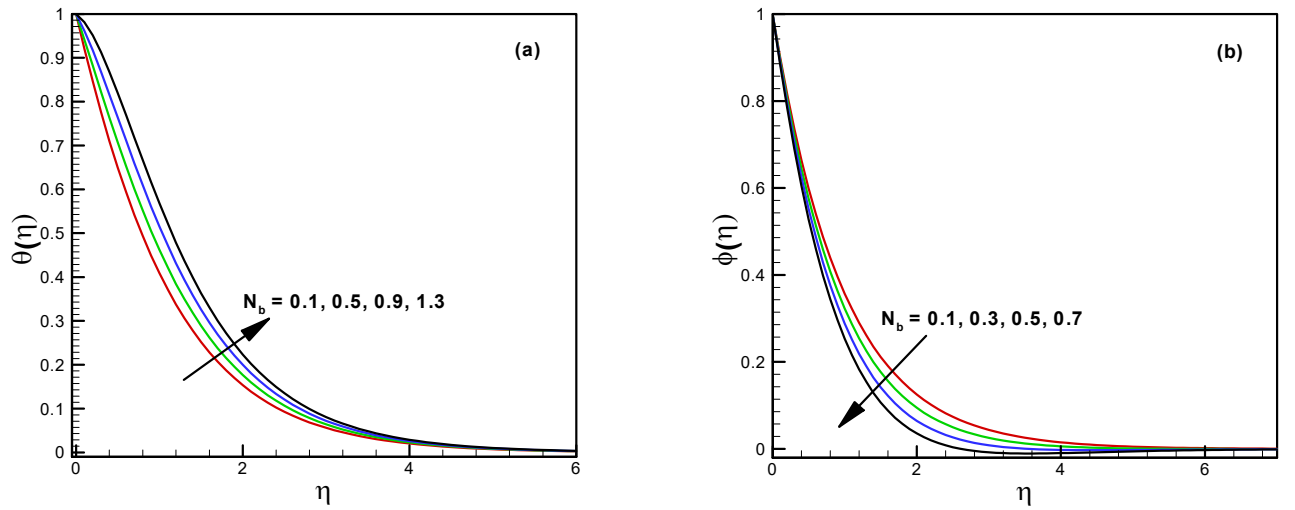


**Figure 8.10:** Temperature and concentration profiles via  $N_b$ .

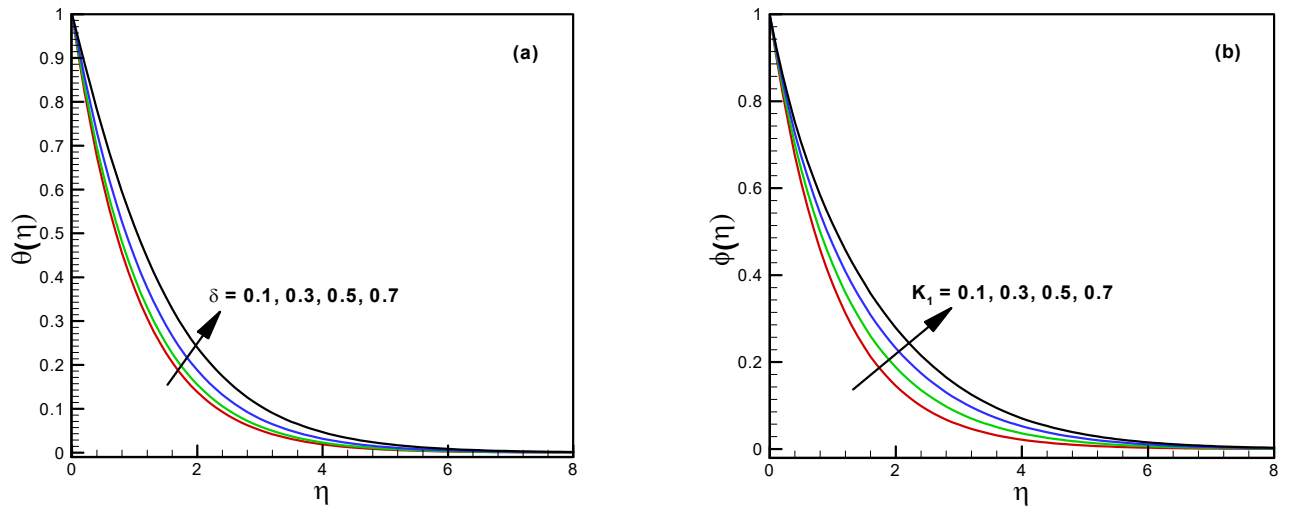


**Figure 8.11:** Temperature and concentration profiles via  $\delta$  and  $K_1$ , respectively.

**Table 8.2:** Comparison of radial, azimuthal velocity gradient and temperature gradient at the surface in limiting case when  $\beta_1 = M = R = N_t = N_b = \beta_t = \beta_c = \delta = K_1 = Le = 0$  and  $Pr = 6.2$ .

	Ref. [80]	Ref. [81]	Ref. [82]	Present results
$F'(0)$	0.5102326	0.5102	0.510116264	0.5000776
$-G'(0)$	0.6159220	0.6159	0.615849279	0.6185207
$-\theta(0)$	0.9338779	0.9337	0.933694112	0.9300460

**Table 8.3:** Comparison of radial, azimuthal velocity gradient at the surface in limiting case when  $\beta_1 = M = N_t = N_b = \beta_t = \beta_c = \delta = K_1 = Le = Pr = 0$  and  $R = 1$ .

	Ref. [83]	Ref. [84]	Present results
$F'(0)$	-0.9483	-0.9483	-0.948316
$-G'(0)$	1.4870	1.4870	1.486953

**Table 8.4:** Comparison of temperature gradient at the surface for various values of Prandtl number  $Pr$  in limiting case when  $\beta_1 = M = R = N_t = N_b = \beta_t = \beta_c = \delta = K_1 = Le = 0$ .

$Pr$	Ref. [85]	Present results
1	0.3925	0.396855
10	1.1341	1.133851
100	2.6871	2.686744

## Chapter 9

# Thesis Summary and Future Recomendations

The idea behind the present theoretical investigation was to analyze the rheological properties of the viscoelastic Maxwell fluid flow generated by stretchable and rotating surfaces. Moreover, in a broad context predicting the transport mechanism of thermal and solutal energy in such flows was also part of this study. The various physical effects were incorporated while studying the flow phenomenon. Both numerical and analytical methodologies have been used to compute the solution of similar governing ODEs to reveal the flow and energy transport characteristics of Maxwell fluid.

### 9.1 Conclusions

The key findings of this theory based analysis are summarized in this chapter in the form of follwoing concluding points:

- An increase in the phenomenon of stress relaxation for a viscoelastic Maxwell fluid resulted in decrease the flow velocity significantly while conduction of heat energy was increased.
- The stretching strength parameter for bi-axially stretching sheet and stretchable rotating disk enhanced the flow of fluid in an axial and radial direction, respectively, whereas an opposite trend was observed in the case of transverse and azimuthal direction, respectively.
- The Reynolds number  $Re$  in three-dimensional flow of fluid due to the stretchable rotating cylinder is the flow controlling parameter and both swirl and axial velocities reduced and decay exponentially for higher values of  $Re$  and fluid motion occurred only near to the surface.
- For  $Re = 0$  the fluid motion occurred near to the surface due to only torsional motion of the cylinder.
- The higher values of  $Re$  also reduced the heat and mass transport in fluid motion due to decrease in the main forced convection mechanism.
- Fluid flow velocity from free stream to rotating disk surface was increased due to higher values of stretching strength parameter.
- The buoyant motion of fluid boosted the velocity field but declined the temperature and concentration distribution in assisting mode.
- The stretching rate of the cylinder decreased due to higher values of the unsteadiness parameter, therefore, the fluid motion declined. Furthermore, the thermal energy transport decreased with higher values of unsteadiness parameter in case of PST but enhanced in the case of CWT.

- Higher rate of heat transport was observed for constant wall temperature (CWT) as compared to prescribed surface temperature (PST).
- The heat generation source, thermal radiation increased the heat transport rate in the fluid and constructive chemical reaction enhanced mass transport. Moreover, advective transport of thermal energy was also enhanced for higher values of Eckert number.
- An increase in thermal energy transport in the flow of Maxwell fluid was noted due to haphazard motion and thermo-migration of nanoparticles.
- The temperature and concentration fields were diminished by thermal and solutal relaxation phenomena, respectively.

## 9.2 Future Recommendations

More of the attention in this thesis has been paid to the analysis of rheological properties of Maxwell fluid flow induced above the rotating and stretching surfaces with thermal and solutal energy transport. However, there is space for further development in this area of research and extension to this can be carried out. So, here are following few suggestions that can be considered in future research, which are listed as follows:

- Unsteady 3D flow Maxwell fluid flow over stretchable rotating cylinder under various physical effects can be part of future investigations. However, a well suitable flow similarity transformations are also needed for this work.
- Stretchable rotating boundaries have been considered here, afterward, the flow of non-Newtonian fluid over purely rotating surfaces may be part of the future investigation.



- The flow of Maxwell fluid induced by rotating sphere with thermal energy transport has not explored yet. Thus, this gap can be filled with detailed theoretical study.
- Several advanced numerical techniques can be utilized e.g. finite element method (FEM) and finite volume method (FVM), for the simulation of such highly non-linear flows phenomena as well.

# Bibliography

- [1] M.F. Naccache and P.R.S. Mendes, Heat transfer to non-Newtonian fluids in laminar flow through rectangular ducts, *Int. J. Heat Fluid Flow*, **17(6)** (1996) 613-620.
- [2] S. Shin, The effect of the shear rate-dependent thermal conductivity of non-newtonian fluids on the heat transfer in a pipe flow, *Int. Commun. Heat Mass Transf.*, **23** (1996) 665-678.
- [3] J.M. Nouri and J.H. Whitelaw, Flow of Newtonian and non-Newtonian fluids in an eccentric annulus with rotation of the inner cylinder, *Int. J. Heat Fluid Flow*, **18(2)** (1997) 236-246.
- [4] H.A. Attia, Numerical study of flow and heat transfer of a non-Newtonian fluid on a rotating porous disk, *Appl. Math. Comput.*, **163** (2005) 327-342.
- [5] S. Dhinakaran, A.M. Afonso, M.A. Alves and F.T. Pinho, Steady viscoelastic fluid flow between parallel plates under electro-osmotic forces: Phan-Thien–Tanner model, *J. Colloid Interface Sci.*, **344(2)** (2010) 513-520.
- [6] K.V. Prasad, D. Pal, V. Umesh and N. P. Rao, The effect of variable viscosity on MHD viscoelastic fluid flow and heat transfer over a stretching sheet, *Commun. Nonlinear Sci. Numer. Simul.*, **15(2)** (2010) 331-344.

- [7] O. Malaspinas, N. Fiétier and M. Deville, Lattice Boltzmann method for the simulation of viscoelastic fluid flows, *J. non-Newton Fluid Mech.*, **165(23-24)** (2010) 1637-1653.
- [8] S. Siddiqa, N. Begum, M.A. Hossain and R.S.R. Gorla, Natural convection flow of a two-phase dusty non-Newtonian fluid along a vertical surface, *Int. J. Heat Mass Transf.*, **113** (2017) 482-489.
- [9] T.R. Mahapatra and S. Sidui, Non-axisymmetric Homann stagnation-point flow of a viscoelastic fluid towards a fixed plate, *Eur. J. Mech.*, **79** (2020) 38-43.
- [10] T. Wenchang, P. Wenxiao and X. Mingyu, A note on unsteady flows of a viscoelastic fluid with the fractional Maxwell model between two parallel plates, *Int. J. Non-Linear Mech.*, **38(5)** (2003) 645-650.
- [11] S. Nadeem, R.U. Haq and Z.H. Khan, Numerical study of MHD boundary layer flow of a Maxwell fluid past a stretching sheet in the presence of nanoparticles, *J. Taiwan Inst. Chem. Eng.*, **45(1)** (2014) 121-126.
- [12] S. Abbasbandy, T. Hayat, A. Alsaedi and M.M. Rashidi, Numerical and analytical solutions for Falkner-Skan flow of MHD Oldroyd-B fluid, *Int. J. Numer. Meth. Heat Fluid Flow*, **24(2)** (2014) 390-401.
- [13] J. Ahmed, M. Khan and L. Ahmad, MHD swirling flow and heat transfer in Maxwell fluid driven by two coaxially rotating disks with variable thermal conductivity, *Chin. J. Phys.*, **60** (2019) 22-34.
- [14] A. Rauf, Y. Mahsud and I. Siddique, Multi-layer flows of immiscible fractional Maxwell fluids in a cylindrical domain, *Chin. J. Phys.*, **67** (2020) 265-282.

- [15] L. J. Crane, Boundary layer flow due to a stretching cylinder, *ZAMP*, **26** (1975) 619-622.
- [16] C.Y. Wang, The three-dimensional flow due to a stretching flat surface, *The Phys. Fluids*, **27** (8) (1984) 1915-1917.
- [17] C.Y. Wang, Free convection on a verticle stretching surface, *ZAMM*, **69** (1989) 418-420.
- [18] K. Vajravelu, Viscous flow over a nonlinearly stretching sheet, *Appli. Math. Comput.*, **124**(3) (2001) 281-288.
- [19] P.D. Ariel, Axisymmetric flow of a second grade fluid past a stretching sheet, *Int. J. Eng. Sci.*, **39**(5) (2001) 529-553.
- [20] T. Fang and S. Yao, Viscous swirling flow over a stretching cylinder, *Chin. Phys. Lett.*, **28**(11) (2011) 114702.
- [21] M.A. Sprague and P.D. Weidman, Three-dimensional flow induced by the torsional motion of a cylinder, *Fluid Dyn. Res.*, **43**(1) (2010) 015501.
- [22] S.V. Subhashini, R. Sumathi and I. Pop, Dual solutions in a thermal diffusive flow over a stretching sheet with variable thickness, *Int. Commun. Heat Mass Transf.*, **48** (2013) 61-66.
- [23] S. Mukhopadhyay, MHD boundary layer flow and heat transfer over an exponentially stretching sheet embedded in a thermally stratified medium, *Alex. Eng. J.*, **52**(3) (2013) 259-265.
- [24] B.S. Dandapat, S.K. Singh and S. Maity, Thin film flow of bi-viscosity liquid over an unsteady stretching sheet: an analytical solution, *Int. J. Mech. Sci.*, **130** (2017) 367-374.

- [25] J. Ahmed, M. Khan and L. Ahmad, Transient thin film flow of nonlinear radiative Maxwell nanofluid over a rotating disk, *Phys. Lett. A*, **383(12)** (2019) 1300-1305.
- [26] M.F. Javed, M.I. Khan, N.B. Khan, R. Muhammad, M.U. Rehman, S.W. Khan and T.A. Khan, Axisymmetric flow of Casson fluid by a swirling cylinder, *Results Phys.*, 9 (2018) 1250-1255.
- [27] P.D. Weidman, Radial stagnation flow on a twisting cylinder, *J. Fluids Eng.*, **141 (11)** (2019) doi:10.1115/1.4043425.
- [28] C. Cattaneo, Sulla conduzione del calore. *Atti semin Mat Fis Univ Modena Rerrio Emilia*. **3** (1948) 83-101.
- [29] C.I. Christov, On a higher-gradient generalization of Fourier's law of heat conduction, *In: AIP Conf Proc.*, **946** (2007) 11-22.
- [30] M.A. Yousif, H.F. Ismael, T. Abbas and R. Ellahi, Numerical study of momentum and heat transfer of MHD Carreau nanofluid over exponentially stretched plate with internal heat source/sink and radiation, *Heat Transf. Res.*, **50(7)** (2019) 649-658.
- [31] M.M. Sarafraz, O. Pourmehran and B. Yang, Arjomandi M, Ellahi R, Pool boiling heat transfer characteristics of iron oxide nano-suspension under constant magnetic field, *Int. J. Therm. Sci.*, **147** (2020) 106131.
- [32] S. Han, L. Zheng, C. Li and X. Zhang, Coupled flow and heat transfer in viscoelastic fluid with Cattaneo-Christov heat flux model, *Appl. Math. Lett.*, **38** (2014) 87-93.

- [33] S.M. Upadhya, Mahesha and C.S.K. Raju, Cattaneo -Christov heat flux model for magnetohydrodynamic flow in a suspension of dust particles towards a stretching sheet, *Nonlinear Eng.*, **7** (2018) 237–246.
- [34] W.A. Khan, M. Irfan and M. Khan, An improved heat conduction and mass diffusion models for rotating flow of an Oldroyd-B fluid, *Results Phys.*, **7** (2017) 3583-3589.
- [35] W. Ibrahim, Three dimensional rotating flow of Powell-Eyring nanofluid with non-Fourier's heat flux and non-Fick's mass flux theory, *Results Phys.*, **8** (2018) 569-577.
- [36] M. Farooq, S. Ahmad, M. Javed and A. Anjum, Analysis of Cattaneo-Christov heat and mass fluxes in the squeezed flow embedded in porous medium with variable mass diffusivity, *Results Phys.* **7** (2017) 3788-3796.
- [37] S.Z. Alamri, A.A. Khan, M. Azeez and R. Ellahi, Effects of mass transfer on MHD second grade fluid towards stretching cylinder: A novel perspective of Cattaneo–Christov heat flux model, *Phys. Lett. A.*, **383** (2019) 276-281.
- [38] J. Ahmed, M. Khan and L. Ahmad, Effectiveness of homogeneous-heterogeneous reactions in Maxwell fluid flow between two spiraling disks with improved heat conduction features, *J. Therm. Anal. Calorim.*, (2019) doi.org/10.1007/s10973-019-08712-9.
- [39] S. Saleem, M. Awais, S. Nadeem, N. Sandeep and M.T. Mustafa, Theoretical analysis of upper-convected Maxwell fluid flow with Cattaneo–Christov heat flux model, *Chin. J. Phys.*, **55(4)** (2017) 1615-1625.
- [40] G. K. Reddy, K. Yarrakula, C.S.K. Raju, and A. Rahbari, Mixed convection analysis of variable heat source/sink on MHD Maxwell, Jeffrey, and Oldroyd-B nanofluids over a cone

- with convective conditions using Buongiorno's model, *J. Therm. Anal. Calorim.*, **132(3)** (2018) 1995-2002.
- [41] R. Ellahi, A. Zeeshan, N. Shehzad, and S. Z. Alamri, Structural impact of Kerosene-Al<sub>2</sub>O<sub>3</sub> nanoliquid on MHD Poiseuille flow with variable thermal conductivity: application of cooling process, *J. Mol. Liq.*, **264** (2018) 607-615.
- [42] V. Tibullo and V. Zampoli, A uniqueness result for the Cattaneo-Christov heat conduction model applied to incompressible fluids, *Mech. Res. Commun.*, **38(1)** (2011) 77-79.
- [43] A. Shahid, M.M. Bhatti, O.A. Bég and A. Kadir, Numerical study of radiative Maxwell viscoelastic magnetized flow from a stretching permeable sheet with the Cattaneo-Christov heat flux model. *Neu. Comp. Appl.*, **30** (2018) 3467-3478.
- [44] W. Ibrahim and B. Hindebu, Magnetohydrodynamic(MHD) boundary layer flow of Eyring-Powell nanofluid past stretching cylinder with Cattaneo-Christov heat flux model, *Nonlinear Eng.*, **8** (2019) 303-317.
- [45] K.K. Anantha, V. Sugunamma and N. Sandeep, Influence of viscous dissipation on MHD flow of micropolar fluid over a slendering stretching surface with modified heat flux model, *J. Therm. Anal. Calorim.*, (2019) doi.org/10.1007/s10973-019-08694-8.
- [46] T. Hayat, S. Qayyum, A. Alsaedi and B. Ahmad, Nonlinear convective flow with variable thermal conductivity and Cattaneo-Christov heat flux, *Neu. Comp. Appl.*, **31** (2019) 295-305.
- [47] S. Rashidi, M. Eskandarian, O. Mahian and S. Poncet, Combination of nanofluid and inserts for heat transfer enhancement, *J. Therm. Anal. Calorim.*, **135(1)** (2019) 437-460.

- [48] G. Huminic and A. Huminic, Application of nanofluids in heat exchangers: A review, *Renew. Sust. Energ.*, **16(8)** (2012) 5625-5638.
- [49] S.U.S. Choi, Enhancing thermal conductivity of fluids with nanoparticles, *ASME Int. Mech. Eng.*, **66** (1995) 99–105.
- [50] J. Buongiorno, Convective transport in nanofluids, *J. Heat Transf.*, **128** (2006) 240.
- [51] C. Sulochan, S.P. Samrat and N. Sandeep, Boundary layer analysis of an incessant moving needle in MHD radiative nanofluid with joule heating, *Int. J. Mech. Sci.*, **128–129** (2017) 326-331.
- [52] M. Turkyilmazoglu, Buongiorno model in a nanofluid filled asymmetric channel fulfilling zero net particle flux at the walls, *Int. J. Heat Mass Transf.*, **126** (2018) 974-979.
- [53] M.N. Rostami, S. Dinarvand and I. Pop, Dual solutions for mixed convective stagnation-point flow of an aqueous silica–alumina hybrid nanofluid, *Chin. J. Phys.*, **5** (2018) 2465-2478.
- [54] M.H. Ahmadi, A. Mirlohi, M.A. Nazari and R. Ghasempour, A review of thermal conductivity of various nanofluids, *J. Mol. Liq.*, **265** (2018) 181-188.
- [55] L. Yang, J. Huang, W. Ji and M. Mao, Investigations of a new combined application of nanofluids in heat recovery and air purification, *Powder Tech.*, (2019) doi: 10.1016/j.powtec.2019.10.053.
- [56] S. Nadeem, M.R. Khan and A.U. Khan, MHD stagnation point flow of viscous nanofluid over a curved surface, *Phys. Scripta*, **94(11)** (2019) 115207.



- [57] A.U. Khan, S. Saleem, S. Nadeem and A.A. Alderremy, Analysis of unsteady non-axisymmetric Homann stagnation point flow of nanofluid and possible existence of multiple solutions, *Phys. A: Stat. Mech. Appli.*, (2019) doi.org/10.1016/j.physa.2019.123920.
- [58] N. Abbas, S. Nadeem and M.Y. Malik, On extended version of Yamada–Ota and Xue models in micropolar fluid flow under the region of stagnation point, *Phys. A: Stat. Mech. Appli.*, (2019) doi.org/10.1016/j.physa.2019.123512.
- [59] S. Nadeem, A. Alblawi, N. Muhammad, I.M. Alarifi, A. Issakhov and M.T. Mustafa, A computational model for suspensions of motile micro-organisms in the flow of ferrofluid, *J. Mol. Liq.*, **298** (2019) 112033.
- [60] N. Abbas, M.Y. Malik and S. Nadeem, Transportation of magnetized micropolar hybrid nanomaterial fluid flow over a Riga surface surface, *Comp. Meth. Prog. Biomedicine*, **185** (2020) 105136.
- [61] A. Wakif, I.L. Animasaun, P.V. S. Narayana and G. Sarojamma, Meta-analysis on thermomigration of tiny/nano-sized particles in the motion of various fluids, *Chin. J. Phys.*, (2019) doi.org/10.1016/j.cjph.2019.12.002.
- [62] I.L. Animasaun, R.O. Ibraheem, B. Mahanthesh and H.A. Babatunde, A meta-analysis on the effects of haphazard motion of tiny/nano-sized particles on the dynamics and other physical properties of some fluids, *Chin. J. Phys.*, (2019) doi.org/10.1016/j.cjph.2019.06.007.

- [63] W.T. Cheng and C.H. Lin, Melting effect on mixed convective heat transfer with aiding and opposing external flows from the vertical plate in a liquid-saturated porous medium, *Int. J. Heat Mass Transf.*, **50** (2007) 3026-3034.
- [64] W. Li and Z.Z. Feng, Laminar mixed convection of large-Prandtl-number in-tube nanofluid flow, Part II: Correlations, *Int. J. Heat Mass Transf.*, **65** (2013) 928-935.
- [65] T. Hayat, I . Ullah, A. Alsaedi, M. Waqas and B. Ahmad, Three-dimensional mixed convection flow of Sisko nanoliquid, *Int. J. Mech. Sci.*, **133** (2017) 273-282.
- [66] S.J. Liao, The proposed homotopy analysis technique for the solution of nonlinear problems, *Ph.D. Thesis, Shanghai Jiao Tong University*, 1992.
- [67] M. Ahmad, I. Ahmad and M. Sajid, Magnetohydrodynamic time-dependent three-dimensional flow of Maxwell fluid over a stretching surface through porous space with variable thermal conditions, *J. Braz. Soc. Mech. Sci. Eng.*, **38 (6)** (2016) 1767-1778.
- [68] I.C. Liu and I. Andersson, Heat transfer over a bidirectional stretching sheet with variable thermal conditions, *Int. J. Heat Mass Transf.*, **51(2008)** 4018–4024.
- [69] T.M. Ajayi, A.J. Omowaye, and I.L. Animasaun, Effects of viscous dissipation and double stratification on MHD Casson fluid flow over a surface with variable thickness: Boundary layer analysis, *Int. J. Eng. Res. Africa*, **28** (2017) 73-89.
- [70] A.S. Butt and A. Ali, Entropy analysis of magnetohydrodynamics flow and heat transfer over a convectively heated radially stretching surface, *J. Taiwan Inst. Chem. Eng.*, **45** (2014) 1197-1203.

- [71] S.K. Soid, A. Ishak and I. Pop, MHD flow and heat transfer over a radially stretching/shrinking disk, *Chin. J. Phys.*, **56(1)** (2018) 58-66.
- [72] M.S. Abel and J.V. Tawade, Nandeppanavar MM, MHD flow and heat transfer for the upper-convected Maxwell fluid over a stretching sheet, *Meccanica*, **47** (2012) 385-393.
- [73] M. Waqas, M.I. Khan, T. Hayat and A. Alsaedi, Stratified flow of an Oldroyd-B nanoliquid with heat generation, *Results Phys.*, **7** (2017) 2489-2496.
- [74] M. Irfan, M. Khan and W.A. Khan, Impact of homogeneous–heterogeneous reactions and non-Fourier heat flux theory in Oldroyd-B fluid with variable conductivity, *J. Braz. Soc. Mech. Sci. Eng.*, **41(3)** (2019) 1-9.
- [75] T.R. Mahapatra, S.K. Nandy and A.S. Gupta, Magnetohydrodynamic stagnation-point flow of a power-law fluid towards a stretching surface, *Int. J. Non-Linear Mech.*, **44** (2009) 124-129.
- [76] A. Mushtaq, M. Mustafa, T. Hayat and A. Alsaedi, Buoyancy effects in stagnation-point flow of Maxwell fluid utilizing non-Fourier heat flux approach, *PLOS ONE*, **13(5)** (2018) e0192685.
- [77] M.S. Abel, J.V. Tawade and M.M. Nandeppanavar, MHD flow and heat transfer for the upper-convected Maxwell fluid over a stretching sheet, *Meccanica*, **47** (2012) 385–393.
- [78] A.M. Megahed, Variable fluid properties and variable heat flux effects on the flow and heat transfer in a non-Newtonian Maxwell fluid over an unsteady stretching sheet with slip velocity, *Chin. Phys. B.*, **22(9)** (2013) 094701

- [79] M. Mustafa, T. Hayat and A. Alsaedi, Rotating flow of Maxwell fluid with variable thermal conductivity: An application to non-Fourier heat flux theory, *Int. J. Heat Mass Transf.*, **106** (2017) 142-148.
- [80] M. Turkyilmazoglu, Nanofluid flow and heat transfer due to a rotating disk. *Comp. Fluids*, **94** (2014) 139-146.
- [81] N. Bachok, A. Ishak and I. Pop, Flow and heat transfer over a rotating porous disk in a nanofluid, *Physica B: Condensed Matter*, **406(9)** (2011) 1767-1772.
- [82] M. Khan, A. Hafeez and J. Ahmed, Impacts of non-linear radiation and activation energy on the axisymmetric rotating flow of Oldroyd-B fluid, *Physica A: Stat. Mech. Appl.*, (2020) 124085.
- [83] M. Turkyilmazoglu, MHD fluid flow and heat transfer due to a stretching rotating disk, *Int. J. Therm. Sci.*, **51** (2012) 195-201.
- [84] M. Khan, J. Ahmed and L. Ahmad, Chemically reactive and radiative von Kármán swirling flow due to a rotating disk, *Appl. Math. Mech.*, **39(9)** (2018) 1295-1310.
- [85] E.M. Sparrow and J.L. Gregg, Heat transfer from a rotating disk to fluids of any Prandtl number, *J. Heat Transf.*, **81(3)** (1959) 249-251.

## Turnitin Originality Report

Flow and Heat Transport of Maxwell Fluid Induced by Stretching and Rotating Surfaces by Awais Ahmed .

From DRSM (DRSM L)



- Processed on 23-Aug-2021 09:50 PKT
- ID: 1634638749
- Word Count: 25078

Similarity Index

14%

Similarity by Source

Internet Sources:

8%

Publications:

11%

Student Papers:

2%

Musood Khan

Focal Person (Turnitin)  
Quaid-i-Azam University  
Islamabad

**sources:**

- 1 1% match (Internet from 24-Sep-2020)  
<https://www.mysciencework.com/publication/facets/keywords/76R05>
- 2 < 1% match (student papers from 19-Feb-2014)  
[Submitted to Higher Education Commission Pakistan on 2014-02-19](#)
- 3 < 1% match (student papers from 28-Feb-2015)  
[Submitted to Higher Education Commission Pakistan on 2015-02-28](#)
- 4 < 1% match (student papers from 25-Oct-2017)  
[Submitted to Higher Education Commission Pakistan on 2017-10-25](#)
- 5 < 1% match (student papers from 06-Jul-2017)  
[Submitted to Higher Education Commission Pakistan on 2017-07-06](#)
- 6 < 1% match (student papers from 14-Dec-2017)  
[Submitted to Higher Education Commission Pakistan on 2017-12-14](#)
- 7 < 1% match (student papers from 14-Dec-2013)  
[Submitted to Higher Education Commission Pakistan on 2013-12-14](#)
- 8 < 1% match (student papers from 08-May-2016)  
[Submitted to Higher Education Commission Pakistan on 2016-05-08](#)
- 9 < 1% match (student papers from 15-Dec-2011)  
[Submitted to Higher Education Commission Pakistan on 2011-12-15](#)
- 10 < 1% match (student papers from 08-Jul-2013)  
[Submitted to Higher Education Commission Pakistan on 2013-07-08](#)
- 11 < 1% match (student papers from 02-Jan-2015)  
[Submitted to Higher Education Commission Pakistan on 2015-01-02](#)
- 12 < 1% match (student papers from 03-Sep-2013)  
[Submitted to Higher Education Commission Pakistan on 2013-09-03](#)
- 13 < 1% match (student papers from 19-Feb-2014)  
[Submitted to Higher Education Commission Pakistan on 2014-02-19](#)
- 14 < 1% match (student papers from 21-Sep-2017)  
[Submitted to Higher Education Commission Pakistan on 2017-09-21](#)
- 15 < 1% match (student papers from 13-Dec-2018)